

Microwave Resonator Filters for Advanced Wireless Systems

by

Ju Seop Lee

A dissertation submitted in partial fulfillment
of the requirements for the degree of
Doctor of Philosophy
(Electrical Engineering)
in The University of Michigan
2009

Doctoral Committee:

Professor Kamal Sarabandi, Chair
Professor Karl Grosh
Professor Amir Mortazawi
Assistant Professor Anthony Grbic

© Ju Seop Lee 2009
All Rights Reserved

To my mother Kil Jung Lee and my father Seung Joo Lee

ACKNOWLEDGEMENTS

Getting Ph.D. was certainly a family endeavor, and my family has endured much sacrifice for the sake of my education. First I would like to thank my parents to whom my debt is simply infinite. I could not have accomplished what I did without their boundless love, sacrifice, support, and encouragement. My gratitude to my parents is more than that can be expressed in words. I also want to thank my brother, Jung Yup Lee, for taking care of my parents while I was in America, and my wife Youn Goung Song for her love and support.

During my Ph.D. study in the University of Michigan, I have been privileged to have Prof. Kamal Sarabandi as my advisor. I would like to thank him for providing me with the opportunity to conduct this Ph.D. research. I am grateful to him for his patient mentoring, supportive advising, and endless editing. I would also like to thank those who have served on my committee, Prof. Karl Grosh, Prof. Amir Mortazawi, and Prof. Anthony Grbic, for their efforts and contribution to the fruition of my dissertation. I am also grateful to Prof. Eric Michielssen for his help in applying for Horace H. Rackham Predoctoral Fellowship.

I would like to acknowledge the support and guidance provided by Prof. Young-Sik Kim at Korea University, Seoul, Korea. I was able to begin the study on microwave engineering when I was a graduate student at his group.

I would like to extend my thanks to my colleagues in the RADLAB (Radiation Laboratory) I have had throughout the years. Wonbin Hong provided me with tremendous technical support over the years. I got a lot of advice from Line van Nieuwstadt when I needed to make an important decision. Technical questions from Young Jun Song and Morteza Nick made me study fundamentals of electromagnetics and microwave engineer-

ing. I am also thankful to my group members for their friendship. I would also like to thank RADLAB administrative staffs, Karla Johnson and Michelle Chapman.

I am also grateful to Dr. In-Bok Yom and Dr. Man Seok Uhm at ETRI (Electronics and Telecommunications Research Institute), Daejeon, South Korea, for giving me opportunities to gain valuable experiences in the field of RF/microwave engineering.

The research presented in this dissertation was supported in part by KOSEF (Korea Science and Engineering Foundation) Fellowship, Horace H. Rackham Predoctoral Fellowship, and IEEE MTT-S (Microwave Theory and Techniques Society) Graduate Fellowship.

TABLE OF CONTENTS

DEDICATION	ii
ACKNOWLEDGEMENTS	iii
LIST OF TABLES	viii
LIST OF FIGURES	ix
CHAPTER	
1 Introduction	1
1.1 Background	1
1.2 Thesis Overview	8
2 Fundamental Theories of Microwave Resonator Filters	12
2.1 Filter Network Theory	12
2.1.1 Polynomials	12
2.1.2 Reflection and Transmission Coefficients	15
2.1.3 Characteristics of Polynomials	16
2.1.4 Normalization of the Polynomials	17
2.1.5 Generalization of the Transmission and Reflection Coefficients	18
2.2 Characteristic Functions and Frequency Responses	20
2.2.1 All-Pole Filters	21
2.2.2 Filters with Transmission Zeros	24
2.2.3 Linear Phase Filters	26
2.2.4 Linear Phase Filters with Transmission Zeros	26
2.3 Coupling Matrix	29
2.3.1 Circuit Model	29
2.3.2 Scattering Parameter	34
2.3.3 $(N + 2) \times (N + 2)$ Coupling Matrix	37
2.3.4 Coupling-Routing Diagram	39
2.4 Physical Elements for Microwave Filter Implementation	41
3 Dual-Passband Microwave Filter	44

3.1	Introduction	44
3.2	Design Theory	47
3.2.1	Lowpass Filter Prototype	47
3.2.2	Frequency Transformation for Dual-passband Filters	50
3.3	Filter Design and Measurement	53
3.3.1	Electrical Design	53
3.3.2	Physical Design and Measurement	58
3.3.3	Sensitivity Considerations	65
3.4	More Examples	68
3.5	Asymmetric Dual-Passband Filter Design	72
3.6	Conclusions	76
4	Triple-Passband Microwave Filter	77
4.1	Introduction	77
4.2	Design Theory	78
4.2.1	Transfer Function	78
4.2.2	Frequency Transformation for Tripple-Passband Filters	79
4.3	Filter Synthesis	82
4.3.1	6th-Order Filter	82
4.3.2	12th-Order Filter	87
4.4	Measurements	93
4.5	Asymmetric Triple-passband filter	96
4.6	Conclusions	97
5	Tunable Microwave Filter with a Constant Frequency Response	99
5.1	Introduction	99
5.2	Design Theory	100
5.2.1	Step-Impedance Resonator	101
5.2.2	Coupling Elements	103
5.2.3	Filter Performance	109
5.3	Design Example and Measurement	111
5.4	Design of Higher-Order Filters	114
5.5	Conclusions	117
5.6	Appendix I: Step Impedance Resonator	118
5.7	Appendix II: The Inverter Circuit	119
6	Planar Miniaturized Microwave Resonator Filter	124
6.1	Introduction	124
6.2	Filter Structure and Design	125
6.3	Fabrication and Measurement	132
6.4	Conclusion	132
7	Conclusions	134
7.1	Summary	134

7.1.1	Multiple-Passband Microwave Resonator Filters	135
7.1.2	Tunable Microwave Resonator Filters	135
7.1.3	Miniaturized Microwave Resonator Filters	136
7.2	Future Work	136
7.2.1	Non-Planar Miniaturized Microwave Resonator Filter . . .	136
7.2.2	High-Pass Filter for the Receiver of Frequency-Modulated Continuous-Wave Radar	140

BIBLIOGRAPHY	149
-------------------------------	------------

LIST OF TABLES

Table

3.1	Physical dimensions of the dual-passband filter.	62
5.1	Design parameters for the 2nd-order tunable filter.	105
5.2	Design result of the tunable filter.	110
5.3	Design parameters for the 2nd-order tunable filter.	111

LIST OF FIGURES

Figure	
2.1	Ideal amplitude spectrum for lowpass filter. 21
2.2	Lowpass response of the 4th-order Butterworth filter. 22
2.3	Lowpass response of the 4th-order all-pole filter with an arbitrary distribution of reflection zeros. 23
2.4	Lowpass response of the 4th-order Chebyshev response filter with 20 db equi-ripple return loss. 24
2.5	Lowpass response of the 4th-order filter with 20 dB equi-ripple return loss within the passband and transmission zeros at $S_p = \pm j2.4$ and $\pm j3.6$ 25
2.6	Lowpass responses of the 4th-order filters in Fig 2.2, Fig. 2.4, and Fig. 2.5. 26
2.7	Position of roots of $P(S)$ and $F(S)$ for the example of the linear phase filter with transmission zero. \times and \circ indicates the roots of $F(S)$ and $P(S)$, respectively. The roots of $F(S)$ are $S_f = \pm j0.9731, \pm j0.7802, \pm j0.4903,$ and $\pm j0.1692$. The roots of $P(S)$ are $S_p = \pm j2.00$ and $\pm 0.60 \pm j0.45$ 27
2.8	Linear phase filter with transmission zeros. (a) the amplitude response, (b) the group delay response. 28
2.9	A bandpass circuit prototype for an N th-order filter. 30
2.10	A bandpass circuit prototype for an N th-order filter. 32
2.11	A lowpass circuit prototype for an N th-order filter. 33
2.12	A circuit network for an N th-order filter. Impedance matrix A represents overall circuit including the source and load termination. Impedance matrix Z represents a purely reactive network operating between a voltage source with internal impedance and a load. 35
2.13	A circuit network representation for an N th order filter (a) using the $N \times N$ matrix (b) using the $(N + 2) \times (N + 2)$ matrix. 37
2.14	The coupling-routing diagram of a 8th-order canonical structure filter. . . . 40
2.15	The coupling-routing diagrams of inline structure filters: (a) 6th-order filter; (b) 8th-order filter. 40
3.1	An example of frequency plan and spatial coverage of a satellite communication system. 45

3.2	A block diagram of a conventional satellite transponder for the frequency plan and spatial coverage shown in Fig. 3.1.	46
3.3	A block diagram of a satellite transponder with dual-passband microwave filters.	46
3.4	The frequency response of the filter in Ω , Ω' , and ω domain. The coupling matrix of the dual-passband filter is obtained from the transfer function in Ω' domain.	48
3.5	Frequency response of a lowpass filter prototype with the transmission zeros at $\pm j2.0$	54
3.6	The frequency response of the dual-passband filter in Ω' domain.	55
3.7	The frequency response of the dual-passband filter in real frequency domain.	58
3.8	The conductor layer of stripline structure for the dual-passband filter.	59
3.9	Coupling structures of coupled stripline open-loop resonators which are separated by a spacing s and may or may not be subject to an offset p : (a) Electric coupling structure. (b) Magnetic coupling structure. (c) Mixed coupling structure. (d) Mixed coupling structure.	60
3.10	Synthesized and simulated frequency response of the dual-passband filter.	63
3.11	The fabricated conductor layer of the stripline structure for the dual-passband filter.	63
3.12	Frequency response of the dual-passband filter: (a) S_{11} , (b) S_{21}	64
3.13	Sensitivity to random variation in coupling coefficients. Random variation less than ± 0.005 is applied to all zero inter-resonator couplings in (3.25): (a) S_{21} , (b) S_{11}	66
3.14	Sensitivity to random variation in coupling coefficients. Random variation less than ± 0.01 is applied to all zero inter-resonator couplings in (3.25): (a) S_{21} , (b) S_{11}	66
3.15	Sensitivity to random variation in coupling coefficients. Random variation less than ± 0.005 is applied to all zero self-couplings in (3.25): (a) S_{21} , (b) S_{11}	67
3.16	Sensitivity to random variation in coupling coefficients. Random variation less than ± 0.01 is applied to all zero self-couplings in (3.25): (a) S_{21} , (b) S_{11}	67
3.17	Sensitivity to random variation in coupling coefficients. Random variation less than $\pm 1\%$ is applied to all non-zero inter-resonator couplings in (3.25): (a) S_{21} , (b) S_{11}	68
3.18	Sensitivity to random variation in coupling coefficients. Random variation less than $\pm 5\%$ is applied to all non-zero inter-resonator couplings in (3.25): (a) S_{21} , (b) S_{11}	68
3.19	Frequency response of a lowpass filter prototype with no transmission zeros at finite frequencies.	69
3.20	Frequency response of a dual-passband filter whose lowpass prototype is shown in Fig. 3.19.	70
3.21	Frequency response of a lowpass filter prototype with no transmission zeros at infinite frequencies	71

3.22	Frequency response of a dual-passband filter whose lowpass prototype is shown in Fig. 3.21.	72
3.23	A typical transmission response of an asymmetric dual-passband filter in Ω and Ω' domains. Frequency transformation from Ω domain to Ω' domain is performed using (3.33) with $\Omega'_{ma} > 0$, $\Omega'_{mb} > 0$, and $\Omega'_z > 0$	74
3.24	Frequency responses of asymmetric dual-passband filters in Ω' domain : (a) $\Omega'_{ma} = 0.1$, $\Omega'_{mb} = 0.7$, $\Omega'_z = 0.5$ (b) $\Omega'_{ma} = -0.8$, $\Omega'_{mb} = 0.2$, $\Omega'_z = -0.3$	75
4.1	The frequency response of the filter in Ω , Ω' , and ω domain. The coupling matrix of the triple-passband filter is obtained from the transfer function in Ω' domain.	80
4.2	The frequency response of a 2nd-order lowpass filter prototype with the transmission zero at $\pm j25.0$ and return loss of 20 dB.	83
4.3	The frequency response of a lowpass filter prototype for triple-passband filter.	84
4.4	The coupling-routing diagram of 6th-order canonical structure filter with a source-load coupling.	85
4.5	The frequency response of a lowpass filter prototype for triple-passband filter. This response is obtained by rearranging the reflection zeros and transmission zeros of the frequency response shown in Fig. 4.3 after removing a pair of outermost transmissions zeros.	86
4.6	The frequency response of a 4th-order lowpass filter prototype with the transmission zero at $\pm j2.0$ and return loss of 20 dB.	88
4.7	The frequency response of a lowpass filter prototype for triple-passband filter.	89
4.8	The coupling-routing diagram of 12th-order canonical structure filter.	89
4.9	The frequency response of a lowpass filter prototype for triple-passband filter. This response is obtained by rearranging the reflection zeros and transmission zeros of the frequency response shown in Fig. 4.7 after removing repeated transmissions zeros at $\pm\Omega'_z$	91
4.10	The coupling-routing diagram of 12th-order canonical structure filter.	91
4.11	The coupling-routing diagram of 12th-order cascaded-quadruplet structure filter.	93
4.12	The microstrip layout of the 12th-order triple-passband open-loop resonator filter. $b = 2.42$, $r = 17.2$, $g_1 = 2.02$, $g_2 = g_3 = g_4 = g_5 = g_6 = 2.36$, $d_{01} = 0.30$, $d_{12} = 0.40$, $d_{23} = 0.70$, $d_{34} = 0.95$, $d_{45} = 0.52$, $d_{56} = 1.10$, $d_{67} = 3.00$, $d_{58} = 10.10$, $d_{49} = 1.36$, and $d_{310} = 2.10$. All dimensions are in mm.	94
4.13	The measured and synthesized frequency response of the 12th-order triple-passband open-loop resonator filter.	95
4.14	The frequency response of the asymmetric triple-passband filter in Ω and Ω' domain.	97
4.15	The frequency response of an asymmetric triple-passband filter in Ω' domain. $\Omega'_{b1} = -0.80$, $\Omega'_{a1} = -0.05$, $\Omega'_{a2} = 0.25$, and $\Omega'_{b2} = 0.60$	98
5.1	A schematic of 2nd-order tunable microstrip filter. Parameters in the parentheses are physical parameters.	101

5.2	A symmetric step-impedance microstrip resonator loaded with a varactor.	102
5.3	The resonant frequencies of the step-impedance resonator.	103
5.4	A generalized N th-order bandpass filter circuit with admittance inverters.	104
5.5	An inverter circuit with a series capacitor.	104
5.6	A 2nd-order tunable filter with varactors. C_{v01} , C_{v12} , and C_{v23} are for inverter circuit and C_v 's are for adjusting the resonant frequencies of the resonators.	106
5.7	An inverter circuit for J_{01} inverter.	107
5.8	An inverter circuit for J_{12} inverter.	109
5.9	Frequency responses of the 2nd-order tunable filter.	110
5.10	The schematic of the 2nd-order tunable microstrip filter.	112
5.11	The fabricated 2nd-order tunable microstrip filter.	112
5.12	Measured and simulated frequency responses of the 2nd-order tunable microstrip resonator filter.	113
5.13	Frequency response of a 3rd-order tunable filter. The design parameters are $L_b-l_{01.1}=20.368$ mm, $L_b-l_{12.1}=14.125$ mm, $Z_a=80 \Omega$, $Z_b=20 \Omega$, $C_{01a}=2.527$ pF, $C_{01b}=1.929$ pF, $C_{12a}=4.751$ pF, $C_{12b}=21.701$ pF. Since the circuit is symmetric, only half of the design parameters are provided.	115
5.14	Frequency response of a 4th-order tunable filter. The design parameters are $L_b-l_{01.1}=20.424$ mm, $L_b-l_{12.1}=14.130$ mm, $L_b-l_{23.2}=14.130$ mm, $Z_a=80 \Omega$, $Z_b=20 \Omega$, $C_{01a}=2.416$ pF, $C_{01b}=2.028$ pF, $C_{12a}=4.658$ pF, $C_{12b}=24.616$ pF, $C_{23a}=4.497$ pF, $C_{23b}=32.207$ pF. Since the circuit is symmetric, only half of the design parameters are provided.	116
5.15	A capacitor-loaded step impedance microstrip resonator.	118
6.1	Two-pole miniaturized double-spiral slot-line resonator filters: (a) a conventional structure and (b) a novel structure. The dimensions are all in mm and are $a=0.30$, $b=0.35$, $d=2.75$, $e=4.00$, $f=7.90$, $g=0.30$, $h=3.30$, $i=0.70$, and $k=1.70$	126
6.2	Signal flow in the two-pole filter with the source-load coupling.	127
6.3	Frequency response of the filter with the coupling matrix in (6.9).	129
6.4	(a) Fabricated 2nd-order slot-line resonator filter, (b) The frequency response of the 2nd-order slot-line resonator filter.	131
7.1	The miniaturized two-pole filter with meandered resonators	138
7.2	Enlarged view for the meandered resonators in Fig. 7.1.	139
7.3	The frequency response of the miniaturized filter shown in Fig. 7.1	140
7.4	A block diagram of an FMCW radar system.	141
7.5	A transmitting, receiving, and beat frequency of an FMCW radar.	142
7.6	The block diagram of the receiver.	143
7.7	The amplitude response of the normalized butterworth-response highpass filter. The cutoff frequency is at $\Omega = 1$	144
7.8	Amplitude responses of 4th-order lowpass prototype filters: (a) with no transmission zeros; (b) with transmission zeros at $S = \pm j4.0$	145

7.9	Amplitude responses of 4th-order lowpass prototype filters: (a) with no transmission zeros; (b) with transmission zeros at $S = \pm j4.0$	146
7.10	The frequency response.	147

CHAPTER 1

Introduction

1.1 Background

The microwave filter is a component which provides frequency selectivity in mobile and satellite communications, radar, electronics warfare, and remote sensing systems operating at microwave frequencies. In general, the electrical performances of the filter are described in terms of insertion loss, return loss, frequency-selectivity (or attenuation at rejection band), group-delay variation in the passband, and so on. Filters are required to have small insertion loss, large return loss for good impedance matching with interconnecting components, and high frequency-selectivity to prevent interference. If the filter has high frequency-selectivity, the guard band between each channel can be determined to be small which indicates that the frequency can be used efficiently. Also, small group-delay and amplitude variation of the filter in the passband are required for minimum signal degradation. In mechanical performance aspect, filters are required to have small volume and mass, and good temperature stability.

There are two methods of filter design. One was originated by Zobel and is well known as the image parameter method. The second was originated by Norton and Bennett and is known as the polynomial method or insertion loss method. The image parameter theory filter is based on the properties of transmission lines. A simple network with lumped

components is described in terms of this continuous structure. Several of such elementary networks with equal characteristic terminal impedances, connected together to produce a chain of ladder networks, will possess a transmission constant equal to the sum of all the individual transmission constants of the elementary sections [1]. In the insertion loss method, a filter response is defined by a transfer function which is the ratio of the output voltage to the input voltage of the filter. The ideal lowpass transfer function is characterized by a magnitude function that is a constant in the passband and zero in the stopband. The corresponding phase is linear in the passband and the phase delay is a constant there. Since such a lowpass network cannot be represented by a quotient of finite-degree rational polynomials, it is necessary to seek some approximation to it [2]. This may be done by having the amplitude, phase and delay stay within prescribed tolerances. The classical four class solutions to the approximation problems are the Butterworth (maximally flat), Chebyshev (equal ripple in the passband), inverse Chebyshev (equal ripple in the stopband) and elliptic (equal ripple in the passband and stopband). It is of note that the former problems are all special cases of the latter one. In practice, either method can be used depending on requirements. If one is forced to use hand calculation, then the image parameter approach is really the only method available, except perhaps in the limited cases where tabulated insertion loss designs can be used. Insertion loss method deals directly with frequency responses and provides an elegant solution to the approximation problem. Today, most microwave filter designs are done with computer-aided design based on insertion loss method. The microwave filter design techniques presented in this thesis also rely on the insertion loss method.

It is not overstatement to say that the classic paper by Cohn paved the way for subsequent works on microwave filters [3]. This paper describes direct-coupled microwave filter where there are only couplings between adjacent resonators. As well known, the direct-coupled microwave filter can support Butterworth and Chebyshev frequency response which do not have transmission zeros in finite frequencies. Since Chebyshev re-

sponse has fairly good frequency selectivity than Butterworth response, it has been widely employed in filter design. The importance of Cohn's paper is that easy-to-use formulas are given for Butterworth and Chebyshev response filter design. It is interesting to note how much Cohn's design formulas are simple compared with precedent Darlington's work [4].

Wireless communications systems have been demanding tighter requirements in terms of electrical specifications as well as drastic reductions of manufacturing costs and development times [5]. Hence, the area of microwave filters, especially for mobile and space applications, has experienced significant improvements in theoretical, technological, and performance subjects. One of significant improvements in filter design theory was utilizing cross-coupling between nonadjacent resonators. Early works by Kurzok described 3rd-order and 4th-order filters with cross-coupling [6][7]. Cross-coupling gives a number of alternative paths which a signal may take between the input and output ports. The multipath effect causes transmission zeros to appear in the transfer function, which, depending on the phasing of the signals, may cause transmission zeros (or attenuation poles) at finite frequencies or group-delay flattening, or even both simultaneously [8]. The cross-coupling configuration makes it easy to design elliptic response filters. Since the transfer function of the elliptic filter has transmission zeros (or attenuation poles) in finite frequencies, the elliptic filter has much higher frequency selectivity than the Chebyshev filter. Also, the cross-coupling technique facilitates the design of linear phase filters which have linear phase in their passband. Since linear phase results in flat group-delay variation in the passband, the linear phase filter does not necessitate the external equalizer for phase linearity. Hence, the linear phase filter is also called self-equalized filter.

Along with the improvement in electrical performances of the filters, many efforts have been made for the enhancement of mechanical performance. Especially, reducing the size and volume of the filter has been main topic for filter designers. Since R. D. Richtmyer [9] showed that dielectric objects can function much like metallic cavities, dielectric resonators have always been a good candidate for this purpose. Dielectric resonator filters

have the advantages of not only small size but also good temperature stability. Another major step in reducing the volume and mass of microwave filters was utilizing dual-mode technique. The paper written by Williams [10] describes the fundamental theory with dual-mode waveguide filter realization. Dual-mode filters use two orthogonal degenerate modes of each resonator, the number of resonators can be reduced by a factor of two. Hence, the small volume and mass were able to be achieved. Although dual-mode filter design technique is initiated from non-planar filter structure, this technique has been also widely applied to planar microwave filters.

Although the significant improvements of the microwave filter design theory and technology have been made as the specifications for the filter become more stringent, many filter design techniques have not been exploited and still need to develop for advanced wireless systems. In satellite communication systems, non-continuous channels might be transmitted to the same geographical region through one beam [11]. Individual conventional single-passband filters might be connected in parallel to establish multiple passbands. One of the methods to connect individual filters is using a power divider and a power combiner at input and output ports, respectively. In this case, the individual filters can be designed with ease using traditional filter design theory but 6 dB loss generated by both a power divider and a power combiner is inevitable. Also, the divider and the combiner make the total structure bulky. Since a multiple-passband filter has multiple passbands, signal dividing and combining structures are not needed. Hence, the multiple-passband filter can make such wireless systems much more simple than the parallel-connected single-passband filters. This advantage of multiple-passband microwave filters brought significant interests.

Since the polynomials, which are essential for insertion loss method, for multiple-passband microwave filters are not well known. Hence, the most common method to synthesize multiple-passbands microwave filters rely on optimization methods. Basic idea to establish multiple passbands is putting transmission zeros inside the passband of the single-passband filter to split it into multiple passbands. However, the performance or efficiency

of optimization methods to find the polynomials depends on initial values. Hence, the study in this proposal embark on developing the analytic method for synthesizing the multiple-passband microwave filters.

Another microwave filter design technique that great efforts need to be dedicated toward is tunable microwave filter design technique since recent broadband receiving and transmitting systems have increased the demand for frequency tunability of microwave components. For example, frequency agile system for naval target control uses 19 channels from 421.5 MHz to 448.5 MHz. This frequency agile system can obtain improved resistance to interference and increased data link reliability. This system senses interference and automatically changes frequencies to avoid it. This frequency change can be achieved by switching from one filter to the other, but the system should have as many filters as the number of the channels. Hence, compared with the bank of switched fixed-frequency filters, one tunable filter can make frequency-agile systems much simple.

The performance of tunable filters may be described by the same criteria as used for fixed-frequency filters. Most important additional parameters for tunable filters could be tuning range, tuning speed, and tuning linearity. Not all of these requirements can be perfectly satisfied simultaneously by a certain tunable filter. Hence, the tunable filter design should take into account the priority of the requirements. If system requirements necessitate that the filter exhibit multioctave tuning range, an YIG (Yttrium-Iron-Garnet) filter is an obvious choice [12][13]. It also has spurious-free response, low insertion loss due to high quality factor of the resonator. However, it cannot be implemented in integrated systems since its structure is not planar. Also, magnetic hysteresis effect limits the tuning speed of the YIG filter. Fast tuning speed can be achieved by varactor tuning technique. Since varactors can be easily integrated on coplanar waveguide and microstrip structures, tremendous applications have been made to microwave tunable filters. General method to tune the filter is to use varactors as part of the resonator. One of the varactors' drawback is power capacity. Since the varactors are originally non-linear devices, the large input

signals generate harmonics. Recently developed technologies such as MEMS (microelectromechanical systems) and BST (Barium Strontium Titanate) have also been applied to tunable filters. MEMS varactors have small size and provide fast tuning speed and low insertion loss. However, serious drawback of narrow tuning range due to poor capacitance ratio is underestimated. Digital MEMS filters show wide tuning range but discrete center frequencies that the filter can have result in relatively low frequency resolution. BST varactors are also small and can be easily implemented in integrated circuits. Also, they are reported to be suitable for high-power applications. However, they suffer from poor quality factor.

Repeatedly, there is no perfect tunable filter satisfying all the requirements at the same time. No matter what type of the tunable filter is used in the research, most research activities have concentrated on methodology of changing the center frequency of the filter and have overlooked the characteristics of frequency responses of the filters. This has resulted in different frequency responses and bandwidths as the filter is adjusted for different center frequencies. However the tunable filter should have same performance for all channels with different center frequencies. Hence, this overlooked important point in tunable filter design is studied in this research.

Finally, with all many kinds of miniaturized filters, minimizing the size of the filter has always received a great attention. Recent solid state device technologies make it possible to implement miniaturized electronic circuits including microwave devices and components. However, one of the exceptions is a distributed passive microwave filter and it still occupies a lot of space of the entire circuit. The large dimension of the distributed filter stems from the fact that it is usually made of a number of resonators whose dimensions are comparable to the guided wavelength. Hence, many researchers made a lot of efforts to developing the topologies of miniaturized resonators.

The resonators can be categorized into planar resonators and non-planar resonators. Most common planar resonators are implemented using the microstrip structure. Microstrip

patch resonators and microstrip line resonators are very representative of planar resonators. Regarding the reducing the size of the resonator, the microstrip resonator line has great advantages. Most successful method to reduce the size of the microstrip line resonator is meandering the microstrip line of the resonator. The meandered microstrip line open-loop resonator is smaller than $\lambda_{g0}/8$ by $\lambda_{g0}/8$, where λ_{g0} is the guided wavelength at the center frequency [14]. For further reduction of the resonator size using meandering the microstrip line, the microstrip line should have very narrow line. However, in general, the quality factor of the resonator becomes worse as the line becomes narrower. This disadvantage of the meandered microstrip line resonator has been overcome by using HTS (High Temperature Superconducting) materials but the required cooler reduces the miniaturization advantage. On the other hand, non-planar resonators have relatively higher quality factor than planar resonators. Although the non-planar resonators are bulky, these filters are employed by the wireless systems where the electrical performances are much more important than the size and volume of the filter. For examples, the waveguide cavity filters have found a lot of applications such as base stations of cellular systems and satellite transponders. Although these systems, compared with handsets, allocate large spaces for the filters, small filters are obviously more favorable. As delineated in the above, two major methods, using the dielectric resonators and dual-mode techniques, have been utilized for designing small non-planar microwave filters. Another approach for producing non-planar filters with reduced size is utilizing the evanescent mode of the waveguide [15]. While the waveguides of the waveguide cavity filters operate above their cutoff frequencies, those of the evanescent mode filters operate below the cutoff frequencies. This technique showed appreciable reduction in size and volume. The above-mentioned trend of the developing small microwave filters shove this research into contriving prototypes of the miniaturized planar and non-planar resonators for small microwave filter design.

1.2 Thesis Overview

With the above-mentioned background, the work carried out during the course of this thesis has been directed toward the design of microwave resonator filters for advanced wireless systems. As modern and next-generation wireless systems use complex frequency allocation and spatial coverage, the size and mass of the entire systems are mainly affected by the microwave filters. For size and mass reduction of the advanced wireless systems, this work particularly focuses on developing the design methods for multiple-passband microwave filters, tunable microwave filters with a constant frequency response, and planar miniaturized microwave filters. These filters can make a significant impact on the advanced wireless systems by replacing the conventional microwave filters.

The organization of this thesis is as follows.

Following the Introduction, Chapter 2 provides the overview of fundamental theories of microwave resonator filters which will be used in the rest of the thesis. Since the filters in this thesis are designed by the insertion loss method, the transfer function and its polynomials and the ripple constants are briefly explored. The characteristics of the polynomials and frequency responses of all-pole filters, filters with transmission zeros, and self-equalized filters are also provided in this chapter. Based on the equivalent circuit model of the microwave resonator filter, the coupling matrix theory, which will later be applied to the filter design in the following chapter, is described. Based on the physical elements for implementation, microwave filters can be categorized into lumped element filter, waveguide filter, printed circuit filter, and dielectric resonator filter. The characteristics of these filters are also provided in this chapter.

Chapter 3 describes a synthesis method for symmetric dual-passband filters. Conventional filter which has one passband can be easily synthesized since the polynomials for the transfer functions are well known. Also, design tables are well established and can be easily referred. However, the polynomials for the transfer function of the dual-passband microwave filters are not easily obtainable and have been usually acquired by optimization

methods whose convergence depends on the initial values and is not always guaranteed. The proposed method employs frequency transformation techniques for finding the locations of reflection zeros and transmission zeros of a desired filter. From the reflection zero and transmission zero information, the polynomials for the transfer functions are obtained. This method can be used to design dual-passband filters with prescribed passbands and attenuation level at stopbands directly without the need for any optimization processes. The frequency transformation for symmetric dual-passband filters is also extended to include asymmetric dual-passband responses. This flexible frequency transformation preserves the attenuation characteristics of the lowpass filter prototype.

Chapter 4 expands the dual-passband microwave filter design theory to a synthesis method for triple-passband microwave filters. Similarly to the dual-passband filter design, a frequency transformation is newly developed for finding the locations of reflection zeros and transmission zeros of the triple-passband filters in an analytical manner. Sometimes, the number of obtained transmission zeros obtained by using the proposed analytic method might be so large that some transmission zeros are redundant to satisfy the frequency selectivity specification. In this case, some transmission zeros can be intentionally removed to reduce the number of the cross-couplings. Small number of the cross-couplings is preferred with respect to physical filter implementation. The reflection zeros and transmission zeros obtained by the frequency transformation are optimized after removing redundant zeros to achieve a transfer function with reduced number of transmission zeros in order to reduce the number of cross-couplings.

Chapter 5 describes an analytic design method for microstrip tunable filters. Especially, this proposal focuses on developing the analytic design method for tunable microwave filters with a prescribed frequency response. An analytic approach for filter design makes it possible to make the tunable filter have same frequency response when the center frequency is adjusted. One possible way to obtain the same frequency response is using tuning elements not only for resonators but also the coupling structure. However, in the this design

method, no tuning elements are used in coupling structures for reducing the tuning complexity. Prescribed frequency response is achieved by designing the coupling structures in such a way that their frequency responses closely follow those of the desired inverters. Step-impedance microstrip line resonators are employed and the resonant frequencies of resonators are adjusted by varactors.

Chapter 6 presents a miniaturized planar 2nd-order microwave filter. The building block of this filter is a high-Q double spiral slot resonator backed by a conductor plane. The provision of a float back conductor plane allows vertical integration of this filter with other passive and active RF electronic components usually found in miniaturized wireless transceivers. The conductor plane also provides a coupling mechanism between the input and output of the filter giving rise to transmission zeros. It is shown that the location of transmission zeros can easily be adjusted and significant out-of-band rejection be achieved using only two miniaturized double-spiral resonators.

The final chapter of the thesis (Chapter 7) presents the conclusions and the suggested works. The significance and contribution of this work is summarized. For the suggested works, along with the miniaturized planar filter in Chapter 6, a miniaturized non-planar filter utilizing a meander resonator is shown. A proposed meander resonator has the quality factor higher than 600, which results in low insertion loss of the filter. Since the resonator has non-planar meander structure, a newly-developed fabrication process called ultrasonic consolidation process is suggested to be used to implement such structure. Design approach and simulation result of the non-planar miniaturized microwave filter are briefly presented. Another suggested work, a highpass filter for the receiver of a frequency-modulated continuous-wave radar is also discussed. The highpass filter can compensate for the amplitude variation of received signal from a target. This highpass filter should have no infinite attenuation in order not to lose signal. Since, no design method for this type of the highpass filter has been provided, a design method is presented and it is suggested that the filter is applied to the receiver of the frequency-modulated continuous-wave radar in order to

effectively increase the dynamic range of an analog-to-digital converter which follows the highpass filter.

CHAPTER 2

Fundamental Theories of Microwave Resonator Filters

2.1 Filter Network Theory

The microwave filter is vital component in a huge variety of electronic systems, including mobile radio, satellite communications and radar. Such component is used to select or reject signal at different frequencies. Although the physical realization of microwave filters may vary, the circuit network theory is common to all. This section provides various network theories for the design of microwave filters.

2.1.1 Polynomials

Filter design using insertion loss method begins with defining the low-pass transfer function which is a ratio of output voltage to input voltage may be written as

$$\frac{V_{out}}{V_{in}} = \frac{a_m S^m + a_{m-1} S^{m-1} + \dots + a_1 S + a_0}{b_n S^n + b_{n-1} S^{n-1} + \dots + b_1 S + b_0} = t(S) \quad (2.1)$$

where $S = \sigma_n + j\Omega$ is the normalized complex frequency. This is the variable commonly encountered in Laplace transformation theory. For this transfer function to represent a stable systems, the denominator of $t(S)$ must be Hurwitz: that is, the roots of the denominator must be in the left half-plane of the complex frequency domain. The ratio of the output

amplitude to the input amplitude can be found by simply evaluating the transfer function $t(S)$ at $S = j\Omega$. Because $S = j\Omega$ corresponds to a sinusoidal frequency, the letter Ω is often said to represent real angular frequencies while the letter S is said to represent complex frequencies.

If the amplitude of a sinusoid at the output of a network is smaller than the amplitude at the input, then the signal is said to have been attenuated. The attenuation is usually expressed in terms of decibels (dB) as

$$A(\Omega) = 20\log \left| \frac{V_{in}(j\Omega)}{V_{out}(j\Omega)} \right|. \quad (2.2)$$

By our definition of the transfer function $t(S)$, this can also be written as

$$A(\Omega) = -20\log |t(j\Omega)|. \quad (2.3)$$

In filter theory it is common practice to consider transfer functions that are ratios of input to output; i.e., we work with

$$\begin{aligned} H(s) &= \frac{1}{t(S)} \\ &= \frac{b_n S^n + b_{n-1} S^{n-1} + \dots + b_1 S + b_0}{a_n S^n + a_{n-1} S^{n-1} + \dots + a_1 S + a_0} \\ &= \frac{E(S)}{P(S)}. \end{aligned} \quad (2.4)$$

It follows that the attenuation can be expressed as

$$A(\Omega) = 20\log |H(j\Omega)|. \quad (2.5)$$

The function $H(S)$ will be referred to simply as an input/output transfer function. In the passband of a filter, the arbitrary shape that we want to approximate is usually just a constant. For simplicity the constant value can be normalized to unity; that is, in the

passband,

$$|H(j\Omega)| \approx 1. \quad (2.6)$$

It is convenient to eliminate this constant term and instead use the characteristic function $K(S)$ defined by

$$H(S)H(-S) = 1 + K(S)K(-S). \quad (2.7)$$

This equation indicates that $H(S)$ and $K(S)$ have the same denominator polynomial; thus if $H(S)$ is written as

$$H(S) = \frac{E(S)}{P(S)} \quad (2.8)$$

and we can write $K(S)$ as

$$K(S) = \frac{F(S)}{P(S)}. \quad (2.9)$$

Making use of (2.7), (2.8), and (2.9), we can relate the polynomials by

$$E(S)E(-S) = P(S)P(-S) + F(S)F(-S). \quad (2.10)$$

The attenuation of the network is given by

$$\begin{aligned} A(\Omega) &= 10\log|H(j\Omega)|^2 \\ &= 10\log\left(1 + |K(j\Omega)|^2\right). \end{aligned} \quad (2.11)$$

Thus, when either $H(j\Omega)$ or $K(j\Omega)$ is infinite, the attenuation is infinite. However, only when $K(j\Omega)$ is zero is there an attenuation zero. The characteristic function is thus the more useful, because it eliminates the unity constant and focuses attention on the attenuation

zeros (reflection zeros) and attenuation poles (transmission zeros).

2.1.2 Reflection and Transmission Coefficients

In transmission-line theory transfer function $t(S)$ is also called transmission coefficient and defined as

$$t(S) = \frac{\text{transmitted wave}}{\text{incident wave}} \quad (2.12)$$

and the reflection coefficient ρ is defined as

$$\rho(s) = \pm \frac{\text{reflected wave}}{\text{incident wave}}. \quad (2.13)$$

The sign of ρ is positive when the ratio is defined in terms of voltages and negative when defined in terms of currents [16].

Since the reflected power plus the transmitted power must equal to the available power, we obtain

$$|\rho(S)|^2 + |t(S)|^2 = 1. \quad (2.14)$$

From (2.10) and (2.14), the reflection coefficient can be expressed by the polynomials as

$$\rho(S) = \frac{F(S)}{E(S)}. \quad (2.15)$$

In terms of decibels, the transmission loss (often termed the attenuation) and reflection loss (often termed the return loss) are defined as

$$\begin{aligned} A &= 10 \log \frac{1}{|t(j\Omega)|^2} = -10 \log |t(j\Omega)|^2 \text{ dB} \\ R &= 10 \log \frac{1}{|\rho(j\Omega)|^2} = -10 \log |\rho(j\Omega)|^2 \text{ dB}. \end{aligned} \quad (2.16)$$

From (2.14), the relationship between the transmission and return loss can be established by

$$\begin{aligned} A &= -10\log\left(1 - 10^{-R/10}\right) \text{ dB} \\ R &= -10\log\left(1 - 10^{-A/10}\right) \text{ dB.} \end{aligned} \tag{2.17}$$

It should be noted that the reflection and transmission coefficients are synonymous with S_{11} and S_{21} , respectively, in terms of scattering parameters.

2.1.3 Characteristics of Polynomials

In filter synthesis, we establish the polynomials $P(S)$ and $F(S)$ from their roots and their roots are determined based on the specifications of the filter. The polynomial $E(S)$ can be obtained by (2.10). For the general case, that includes the realization of symmetric and asymmetric N th-order lowpass prototype filters, the polynomials have the certain properties.

The roots of $F(S)$ lie on the imaginary axis of where the degree is N . The roots represent frequencies at which no power is reflected, often termed reflection zeros. At this frequencies, the filter loss is zero.

The roots of $P(S)$ lie on the imaginary axis. Such roots represent frequencies at which no power is transmitted, and the filter loss is infinite. These frequencies are referred to as transmission zeros or attenuation poles. Its roots can also appear as pairs located symmetrically with respect to the imaginary axis. Such roots lead to linear phase filters. The roots' degree is less than or equal to N .

$E(S)$ is a Hurwitz polynomial of degree N . All its roots lie in the left half-plane of S .

2.1.4 Normalization of the Polynomials

The input/output transfer function $H(S)$ is defined in terms of the characteristic function $K(S)$ in (2.7) as

$$|H(S)|^2 = 1 + |K(S)|^2. \quad (2.18)$$

Without loss of generality, we can introduce an arbitrary constant factor ϵ and restate the relationship as

$$|H(S)|^2 = 1 + \epsilon^2 |K(S)|^2 \quad (2.19)$$

where ϵ is the ripple factor. It is employed to normalize the maximum attenuation of the filter in the passband.

In the filter synthesis procedure, polynomials $F(S)$ and $P(S)$ are normalized so that their highest coefficients are unity. This is accomplished by extracting the highest coefficients of these polynomials and representing their ratio as a constant factor that can be readily absorbed within the ripple factor. Thus, the ripple factor ϵ is used to normalize $F(S)$ and $P(S)$, as well as the prototype amplitude response given by equation (2.19).

From (2.19), the transmitted power can be expressed by

$$\begin{aligned} |t(S)|^2 &= \frac{1}{1 + \epsilon^2 |K(S)|^2} \\ &= \frac{1}{\epsilon^2} \frac{|P(S)|^2}{|E(S)|^2} \end{aligned} \quad (2.20)$$

where

$$|E(S)|^2 = |F(S)|^2 + \frac{|P(S)|^2}{\epsilon^2}. \quad (2.21)$$

Hence, the transmission and reflection coefficients are given by

$$\begin{aligned}
t(S) &= \frac{1}{\varepsilon} \frac{P(S)}{E(S)} \\
\rho(S) &= \frac{F(S)}{E(S)}.
\end{aligned}
\tag{2.22}$$

The filter response depends on the choices of ε . For equi-ripple passbands, ε determines the magnitude of the ripple. For maximally flat passband or non-equi-ripple passband, ε is normally chosen with respect to the maximum permissible ripple. If the filter has the maximum ripple A_1 dB in the passband at Ω_1 , then

$$|t(j\Omega_1)|^2 = 10^{-A_1/10} = \frac{1}{1 + \varepsilon^2 |K(j\Omega_1)|^2}.
\tag{2.23}$$

Hence, the ripple constant is determined to be

$$\varepsilon = \sqrt{\frac{10^{A_1/10} - 1}{|K(j\Omega_1)|^2}}.
\tag{2.24}$$

The ripple constant can also be expressed by return loss as

$$\varepsilon = \sqrt{\frac{1}{10^{R_1/10} - 1} \frac{1}{|K(j\Omega_1)|^2}}
\tag{2.25}$$

where return loss R_1 corresponds to the maximum ripple A_1 . For normalized lowpass filter prototypes, Ω_1 is referred to as the cutoff frequency and is normally chosen to be unity.

2.1.5 Generalization of the Transmission and Reflection Coefficients

In previous sections, we dealt with polynomials of the N th-order filter which has finite-frequency transmission zeros less than N . In general, the N th-order filter can have at most N finite-frequency transmission zeros. In this case, the transmission and reflection coefficients are in the form

$$\begin{aligned}
t(S) &= \frac{1}{\epsilon} \frac{P(S)}{E(S)} \\
\rho(S) &= \frac{1}{\epsilon_R} \frac{F(S)}{E(S)}.
\end{aligned} \tag{2.26}$$

In (2.26), the polynomials $E(S)$, $F(S)$, and $P(S)$ are normalized so that their highest degree coefficients are unity as in the previous section.

From the conservation of the energy equation (2.14), the third polynomial can be derived from the two of the three polynomials as follows:

$$|E(S)|^2 = \frac{|F(S)|^2}{\epsilon_R^2} + \frac{|P(S)|^2}{\epsilon^2}. \tag{2.27}$$

Both $E(S)$ and $F(S)$ are N th degree polynomials and their highest degree coefficients are normalized to unity, whilst $P(S)$, which contains the finite-frequency transmission zeros, is of degree Z , where Z is the number of finite-frequency transmission zeros. For a realizable network, Z must be less than or equal to N .

Since $E(S)$ and $F(S)$ are N th degree polynomials whose highest degree coefficients are unity, ϵ_R must be unity for cases that $Z < N$. When $Z = N$, that is $P(S)$ is an N th degree polynomial, then the attenuation at $S = \pm j\infty$ is finite and (2.14) can be expressed as

$$\frac{1}{\epsilon_R^2} \frac{|F(\pm j\infty)|^2}{|E(\pm j\infty)|^2} + \frac{1}{\epsilon^2} \frac{|P(\pm j\infty)|^2}{|E(\pm j\infty)|^2} = 1. \tag{2.28}$$

For $Z = N$ (i.e. the fully canonical case), $E(S)$, $F(S)$, and $P(S)$ are all N th degree polynomials and their highest-degree coefficients are unity. Therefore, at $S = \pm j\infty$, we obtain

$$\frac{1}{\epsilon_R^2} + \frac{1}{\epsilon^2} = 1. \tag{2.29}$$

From (2.26) and (2.27), the transmitted power can be obtained in generalized form as

$$|t(S)|^2 = \frac{1}{1 + \frac{\epsilon^2 |F(S)|^2}{\epsilon_R^2 |P(S)|^2}} \quad (2.30)$$

and the ripple constant can also be expressed in generalized form as

$$\epsilon = \epsilon_R \sqrt{\frac{1}{10^{R_1/10} - 1} \frac{1}{|K(j\Omega_1)|^2}}. \quad (2.31)$$

The ripple factor ϵ_R can be found by substituting (2.31) to (2.29):

$$\epsilon_R = \sqrt{1 + (10^{R_1/10} - 1) |K(j\Omega_1)|^2}. \quad (2.32)$$

For $Z = N$, ϵ_R will have a value slightly greater than unity. If the attenuation at $S = \pm j\infty$ is very high, then the ripple factor ϵ_R will be almost unity. In this case, the transmitted power expression in (2.30) and the ripple factor expression in (2.31) is almost identical to (2.20) and (2.25), respectively.

2.2 Characteristic Functions and Frequency Responses

A filter is defined as a network which passes a certain portion of a frequency spectrum and blocks the remainder of the spectrum [17]. By the term "blocking," we imply that the magnitude response of the filter is approximately zero for that frequency range. Thus, an ideal lowpass filter is a network which passes all frequencies up to a cutoff frequency and blocks all frequencies above the cutoff frequency, as shown in Fig. 2.1.

Since the frequency response shown in Fig. 2.1 is not realizable, we approach the ideal characteristic as closely as desired. The problem of obtaining a realizable transfer function $t(j\Omega)$ is generally referred to as the approximation problem.

In this section, the approximation problem for obtaining the realizable transfer function is described. Basic forms of the characteristic functions and the resulting response shapes

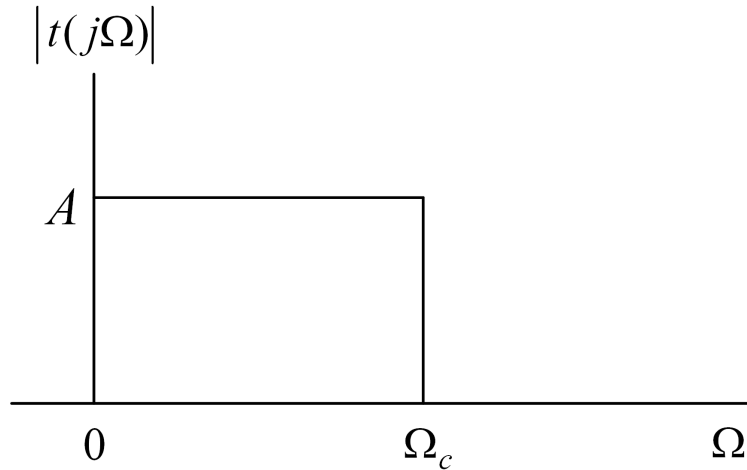


Figure 2.1: Ideal amplitude spectrum for lowpass filter.

for the normalized lowpass prototype filters are provided.

2.2.1 All-Pole Filters

The characteristic function for the all-pole filter is characterized by

$$K(S) = \frac{F(S)}{P(S)} \quad (2.33)$$

where $P(S) = 1$. Therefore, the transfer function is given by

$$t(S) = \frac{1}{E(S)}. \quad (2.34)$$

There are no transmission zeros at finite frequencies. All transmission zeros are located at infinity. The frequency response of the filter is determined by the polynomial $F(S)$.

The roots of the polynomial $F(S)$ are the reflection zeros and if these roots are all located at the origin then this frequency response is characterized by a maximally-flat response. This response is also known as the Butterworth response. For the N th-order Butterworth response filter, the characteristic function is given by

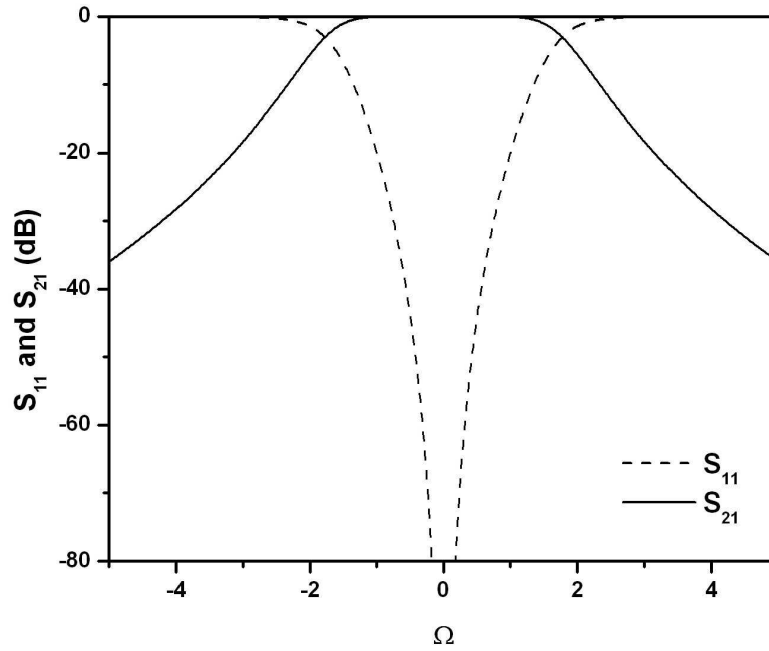


Figure 2.2: Lowpass response of the 4th-order Butterworth filter.

$$\begin{aligned}
 K(S) &= F(S) \\
 &= S^N
 \end{aligned}
 \tag{2.35}$$

and the transmitted power is given by

$$|t(S)|^2 = \frac{1}{1 + \epsilon^2 S^N}.
 \tag{2.36}$$

The ripple factor ϵ defines the maximum amplitude variation over the passband. For example, the choice of ϵ as unity implies that the half of the power is transmitted at the cutoff frequency $\Omega_c = 1$. The amplitude response of a 4th-order maximally-flat filter with $\epsilon = 0.1005$ is shown in Fig. 2.2. This ripple constant corresponds to 20 dB return loss at $\Omega = \pm 1$.

The roots of the polynomial $F(S)$ can be located at finite frequencies and the characteristic function is given by

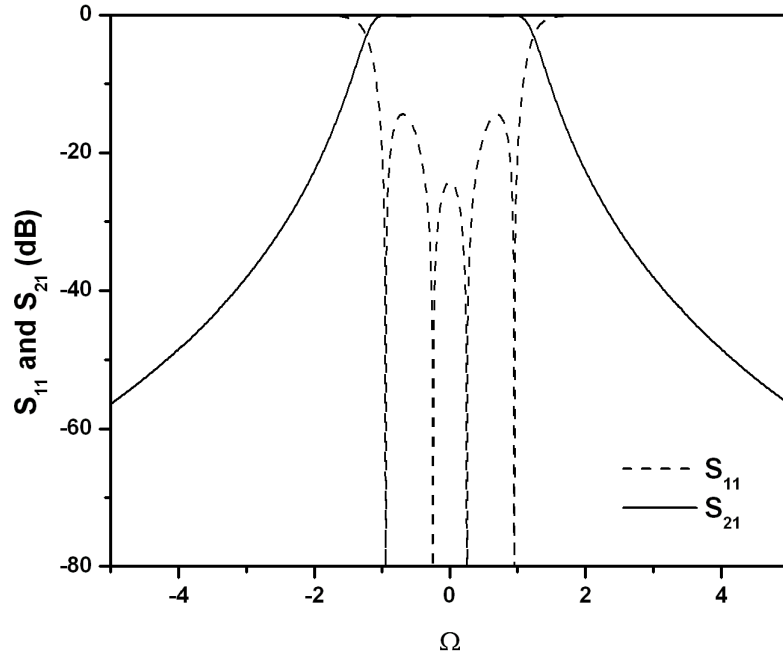


Figure 2.3: Lowpass response of the 4th-order all-pole filter with an arbitrary distribution of reflection zeros.

$$\begin{aligned}
 K(S) &= F(S) \\
 &= (S - S_{f1})(S - S_{f2}) \cdots (S - S_{fN})
 \end{aligned}
 \tag{2.37}$$

where S_{fi} 's lie on imaginary axis. Fig. 2.3 shows lowpass amplitude response of 4th-order all-pole filter with arbitrarily distributed reflection zeros. The reflection zeros are $S_f = \pm j0.95$ and $S_f = \pm j0.25$. The ripple constant $\epsilon = 1.09953$ makes the filter have return loss of 20 dB at $\Omega = \pm 1$.

If the roots are located in such a way that the frequency response in the passband is the equi-ripple response, then this response is generally known as Chebyshev response. Fig. 2.4 shows lowpass amplitude response of 4th-order Chebyshev filter with 20 dB equi-ripple return loss. The reflection zeros for Chebyshev response (equi-ripple response) can be chosen via the Chebyshev polynomial [16]. The reflection zeros in Fig. 2.4 are $S_f = \pm j0.9239, \pm j0.3827$ and the ripple constant is $\epsilon = 0.80425$.

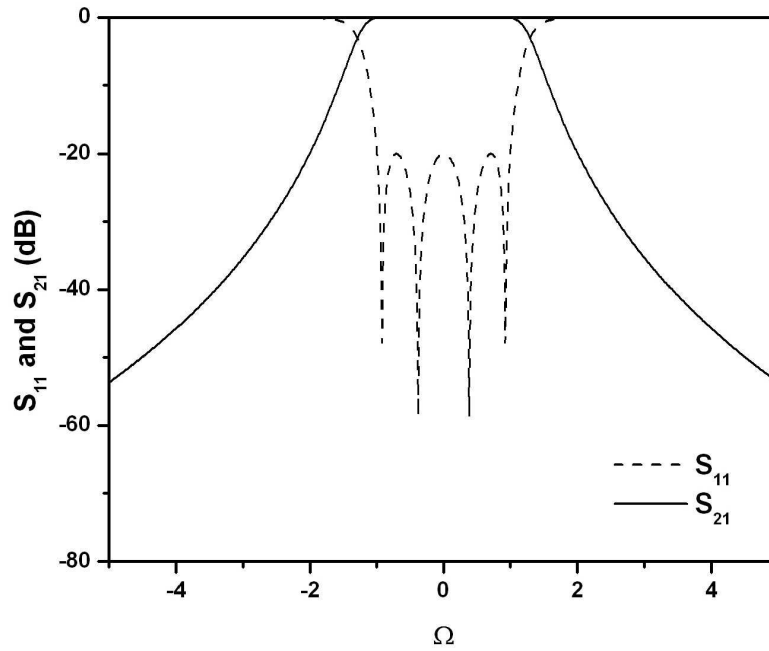


Figure 2.4: Lowpass response of the 4th-order Chebyshev response filter with 20 db equi-ripple return loss.

2.2.2 Filters with Transmission Zeros

The characteristic function for the filters with transmission zeros is given by

$$\begin{aligned}
 K(S) &= \frac{F(S)}{P(S)} \\
 &= \frac{(S - S_{f1})(S - S_{f2}) \cdots (S - S_{fN})}{(S - S_{p1})(S - S_{p2}) \cdots (S - S_{pT})}
 \end{aligned} \tag{2.38}$$

where T represents the number of finite-frequency transmission zeros and must be equal to or less than N . S_{fi} 's and S_{pi} 's lie on imaginary axis. Based on the location of roots of $F(S)$ and $P(S)$, the filter can have equi-ripple response in the passband or the stopband or in both of them. The filter response which is equi-ripple in both passband and stopband is called elliptic function response. The characteristic function $K(S)$ for elliptic function response is expressed in terms of Jacobian elliptic function. However, in general, filters are designed to have non-equi-ripple response in stopband for good near-band rejection characteristic

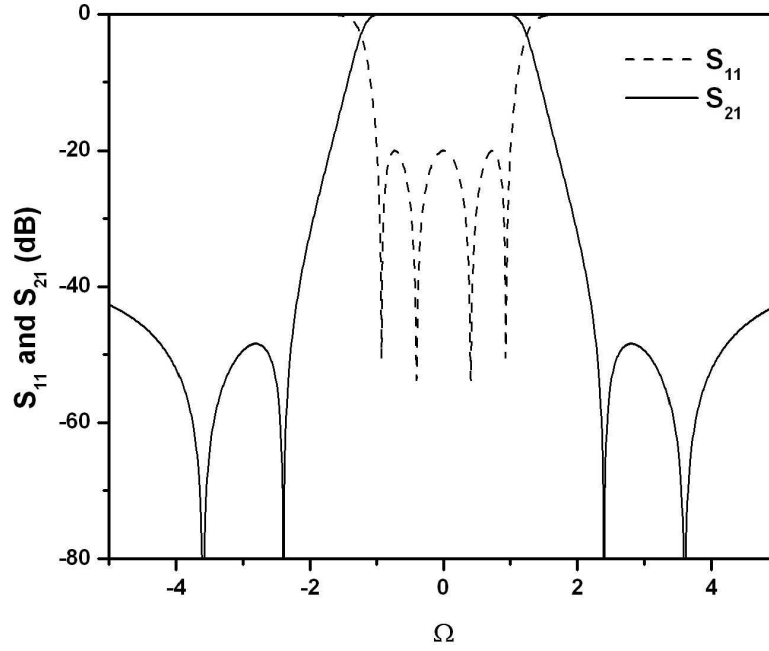


Figure 2.5: Lowpass response of the 4th-order filter with 20 dB equi-ripple return loss within the passband and transmission zeros at $S_p = \pm j2.4$ and $\pm j3.6$.

while the passband response is equi-ripple. Fig. 2.5 shows a frequency response of 4th-order filter with transmission zeros at $S_p = \pm j2.4$ and $\pm j3.6$. The reflection zeros for equi-ripple response in the passband can be found via the characteristic function $K(S)$ [18]:

$$K(j\Omega) = \cosh \left(\sum_{i=1}^N \cosh^{-1} \left(\frac{\Omega - 1/\Omega_i}{1 - \Omega/\Omega_i} \right) \right) \quad (2.39)$$

where Ω_i is the location of the i th transmission zero. The reflection zeros can be easily obtained from computing the reflection coefficient of the filter.

The filter with transmission zeros has higher selectivity near the passband than the all-pole filter. However, the all-pole filter has better wideband selectivity. Fig. 2.6 compares transmission coefficients shown in Fig. 2.2, Fig. 2.4, and Fig. 2.5. All filters have return loss of 20 dB at $\Omega = \pm 1$.

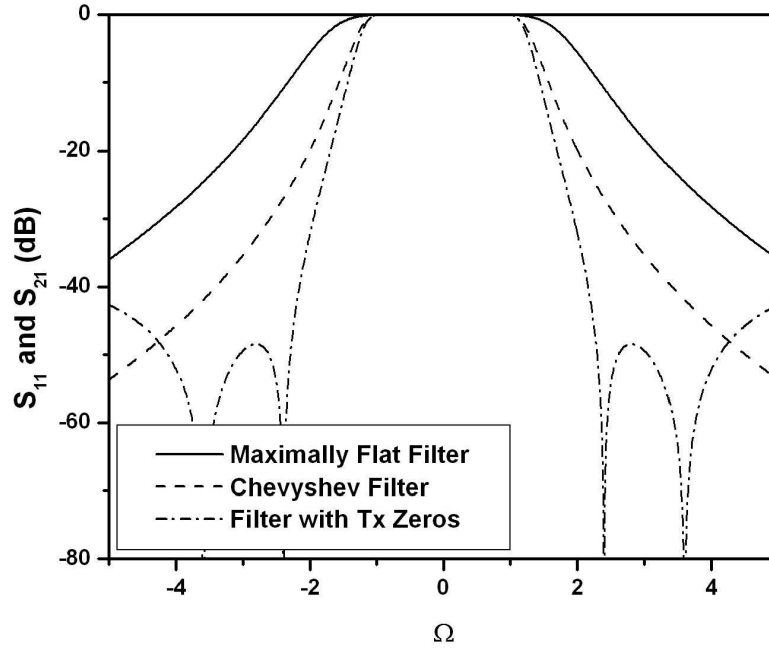


Figure 2.6: Lowpass responses of the 4th-order filters in Fig 2.2, Fig. 2.4, and Fig. 2.5.

2.2.3 Linear Phase Filters

The characteristic function for the linear phase filters is given by

$$\begin{aligned}
 K(S) &= \frac{F(S)}{P(S)} \\
 &= \frac{(S - S_{f1})(S - S_{f2}) \cdots (S - S_{fN})}{(S - S_{p1})(S - S_{p2}) \cdots (S - S_{pT})}
 \end{aligned} \tag{2.40}$$

where the roots of $P(S)$ should locate symmetrically with respect to the imaginary axis. For example, if S_{p1} is $\sigma_{n1} + j\Omega_1$, then the one of the roots of $P(S)$ should be $-\sigma_{n1} + j\Omega_1$. The passband of linear phase filters could be maximally flat, equi-ripple, or non-equi-ripple.

2.2.4 Linear Phase Filters with Transmission Zeros

The characteristic function for the linear phase filters with transmission zeros is similar to (2.40) except that the polynomial $P(S)$ has the roots which lie on the imaginary axis

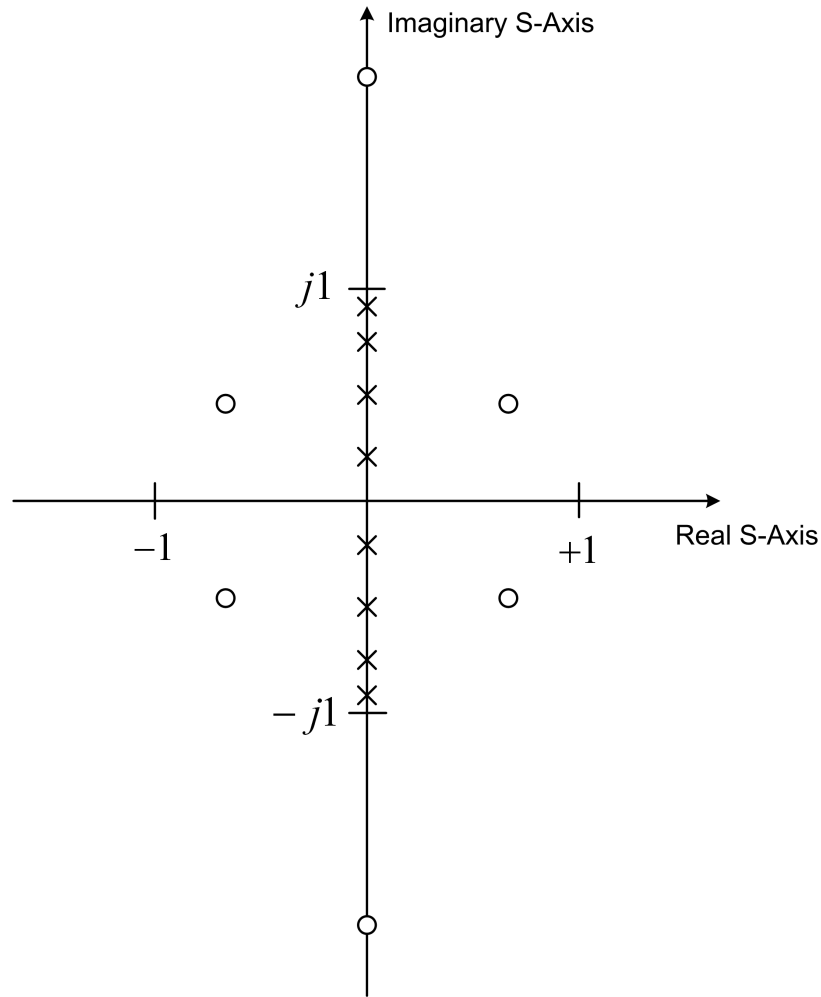
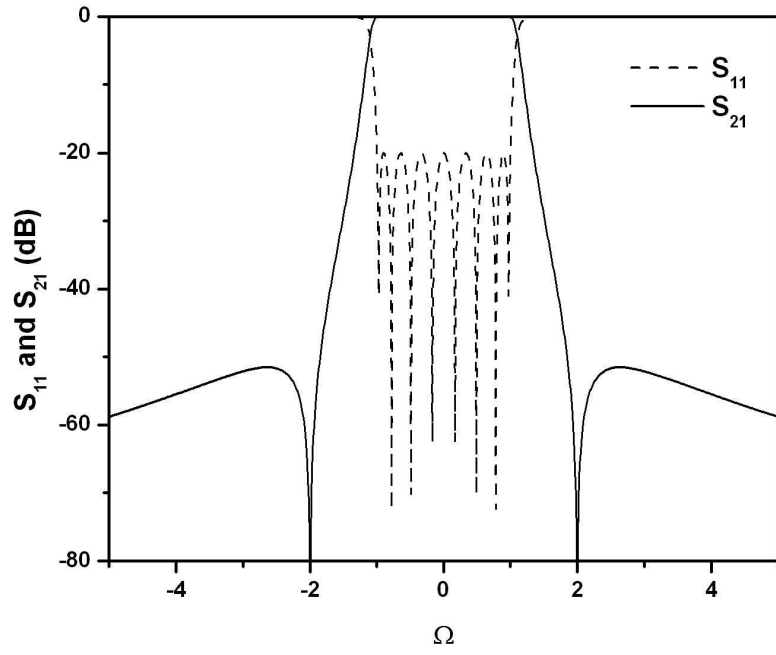
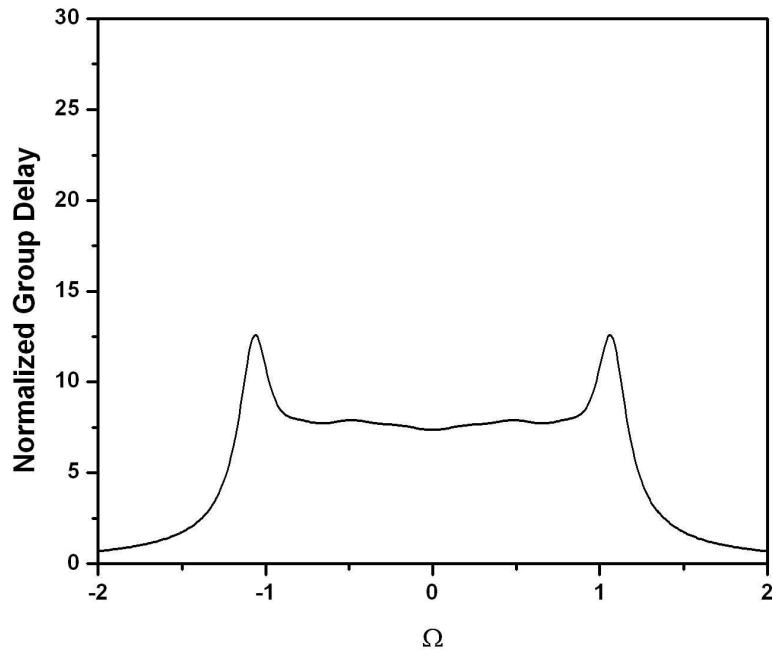


Figure 2.7: Position of roots of $P(S)$ and $F(S)$ for the example of the linear phase filter with transmission zero. \times and \circ indicates the roots of $F(S)$ and $P(S)$, respectively. The roots of $F(S)$ are $S_f = \pm j0.9731, \pm j0.7802, \pm j0.4903, \text{ and } \pm j0.1692$. The roots of $P(S)$ are $S_p = \pm j2.00$ and $\pm 0.60 \pm j0.45$

and the ones which locate symmetrically with respect to the imaginary axis. The roots on the imaginary axis are for transmission zeros at finite frequencies and pairs of roots which locate symmetrically with respect to the imaginary axis are for linear phase in the passband. Fig. 2.7 shows the position of the roots of $F(S)$ (S_f) and roots of $P(S)$ (S_p) for the example of the linear phase filter with transmission zero. A pair of roots of $P(S)$ lies on the imaginary axis and complex roots of $P(S)$ lies in quadruplets in the S -plane. Fig. 2.8 shows the amplitude and group delay response of the filter. It is of note that the group delay is equalized in the passband due to the complex roots of $P(S)$. The group delay of



(a)



(b)

Figure 2.8: Linear phase filter with transmission zeros. (a) the amplitude response, (b) the group delay response.

the lowpass filter is given by

$$T(\Omega) = -\frac{d\phi(\Omega)}{d\Omega} \quad (2.41)$$

where ϕ is the phase of the $t(\Omega)$ in radians. The frequency response of a bandpass filter is given by the conventional frequency transformation

$$\Omega = \frac{1}{B} \left(\frac{f}{f_0} - \frac{f_0}{f} \right) \quad (2.42)$$

where f_0 is the center frequency and B is the fractional bandwidth. The group delay response of the bandpass filter is then computed with

$$\tau(f) = \frac{T(\Omega)}{2\pi B f_0} \left[1 + \left(\frac{f_0}{f} \right)^2 \right]. \quad (2.43)$$

2.3 Coupling Matrix

2.3.1 Circuit Model

In the early 1970s, Williams and Atia [10][19] introduced the concept of the coupling matrix as applied to dual-mode narrow-band waveguide filters. The coupling matrix was extracted from the voltage-current relationship of the equivalent circuit model. The equivalent circuit model they developed was a narrow-band bandpass prototype shown in Fig. 2.9. The circuit is driven by a source of open-circuit voltage e_S with resistance R_S and terminated by the load R_L . The circuit model is composed of lumped-element series resonators which are coupled by transformers. i depicts the current flowing in each series resonator. Self inductance and capacitance of each resonator are 1 H and 1 F. This results in a center frequency of 1 rad/s and the couplings are normalized for a bandwidth of 1 rad/s [20]. Each loop is coupled to every other loop through mutual couplings and these couplings are assumed to be frequency-independent due to the narrow-band approximation. A

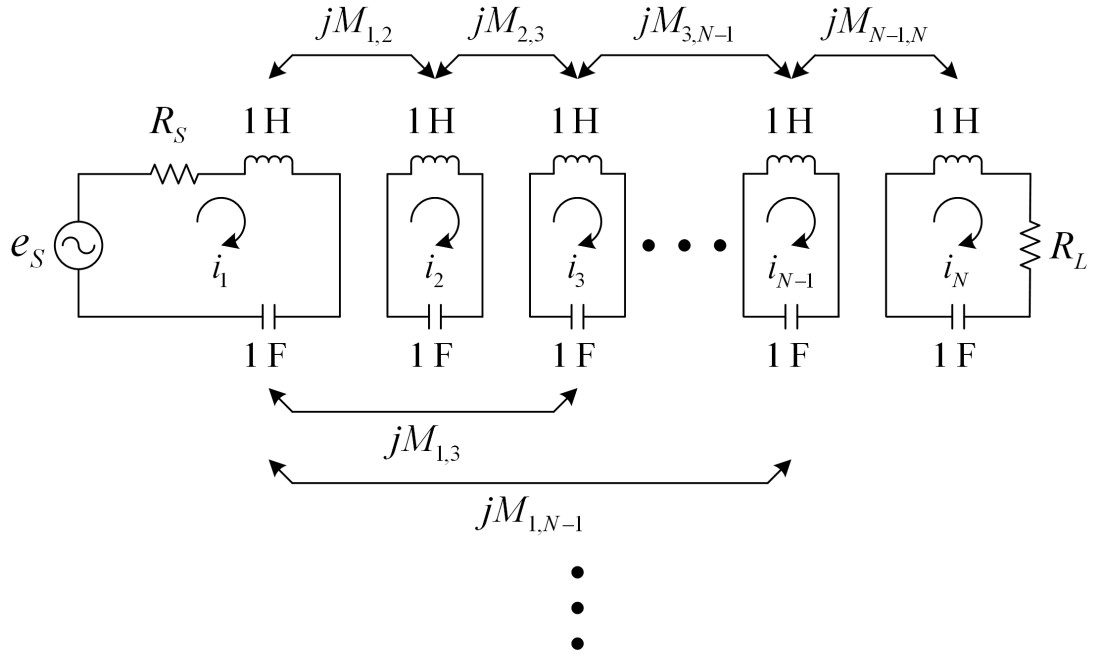


Figure 2.9: A bandpass circuit prototype for an N th-order filter.

voltage-current relationship for each loop in the circuit prototype shown in Fig. 2.9 can be combined into the matrix form which is convenient to manipulate as follows:

$$\begin{bmatrix} e_S \\ 0 \\ \vdots \\ 0 \\ 0 \end{bmatrix} = \begin{bmatrix} R_S + j\left(\omega - \frac{1}{\omega}\right) & jM_{1,2} & \cdots & jM_{1,N-1} & jM_{1,N} \\ jM_{2,1} & j\left(\omega - \frac{1}{\omega}\right) & \cdots & jM_{2,N-1} & jM_{2,N} \\ \vdots & \vdots & \ddots & \vdots & \vdots \\ jM_{N-1,1} & jM_{N-1,2} & \cdots & j\left(\omega - \frac{1}{\omega}\right) & jM_{N-1,N} \\ jM_{N,1} & jM_{N,2} & \cdots & jM_{N,N-1} & R_L + j\left(\omega - \frac{1}{\omega}\right) \end{bmatrix} \begin{bmatrix} i_1 \\ i_2 \\ \vdots \\ i_{N-1} \\ i_N \end{bmatrix} \quad (2.44)$$

The voltage-current relationship in (2.44) is usually written in simplified form:

$$\begin{aligned} \mathbf{E} &= \mathbf{A}\mathbf{I} \\ &= \left(j\left(\omega - \frac{1}{\omega}\right)\mathbf{U} + \mathbf{R} + j\mathbf{M} \right) \mathbf{I}, \end{aligned} \quad (2.45)$$

where \mathbf{E} is the matrix in left-hand side of (2.44) and \mathbf{U} is the identity matrix. \mathbf{I} , \mathbf{R} , and \mathbf{M} are

$$\mathbf{I} = \begin{bmatrix} i_1 \\ i_2 \\ \vdots \\ i_{N-1} \\ i_N \end{bmatrix} \quad (2.46)$$

$$\mathbf{R} = \begin{bmatrix} R_S & 0 & \cdots & 0 & 0 \\ 0 & 0 & \cdots & 0 & 0 \\ \vdots & \vdots & \ddots & \vdots & \vdots \\ 0 & 0 & \cdots & 0 & 0 \\ 0 & 0 & \cdots & 0 & R_L \end{bmatrix} \quad (2.47)$$

$$\mathbf{M} = \begin{bmatrix} 0 & M_{1,2} & \cdots & M_{1,N-1} & M_{1,N} \\ M_{2,1} & 0 & \cdots & M_{2,N-1} & M_{2,N} \\ \vdots & \vdots & \ddots & \vdots & \vdots \\ M_{N-1,1} & M_{N-1,2} & \cdots & 0 & M_{N-1,N} \\ M_{N,1} & M_{N,2} & \cdots & M_{N,N-1} & 0 \end{bmatrix}. \quad (2.48)$$

Here, the matrix \mathbf{M} is called the coupling matrix. Since all series resonators have the same resonant frequency, the filter of the equivalent circuit model is synchronously tuned circuit. For asynchronously tuned filter, we modify the bandpass prototype by including hypothetical frequency-invariant reactive elements in each series resonator as shown in Fig. 2.10. These frequency-invariant reactive elements make resonators have different resonant frequencies. In this case, the coupling matrix is given by

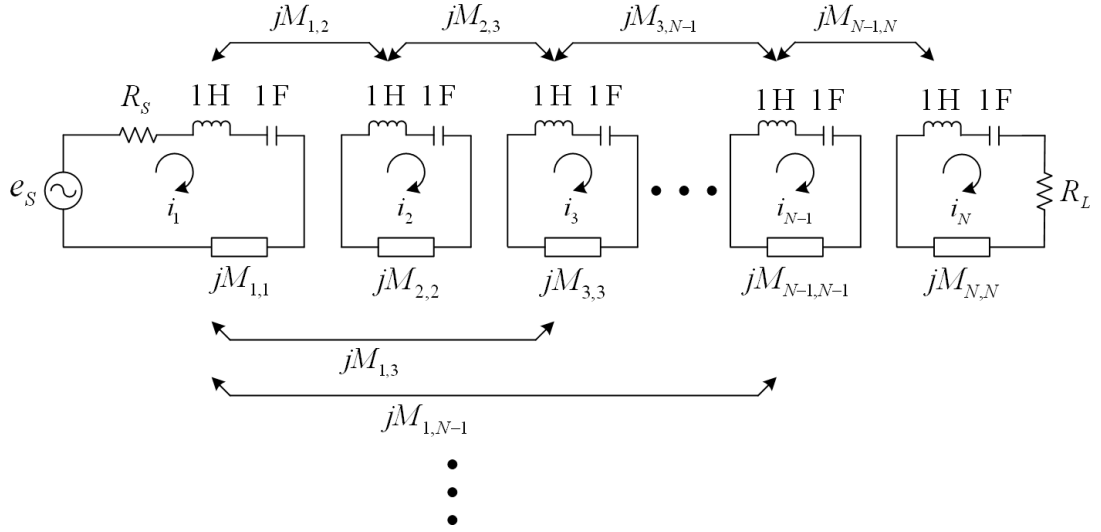


Figure 2.10: A bandpass circuit prototype for an N th-order filter.

$$\mathbf{M} = \begin{bmatrix} M_{1,1} & M_{1,2} & \cdots & M_{1,N-1} & M_{1,N} \\ M_{2,1} & M_{2,2} & \cdots & M_{2,N-1} & M_{2,N} \\ \vdots & \vdots & \ddots & \vdots & \vdots \\ M_{N-1,1} & M_{N-1,2} & \cdots & M_{N-1,N-1} & M_{N-1,N} \\ M_{N,1} & M_{N,2} & \cdots & M_{N,N-1} & M_{N,N} \end{bmatrix}. \quad (2.49)$$

The goal of synthesizing microwave resonator filters is obtaining this coupling matrix along with R_S and R_L with given lowpass transfer function. Therefore voltage-current relationship for bandpass prototype needs to be expressed by lowpass terminology. The lowpass-to-bandpass transformation is give by

$$\Omega = \frac{\omega_0}{\Delta\omega} \left(\frac{\omega}{\omega_0} - \frac{\omega_0}{\omega} \right) \quad (2.50)$$

where ω_0 and $\Delta\omega$ are the center frequency and the bandwidth in rad/s of the bandpass filter, respectively. Since the bandpass topology in Fig. 2.10 has the center frequency of 1 rad/s and bandwidth of 1 rad/s, the voltage-current relationship for the bandpass topology given in (2.45) can be expressed by lowpass terminology as follows:

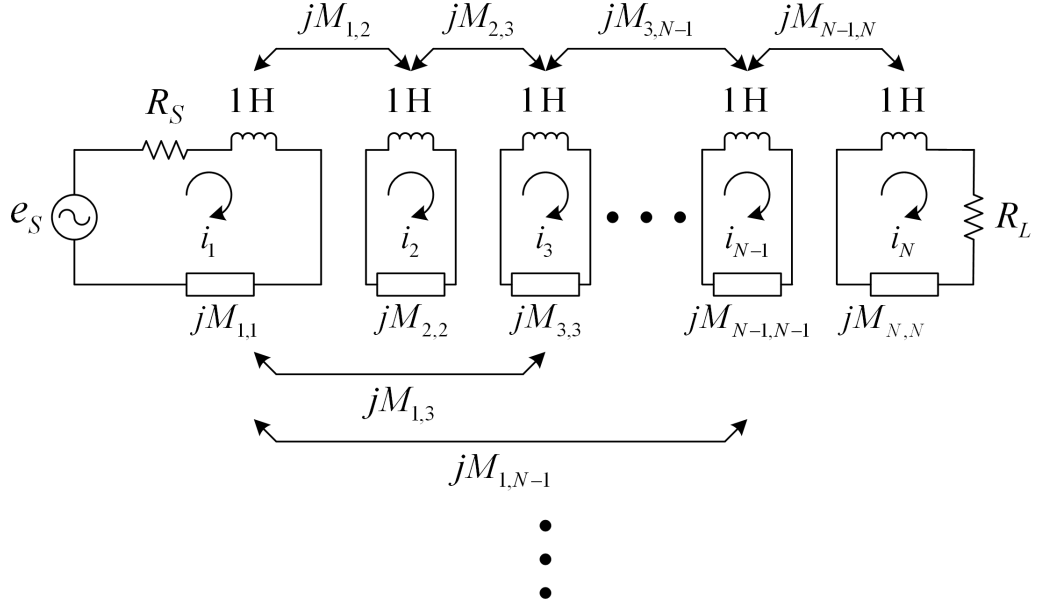


Figure 2.11: A lowpass circuit prototype for an N th-order filter.

$$\begin{aligned}
 \mathbf{E} &= \mathbf{A}\mathbf{I} \\
 &= (j\Omega\mathbf{U} + \mathbf{R} + j\mathbf{M})\mathbf{I} \\
 &= (S\mathbf{U} + \mathbf{R} + j\mathbf{M})\mathbf{I}.
 \end{aligned} \tag{2.51}$$

Similarly, the bandpass prototype can be transformed to the lowpass prototype by replacing the series resonators by inductors as shown in Fig. 2.11 [21]. It is obvious that the voltage-current relationship of the lowpass prototype in Fig. 2.11 results in (2.51).

The $N \times N$ matrix in (2.49) contains the values of the mutual couplings between the nodes of the network [20]. If the coupling between sequentially numbered nodes, it is referred to as a direct coupling. The entries on the main diagonal, $M_{i,i}$ are the self-coupling, whereas all the other couplings between the nonsequentially numbered nodes are known as cross couplings. As mentioned earlier, the self-couplings account for differences in the resonant frequencies of the different resonators. Because of the reciprocity of the passive network, $M_{i,j} = M_{j,i}$.

The diagonal matrix SU contains the frequency-variable portion of the impedance in each loop, giving rise to an $N \times N$ matrix with all entries at zero except for the the diagonal filled with $S = j\Omega$ as follows:

$$SU = \begin{bmatrix} S & 0 & \cdots & 0 & 0 \\ 0 & S & \cdots & 0 & 0 \\ \vdots & \vdots & \ddots & \vdots & \vdots \\ 0 & 0 & \cdots & S & 0 \\ 0 & 0 & \cdots & 0 & S \end{bmatrix}. \quad (2.52)$$

For bandpass filters, the effect of the unloaded quality factor Q_u of the resonator can be taken into account by offsetting S by a positive real factor δ , where $\delta = f_0/(BW \cdot Q_u)$, f_0 is the center frequency, and BW is design bandwidth.

2.3.2 Scattering Parameter

The lowpass circuit prototype in Fig. 2.11 operates between a voltage source generating e_S volts and an internal impedance of R_S ohms and a load impedance of R_L ohms. The overall circuit including the source and load terminations can be represented by the impedance matrix \mathbf{A} as shown in Fig. 2.12. This impedance matrix can also be split into the matrix's purely resistive and purely reactive parts by

$$\mathbf{A} = \mathbf{R} + j\mathbf{M} + SU = \mathbf{R} + \mathbf{Z}. \quad (2.53)$$

Now, the impedance matrix \mathbf{Z} represents a purely reactive network operating between a voltage source with internal impedance R_S and a load R_L .

From (2.45), the current in each loop can be found by

$$\mathbf{I} = \mathbf{A}^{-1}\mathbf{E} \quad (2.54)$$

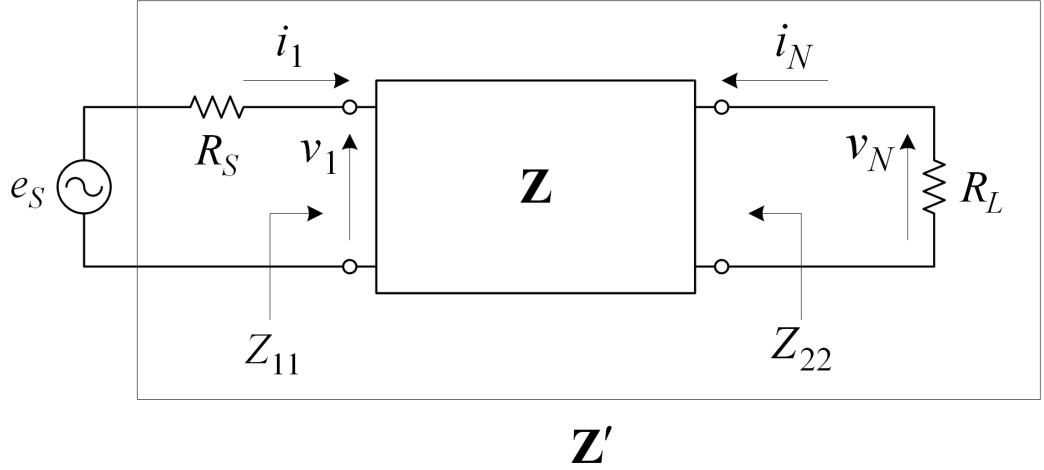


Figure 2.12: A circuit network for an N th-order filter. Impedance matrix \mathbf{A} represents overall circuit including the source and load termination. Impedance matrix \mathbf{Z} represents a purely reactive network operating between a voltage source with internal impedance and a load.

where \mathbf{A} is the network open-circuit impedance matrix with the source and load impedances included. The inverse of the square matrix \mathbf{A} is given by

$$\mathbf{A}^{-1} = \frac{adj(\mathbf{A})}{|\mathbf{A}|} \quad (2.55)$$

where $|\mathbf{A}|$ is the determinant of the square matrix \mathbf{A} and $adj(\mathbf{A})$ is the adjoint of the matrix \mathbf{A} . The adjoint of the matrix is the transpose of the matrix whose (i,j) entry is the cofactor $a_{i,j}$ which is the determinant of the $(N-1) \times (N-1)$ matrix obtained from \mathbf{A} by removing the row number i and the column number j multiplied by $(-1)^{i+j}$. Especially it is necessary to find the current in the first and last loop and they are

$$\begin{aligned} i_1 &= \mathbf{A}_{1,1}^{-1} \mathbf{E} \\ i_N &= \mathbf{A}_{N,1}^{-1} \mathbf{E} = \frac{v_N}{R_L}. \end{aligned} \quad (2.56)$$

The transmission coefficient S_{21} can be found by substituting (2.56) into the definition [22]:

$$\begin{aligned}
S_{21} &= 2\sqrt{\frac{R_S}{R_L}} \cdot \frac{v_N}{e_S} \\
&= 2\sqrt{\frac{R_S}{R_L}} \cdot R_L \mathbf{A}_{N,1}^{-1} \\
&= 2\sqrt{R_S R_L} \cdot \mathbf{A}_{N,1}^{-1}.
\end{aligned} \tag{2.57}$$

The reflection coefficient at the input port S_{11} is given by

$$\begin{aligned}
S_{11} &= \frac{Z_{11} - R_S}{Z_{11} + R_S} \\
&= \frac{Z_{11} + R_S - 2R_S}{Z_{11} + R_S} \\
&= 1 - \frac{2R_S}{Z_{11} + R_S}
\end{aligned} \tag{2.58}$$

where $Z_{11} = v_1/i_1$ is the impedance looking in at the input port. The potential divider at the input port gives v_1 and (2.56) yields i_1 . Therefore, Z_{11} is expressed as

$$Z_{11} = \frac{v_1}{i_1} = \frac{e_S Z_{11}}{Z_{11} + R_S} \cdot \frac{1}{e_S \mathbf{A}_{1,1}^{-1}} \tag{2.59}$$

which results in

$$\frac{1}{Z_{11} + R_S} = \mathbf{A}_{1,1}^{-1}. \tag{2.60}$$

We can find the reflection coefficient at input port by substituting (2.60) into (2.58):

$$S_{11} = 1 - 2R_S \mathbf{A}_{1,1}^{-1}. \tag{2.61}$$

Similarly, the reflection coefficient at output port is given by

$$S_{22} = 1 - 2R_L \mathbf{A}_{N,N}^{-1}. \tag{2.62}$$

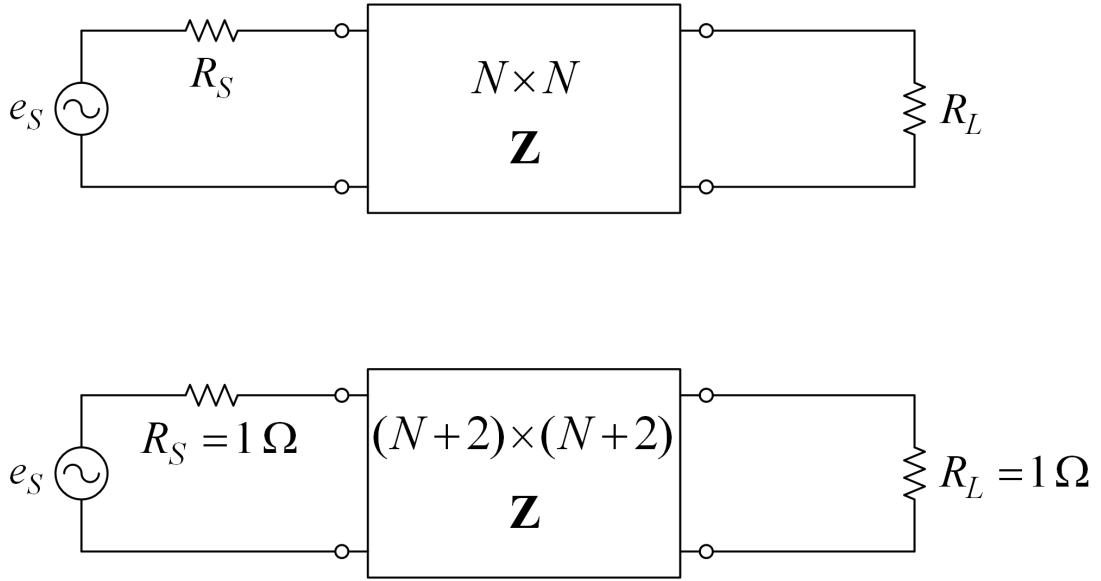


Figure 2.13: A circuit network representation for an N th order filter (a) using the $N \times N$ matrix (b) using the $(N+2) \times (N+2)$ matrix.

Filter synthesis is determining the coupling matrix, R_S , and R_L so that the S parameters given by (2.57) and (2.61) reproduce the predetermined insertion loss and return loss. It can be performed either by using analytic methods or optimization methods. In analytic methods, filter is synthesized by equating the coefficients of polynomials of $t(S)$ with those of (2.57). This process can also be executed by using optimization method [23].

2.3.3 $(N+2) \times (N+2)$ Coupling Matrix

Typically, the source and load terminations are nonzero, and can be normalized to unity impedance by insertion of impedance inverters $M_{S,1}$ and $M_{N,L}$ of impedance values $\sqrt{R_S}$ and $\sqrt{R_L}$, respectively, on the source and load side of the network. These inverters can be absorbed in $N \times N$ matrix creating $(N+2) \times (N+2)$ matrix (see Fig. 2.13):

$$\mathbf{M} = \begin{bmatrix} 0 & M_{S,1} & 0 & \cdots & 0 & 0 & 0 \\ M_{S,1} & M_{1,1} & M_{1,2} & \cdots & M_{1,N-1} & M_{1,N} & 0 \\ 0 & M_{1,2} & M_{2,2} & \cdots & M_{2,N-1} & M_{2,N} & 0 \\ \vdots & \vdots & \ddots & \vdots & \vdots & & \\ 0 & M_{1,N-1} & M_{2,N-1} & \cdots & M_{N-1,N-1} & M_{N-1,N} & 0 \\ 0 & M_{1,N} & M_{2,N} & \cdots & M_{N-1,N} & M_{N,N} & M_{N,L} \\ 0 & 0 & 0 & \cdots & 0 & M_{N,L} & 0 \end{bmatrix} \quad (2.63)$$

where $M_{S,1} = \sqrt{R_S}$ and $M_{N,L} = \sqrt{R_L}$. In addition to the couplings $M_{S,1}$ and $M_{N,L}$, it is possible to include other couplings between the source and/or load terminations, and the internal nodes within the core $N \times N$ matrix. Also, it is possible to accommodate the direct source-load coupling $M_{S,L}$ in order to realize fully canonical filter functions. The full $(N+2) \times (N+2)$ coupling matrix is

$$\mathbf{M} = \begin{bmatrix} 0 & M_{S,1} & M_{S,2} & \cdots & M_{S,N-1} & M_{S,N} & M_{S,L} \\ M_{S,1} & M_{1,1} & M_{1,2} & \cdots & M_{1,N-1} & M_{1,N} & M_{1,L} \\ M_{S,2} & M_{1,2} & M_{2,2} & \cdots & M_{2,N-1} & M_{2,N} & M_{2,L} \\ \vdots & \vdots & \ddots & \vdots & \vdots & & \\ M_{S,N-1} & M_{1,N-1} & M_{2,N-1} & \cdots & M_{N-1,N-1} & M_{N-1,N} & M_{N-1,L} \\ M_{S,N} & M_{1,N} & M_{2,N} & \cdots & M_{N-1,N} & M_{N,N} & M_{N,L} \\ M_{S,L} & M_{1,L} & M_{2,L} & \cdots & M_{N-1,L} & M_{N,L} & 0 \end{bmatrix}. \quad (2.64)$$

Fully canonical filtering functions (i.e., N th-degree characteristics with N finite-frequency transmission zeros) can be synthesized by using the $(N+2) \times (N+2)$ coupling matrix.

For the $(N+2) \times (N+2)$ coupling matrix, the voltage-current relationship is expressed as

$$\begin{aligned}\mathbf{E} &= \mathbf{A}\mathbf{I} \\ &= (\mathbf{R} + j\Omega\mathbf{W} + j\mathbf{M})\mathbf{I},\end{aligned}\tag{2.65}$$

where $\mathbf{E} = [e_S, 0, 0, \dots, 0]^t$, \mathbf{R} is a $(N+2) \times (N+2)$ matrix whose only nonzero entries are $R_{1,1} = R_{N+2,N+2} = 1$, \mathbf{W} is similar to the $(N+2) \times (N+2)$ identity matrix, except that $W_{1,1} = W_{N+2,N+2} = 0$, and $\mathbf{I} = [i_S, i_1, i_2, \dots, i_L]^t$. In this case the transmission and reflection coefficients are given by

$$S_{21} = 2 \cdot \mathbf{A}_{N+2,1}^{-1}\tag{2.66}$$

and

$$S_{11} = 1 - 2 \cdot \mathbf{A}_{1,1}^{-1}.\tag{2.67}$$

2.3.4 Coupling-Routing Diagram

Model of the circuit prototypes describes the coupling mechanism of the cross-coupled filters and from which the coupling matrix has been extracted. However, using the mode of the circuit prototype, it is not comfortable to observe which couplings between resonators exist and which do not. Hence, the coupling-routing diagram is employed which provides convenient insight into the coupling structure of the filter.

Fig. 2.14 shows the coupling-routing diagram of a 8th-order canonical structure filter. It can be easily seen that there are direct couplings between consecutively-numbered resonators and the cross couplings between nonconsecutively-numbered resonators. Fig. 2.15 shows the coupling-routing diagrams of one of 6th-order and 8th-order inline structure filters. These structures are also called cascaded-triplet structure and cascaded-quadruplet structure, respectively.

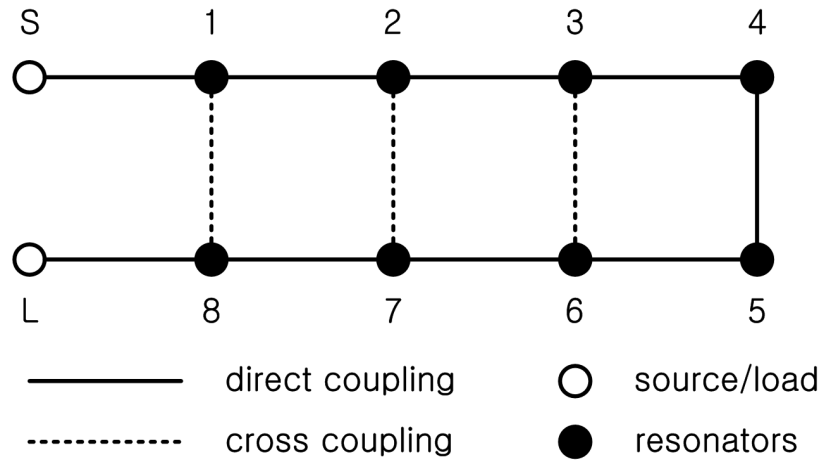


Figure 2.14: The coupling-routing diagram of a 8th-order canonical structure filter.

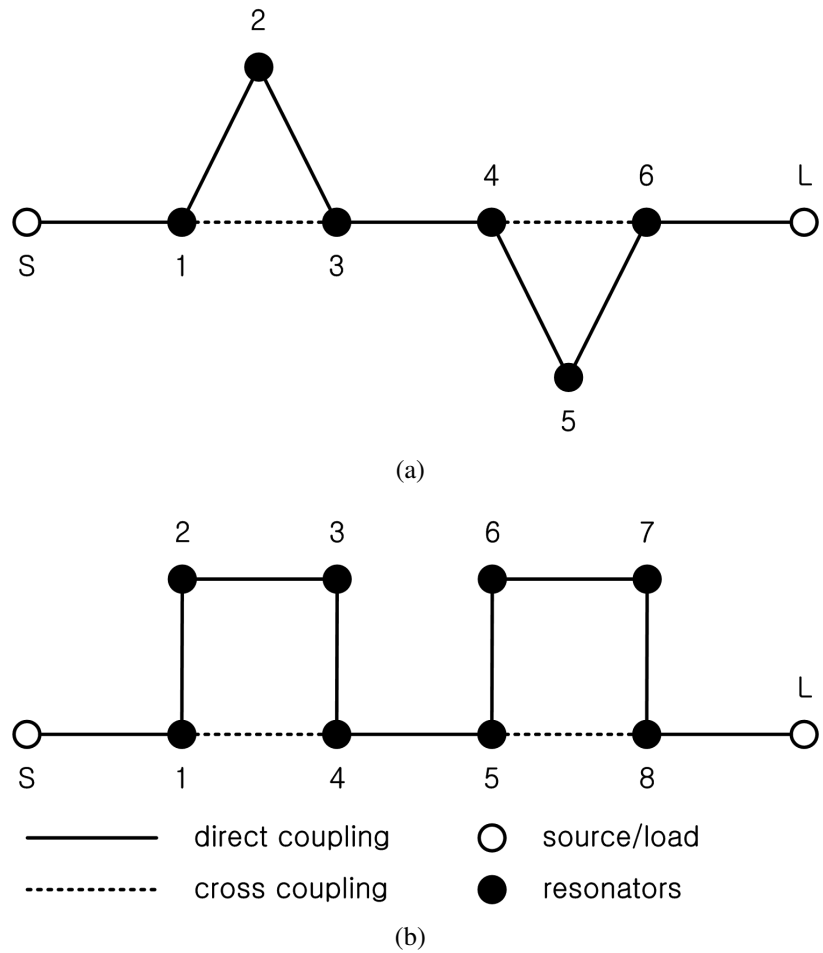


Figure 2.15: The coupling-routing diagrams of inline structure filters: (a) 6th-order filter; (b) 8th-order filter.

Although there is no coupling between the source and load in Fig. 2.14 and Fig. 2.15, we might employ cross coupling between the source and load. The main reason to include the source-load coupling is to increase the number of realizable transmission zeros. For example, 6 transmission zeros can be established at most in 8th-order canonical structure filter in Fig. 2.14. If we include the source-load coupling, it is possible to make 8th-order filter have 8 transmission zeros.

The coupling-routing diagram are used to illustrate the relative phase shifts of multiple signal paths and to understand how the transmission zeros are produced. Many illustrative examples including cascaded-triplet structure, cascaded-quadruplet structure, and the structure with nested cross couplings can be found in [24].

2.4 Physical Elements for Microwave Filter Implementation

Choosing the physical elements is one of the key issues in the realization of filters and it is related to many factors such as frequency range, physical size, quality factor, power handling capability, temperature drift, and production cost [25]. The several media for implementation and corresponding filter technologies include lumped element filter, waveguide filters, printed circuit filters, and dielectric resonator filters.

The main elements of a filter are reactances-lumped capacitances and lumped inductances. It is possible to design some filters by using only capacitors and inductors. The lumped element filters operate typically in hundreds of MHz's, with unloaded quality factor in the hundreds. Their dimensions are much smaller than the operating wavelength and, thus, at high frequencies it is difficult to implement the lumped element filter with good performance. Hence, the distributed components are used for higher frequencies [25].

Microwave filters have been implemented in waveguide technology when low losses and high power handling capabilities are required. For air-filled silver-plated rectangular

and circular waveguide resonators, the quality factor of 10000 to 20000 can be achieved. Also, for a 1 mm silver-plated gap can take up to 630 V peak voltage according to the parallel plate model [26][27]. However, since waveguide structures are typically bulky and have poor temperature stability, significant advances in reducing the mass, volume, and temperature drift have been provided in the past [5]. For instance, the replacement of traditional weighty materials like aluminum by lighter ones, such as Kevlar, have been performed. Additionally, the use of graphite waveguides or carbon fiber technology has also been successfully considered. When using these lighter materials, a deposit of silver onto them is typically required to achieve the good quality factor. Excellent temperature stability has been achieved by using Invar.

A small disc or cube of low-loss high dielectric constant material can also be used as a microwave resonator. Such dielectric resonators are similar in principle to the rectangular or cylindrical waveguide resonators. If the dielectric constant is high, the electric and magnetic fields of a given resonant mode will be confined in an near the resonator and will attenuate to negligible values within a small distance relative to the free-space wavelength. Therefore, radiation loss is minimal, and the unloaded quality factor of the resonator is limited mainly by losses inside the dielectric body [28]. Two types of cylindrical dielectric resonator filters are commonly used. One type is the dual-mode filter, operating in HE_{11} mode, providing low loss, smaller volume, and elliptic function realizations [29]. The other type is the single-mode filter with all cylindrical dielectric resonators operating in $TE_{01\delta}$ mode, providing low loss, flexible layout structure [30]. The drawback of the dielectric resonator filters is their inferior spurious response, and relatively low power handling capability.

Planar structures are mostly employed for microwave integrated circuits and monolithic microwave integrated circuits. Microstrip lines, striplines, coplanar waveguide lines belong to this category. Due to practical features including a small size, easy processing by photolithography, and good affinity with active circuit elements, many circuits utilize the

planar structure resonator. Another advantage of the planar structures is a wide applicable frequency range which can be obtained by employing various kinds of substrate materials. However, a major drawback of the planar structures is low quality factor, making it difficult to apply such planar structures to narrow band filters [31].

CHAPTER 3

Dual-Passband Microwave Filter

3.1 Introduction

Modern wireless communication systems require high performance microwave filters with low insertion loss, high frequency selectivity, and small group-delay variation. For high frequency selectivity, synthesis and design techniques for filters with transmission zeros near passband have been developed [6][7][10]. For those filters, flat group-delay in passband is accomplished using the external equalizer or the self-equalization design technique [32][33]. Although microwave filter technology has gone through a series of innovations, novel filter design techniques are still required as wireless systems evolve.

Since modern communications systems, especially satellite communications systems, have complex frequency and spatial coverage plan, non-contiguous channels might need be amplified and transmitted to one geographical region through one beam. Fig. 3.1 shows an example of frequency and geographical coverage plan. In this case, a conventional approach for implementing such a system includes designing individual single-passband filters and connecting them using signal dividing or combining structures. Fig. 3.2 shows a generic block diagram of a satellite transponder which can meet the frequency plan and spatial coverage shown in Fig. 3.1. In this system, single-passband filters are designed for each channel and non-contiguous channels are transmitted to one geographical region

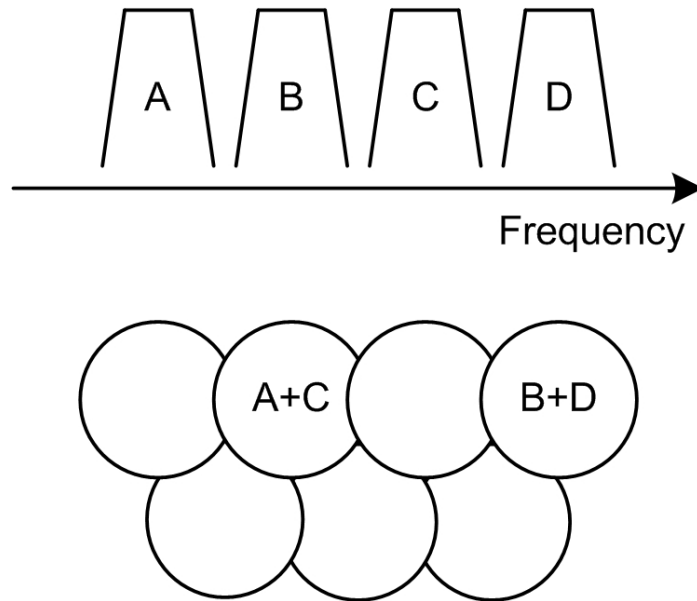


Figure 3.1: An example of frequency plan and spatial coverage of a satellite communication system.

through one beam. Here, signal dividing and combining structures such as circulator structure and manifold structure causes design complexity and increase in size and mass. On the other hand, a novel approach is to include dual-passband filters which can reduce the size and mass of the entire system. This approach requires the synthesis of an advanced filtering function but makes the system simple compared with conventional approach. Fig. 3.3 shows a generic block diagram of a satellite transponder which employs dual-passband filters. It is shown that dual-passband filters can simplify the entire system by replacing individual single-passband filters connected in parallel.

Dual-passband filters of canonical structure with single-mode technique [34], that of in-line structure with dual-mode technique [11], that of canonical structure with dual-mode technique [35] have been designed and realized. Also, synthesis method of a self-equalized dual-passband filter has been presented [36]. These design methods are all based on the optimization techniques in the filter synthesis process.

To avoid the numerical optimization, a method known as frequency transformation technique has been introduced in designing dual-passband filters [37]. Basically this syn-

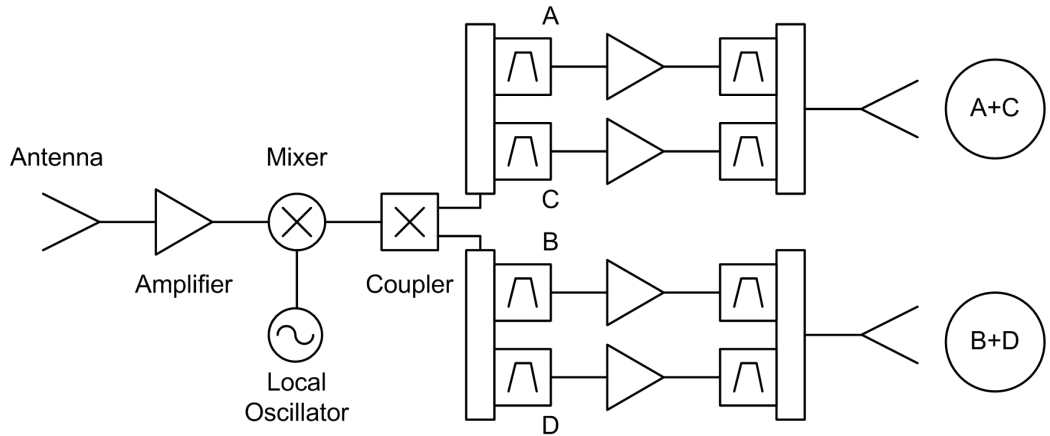


Figure 3.2: A block diagram of a conventional satellite transponder for the frequency plan and spatial coverage shown in Fig. 3.1.

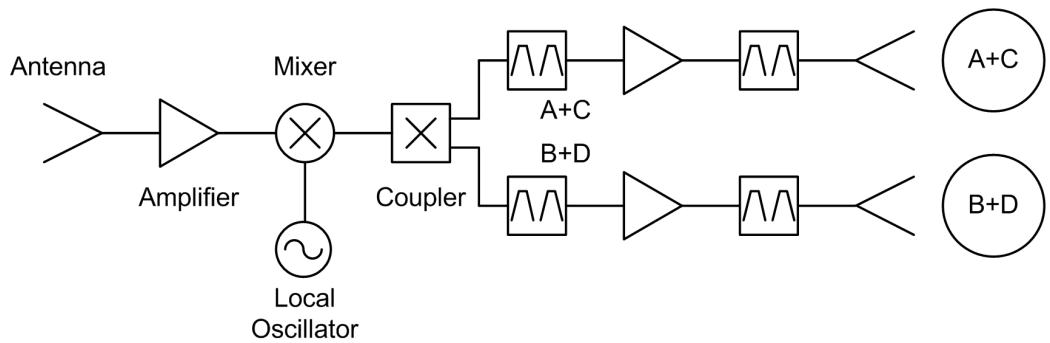


Figure 3.3: A block diagram of a satellite transponder with dual-passband microwave filters.

thesis for designing a dual-passband filter is accomplished by applying a frequency transformation to a lowpass filter prototype. Since the stopband response of the dual-passband filter obtained by using the frequency transformation is not identical to that of lowpass filter prototype, a few attempts are required to find a suitable placement of transmission zeros to acquire the desired attenuation value. One of the frequency transformation in [37] can be adopted for designing asymmetric dual-passband filter. However, this transformation cannot provide the equiripple response in stopband which enables high frequency selectivity.

Filters with dual stopbands and the associated frequency transformation are presented in [38]. Similar to the transformation in [37], this transformation also requires the optimization to achieve equiripple response in stopband and its applications to asymmetric

dual-passband or dual-stopband filters are not discussed.

In this chapter, a synthesis technique for symmetric dual-passband filters using frequency transformation without the need for optimization is presented. Two frequency transformations are given and applied consecutively to the lowpass filter prototype to obtain the dual-passband filter response. With this method, the dual-passband filters can be designed with prescribed passbands and attenuation value in the stopband since the transformation preserves the lowpass filter prototype characteristics. Also, the frequency transformation in general form is given for designing asymmetric dual-passband filters. This transformation is flexible enough to allow for the design of filters with two passbands of highly different bandwidths. This transformation also preserves the lowpass filter prototype characteristics.

3.2 Design Theory

In this section, a procedure for designing dual-passband microwave filters using two frequency transformations is introduced. Fig. 3.4 shows the frequency response of the filter in 3 different frequency domains. ω domain is the actual frequency domain where the filter operates and Ω is a normalized frequency for the lowpass prototype. Generally, single-passband filters are designed in Ω domain and the frequency transformation is applied to make filter operate in ω domain. For dual-passband filter design, an intermediate normalized frequency Ω' is used. The frequency response in ω domain can be obtained by applying two frequency transformations consecutively to the frequency response in Ω domain. The coupling matrix of the dual-passband filter is obtained from the transfer function of the filter in Ω' domain.

3.2.1 Lowpass Filter Prototype

Generally, the transfer function of an N th-order lowpass filter prototype can be expressed by

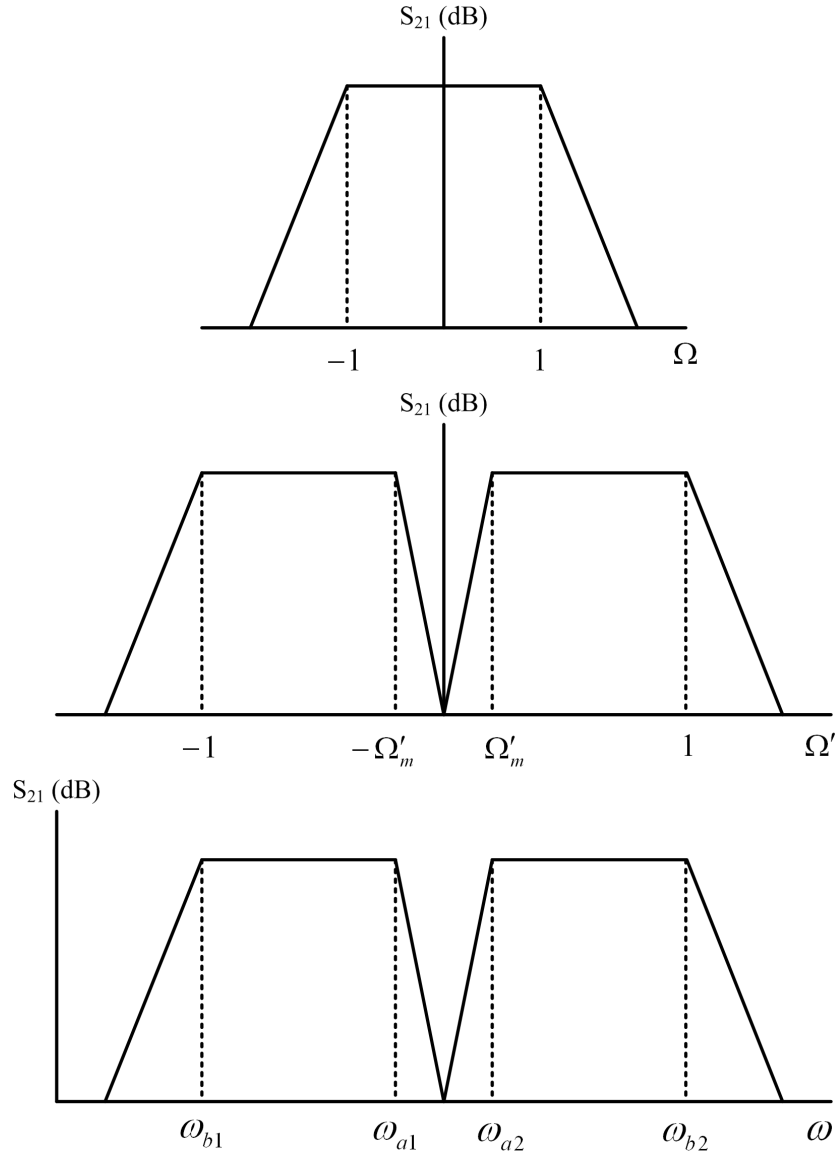


Figure 3.4: The frequency response of the filter in Ω , Ω' , and ω domain. The coupling matrix of the dual-passband filter is obtained from the transfer function in Ω' domain.

$$|t(S)|^2 = \frac{1}{1 + \epsilon^2 |K(S)|^2} \quad (3.1)$$

where $S = j\Omega$ with the assumption that the characteristic function $K(S)$ has only pure imaginary poles and zeros in S domain, and ϵ is the ripple constant related to the passband return loss R_1 at $\Omega = \Omega_1$ by

$$\varepsilon = \sqrt{\frac{1}{10^{R_1/10} - 1} \frac{1}{|K(j\Omega_1)|^2}}. \quad (3.2)$$

Since here we do not deal with self-equalized dual-passband filters, pure imaginary reflection zeros and transmission zeros are sufficient for our design. For the case of pure imaginary reflection zeros and transmission zeros, the characteristic function of the elliptic function filter is given by [39]

$$K(\Omega) = \cosh \left(\sum_{i=1}^N \cosh^{-1}(x_i) \right) \quad (3.3)$$

where

$$x_i = \frac{\Omega - 1/\Omega_i}{1 - \Omega/\Omega_i} \quad (3.4)$$

In (3.4), Ω_i is the location of the i th transmission zero. Note that the magnitude of $K(\Omega)$ is 1 at $\Omega_1 = \pm 1$ for all N . Therefore, in this case, the ripple constant becomes

$$\varepsilon = \sqrt{\frac{1}{10^{R_1/10} - 1}} \quad (3.5)$$

Once the transmission zeros are decided, the reflection zeros can be obtained easily from computing the return loss of the filter. Based on the reflection zero and transmission zero locations, we can rewrite the characteristic function as a rational function:

$$\begin{aligned} K(S) &= \frac{F(S)}{P(S)} \\ &= \frac{\prod_{i=1}^N (S - S_{fi})}{\prod_{i=1}^Z (S - S_{pi})} \end{aligned} \quad (3.6)$$

where N is the number of reflection zeros and Z is the number of transmission zeros. N is

also referred to as the order of the filter. Here, it is assumed that $Z < N$.

The basic idea in establishing two passbands is based on putting transmission zeros within the passband of a single-passband filter to split it into two passbands. Since (3.3) is valid for $|\Omega_i| > 1$, it cannot be used for computing the reflection zeros with given transmission zeros. Therefore, this work presents frequency transformation technique for determining reflection zeros and transmission zeros of dual-passband microwave filters.

3.2.2 Frequency Transformation for Dual-passband Filters

Let's assume that the dual-passband filter has two symmetric passbands and their passband regions are specified by $(\omega_{b1}, \omega_{a1})$ and $(\omega_{a2}, \omega_{b2})$ (Fig.3.4). The coupling matrix is obtained from the frequency response in the normalized frequency Ω' . For dual-passband filter synthesis, the previous studies [35][36] start from Ω' domain by finding the locations of reflection zeros and transmission zeros of the filters by direct optimization.

In this chapter, we obtain the reflection zeros and transmission zeros of the dual-passband filter by analytic frequency transformation technique. The frequency transformation from Ω to Ω' can be expressed as follows:

$$\begin{aligned} S &= \frac{S'}{c_1} + \frac{c_2}{S'} & \text{for } \Omega' > 0 \\ S &= -\left(\frac{S'}{c_1} + \frac{c_2}{S'}\right) & \text{for } \Omega' < 0 \end{aligned} \quad (3.7)$$

where $S = j\Omega$ and $S' = j\Omega'$. Since we are interested in how Ω domain maps to Ω' domain, we rewrite (3.7) so that

$$\begin{aligned} \Omega &= \frac{\Omega'}{c_1} - \frac{c_2}{\Omega'} & \text{for } \Omega' > 0 \\ \Omega &= -\left(\frac{\Omega'}{c_1} - \frac{c_2}{\Omega'}\right) & \text{for } \Omega' < 0. \end{aligned} \quad (3.8)$$

Since 1 and -1 in Ω domain are transformed to 1 and Ω'_m in Ω' domain for $\Omega' > 0$, respectively, and 1 and -1 in Ω domain are transformed to -1 and $-\Omega'_m$ in Ω' for $\Omega' < 0$, respectively, we must enforce

$$\begin{aligned} 1 &= \frac{c_1}{2} \left(1 + \sqrt{1 + 4\frac{c_2}{c_1}} \right) \\ \Omega'_m &= \frac{c_1}{2} \left(-1 + \sqrt{1 + 4\frac{c_2}{c_1}} \right). \end{aligned} \quad (3.9)$$

From (3.9), the constant in (3.7) and(3.8) can be expressed in terms of the band edge frequency of the dual-passband filter in Ω' domain:

$$\begin{aligned} c_1 &= 1 - \Omega'_m \\ c_2 &= \frac{\Omega'_m}{1 - \Omega'_m}. \end{aligned} \quad (3.10)$$

Similarly, the frequency transformation from Ω' to ω for narrow bandpass filters is expressed as

$$S' = \frac{s}{d_1} + \frac{d_2}{s} \quad (3.11)$$

where $s = j\omega$. The frequency transformation in (3.11) can be rewritten as

$$\Omega' = \frac{\omega}{d_1} - \frac{d_2}{\omega}. \quad (3.12)$$

Since band edge frequencies in Ω' domain are transformed to those in ω domain as

$$\begin{aligned}
1 &\rightarrow \omega_{b2} \\
\Omega'_m &\rightarrow \omega_{a2} \\
-\Omega'_m &\rightarrow \omega_{a1} \\
-1 &\rightarrow \omega_{b1}
\end{aligned} \tag{3.13}$$

therefore, the relationship between the band edge frequencies in ω domain and the coefficients in (3.11) are as follows:

$$\begin{aligned}
\omega_{b2} &= \frac{d_1}{2} \left(1 + \sqrt{1 + 4 \frac{d_2}{d_1}} \right) \\
\omega_{b1} &= \frac{d_1}{2} \left(-1 + \sqrt{1 + 4 \frac{d_2}{d_1}} \right) \\
\omega_{a2} &= \frac{d_1}{2} \left(\Omega'_m + \sqrt{\Omega_m'^2 + 4 \frac{d_2}{d_1}} \right) \\
\omega_{a1} &= \frac{d_1}{2} \left(-\Omega'_m + \sqrt{\Omega_m'^2 + 4 \frac{d_2}{d_1}} \right).
\end{aligned} \tag{3.14}$$

From (3.14), we can express d_1 , d_2 , and Ω'_m in terms of band edge frequencies of the dual-passband filter:

$$\begin{aligned}
d_1 &= \omega_{b2} - \omega_{b1} \\
d_2 &= \frac{\omega_{b1} \omega_{b2}}{\omega_{b2} - \omega_{b1}} \\
\Omega'_m &= \frac{\omega_{a2} - \omega_{a1}}{\omega_{b2} - \omega_{b1}}.
\end{aligned} \tag{3.15}$$

Using (3.10) and (3.15), the constant in (3.7) can also be expressed in terms of band edge frequencies of the dual-passband filter. Therefore, the frequency transformations can be

expressed in terms of band edge frequencies of the dual-passband filter.

In addition, for convenient application to filter design, the frequency transformation in (3.12) can be rewritten using real frequency as

$$\Omega' = \frac{f}{d_1} - \frac{d_2}{f} \quad (3.16)$$

and variables in (3.15) should be modified as

$$\begin{aligned} d_1 &= f_{b2} - f_{b1} \\ d_2 &= \frac{f_{b1}f_{b2}}{f_{b2} - f_{b1}} \\ \Omega'_m &= \frac{f_{a2} - f_{a1}}{f_{b2} - f_{b1}}. \end{aligned} \quad (3.17)$$

where $f_{a1} = \omega_{a1}/2\pi$, $f_{a2} = \omega_{a2}/2\pi$, $f_{b1} = \omega_{b1}/2\pi$, and $f_{b2} = \omega_{b2}/2\pi$. Based on the prescribed narrow passbands ($\omega_{b1} - \omega_{a1}$, $\omega_{a2} - \omega_{b2}$) of the dual-passband filter, the frequency transformations can be defined and, consequently, the transfer functions and coupling matrices can be determined.

The following section describes the application of the frequency transformations and then direct applications for designing dual-passband filters.

3.3 Filter Design and Measurement

3.3.1 Electrical Design

In this section, the filter with two passbands is designed and realized to describe the presented filter synthesis theory. The passbands of the dual-passband filter are chosen to be 3.90 - 3.95 GHz and 4.05 - 4.10 GHz. Each passband is set to have 4 reflection zeros and a maximum return loss of 20 dB. Minimum attenuation over stopbands is set to be 30 dB.

Since we are seeking a 4th-order passband response, we start from a 4th-order lowpass

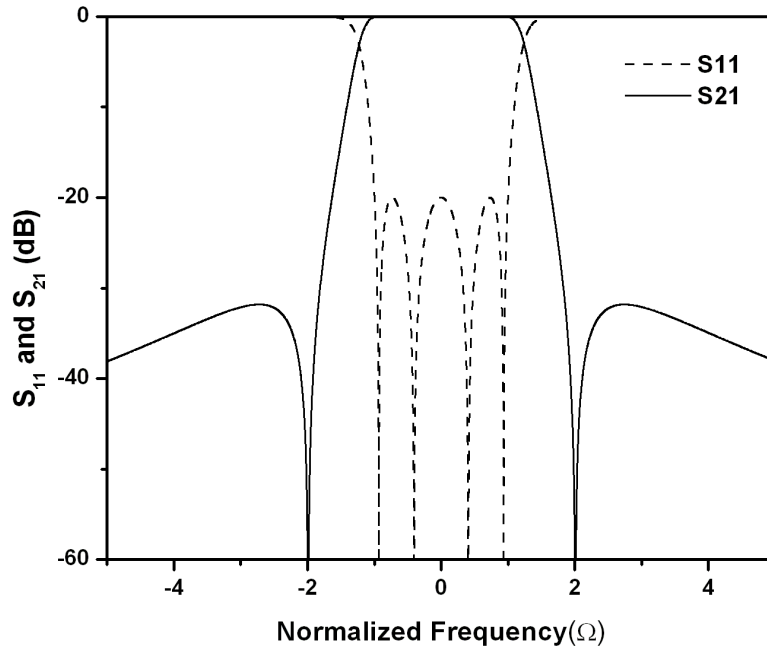


Figure 3.5: Frequency response of a lowpass filter prototype with the transmission zeros at $\pm j2.0$.

prototype. Fig. 3.5 shows the frequency response of the lowpass filter prototype with the transmission zeros at $S = \pm j2.0, \pm\infty$. This filter prototype has a pair of transmission zeros at finite frequencies and their locations are determined based on the attenuation requirement over stopband. Using (3.1) - (3.3), we can find the locations of the reflection zeros with given transmission zeros, return loss, and the order of the filter. The reflection zeros of the filter are found to be located at $S = \pm j0.9330, S = \pm j0.4062$. Since band edge frequencies of the dual-passband filter are $f_{b1} = 3.90$ GHz, $f_{b2} = 4.10$ GHz, $f_{a1} = 3.95$ GHz, and $f_{a2} = 4.05$ GHz, we have $\Omega'_m = 0.5$ from (3.17). From the frequency transformation in (3.7), the reflection zeros and transmission zeros of the dual-passband filter at finite frequencies in Ω' domain can be determined:

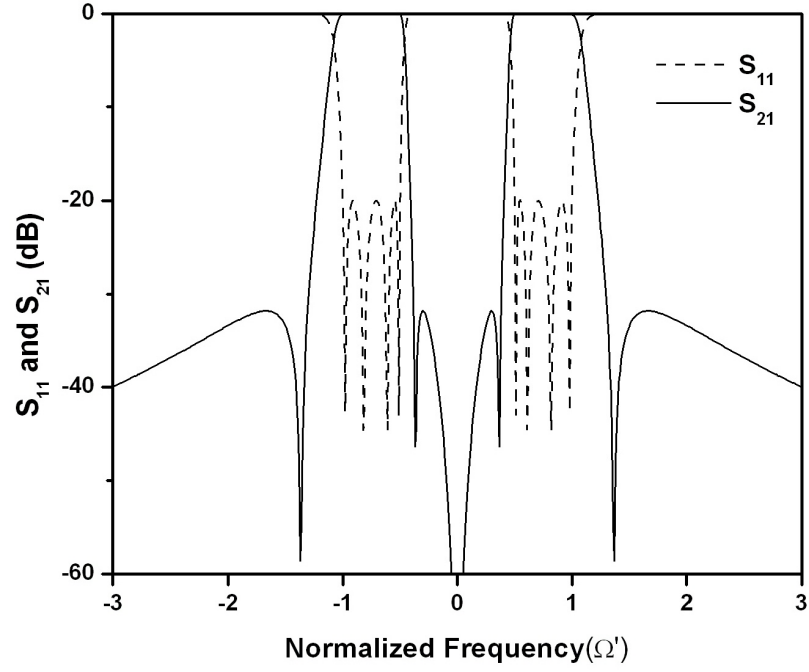


Figure 3.6: The frequency response of the dual-passband filter in Ω' domain.

$$\begin{aligned}
 S'_{p1} &= -j1.366, & S'_{p2} &= -j0.366, & S'_{p3} &= -j0.000, \\
 S'_{p4} &= +j0.000, & S'_{p5} &= +j0.366, & S'_{p6} &= +j1.366, \\
 S'_{f1} &= -j0.978, & S'_{f2} &= -j0.816, & S'_{f3} &= -j0.613, \\
 S'_{f4} &= -j0.511, & S'_{f5} &= +j0.511, & S'_{f6} &= +j0.613, \\
 S'_{f7} &= +j0.816, & S'_{f8} &= +j0.978.
 \end{aligned} \tag{3.18}$$

Fig. 3.6 shows the frequency response of the dual-passband filter with reflection zeros and transmission zeros in (3.18). With the given reflection zeros and transmission zeros of the dual-passband filter in Ω' domain, we can obtain the transfer function in the form given by (3.1).

$$\begin{aligned}
|t(S')|^2 &= \frac{1}{1 + \epsilon'^2 |K(S')|^2} \\
&= \frac{1}{1 + \epsilon'^2 \left| \frac{F(S')}{P(S')} \right|^2} \\
&= \frac{1}{1 + \epsilon'^2 \frac{F(S')F(-S')}{P(S')P(-S')}}
\end{aligned} \tag{3.19}$$

where

$$\begin{aligned}
F(S') &= \prod_i (S' - S'_{fi}) \\
P(S') &= \prod_i (S' - S'_{pi})
\end{aligned} \tag{3.20}$$

and the ripple constant is determined by the return loss R_1 at Ω'_1 :

$$\epsilon' = \sqrt{\frac{1}{10^{R_1/10} - 1} \frac{1}{|K(j\Omega'_1)|^2}}. \tag{3.21}$$

From (3.19), $|t(S')|^2$ can be expressed as a rational function as follows:

$$|t(S')|^2 = \frac{1}{\epsilon'^2} \frac{P(S')P(-S')}{E(S')E(-S')}. \tag{3.22}$$

Using the fact that $|t(S')|^2 = t(S')t(-S')$, we can obtain the expanded form of the transfer function $t(S')$. Using $t(S')$, we synthesize the filter circuit in such a way that the filter exhibits the prescribed transmitted power ratio $|t(S')|^2$. The transfer function $t(S')$ is given by

$$t(S') = \frac{1}{\epsilon'} \frac{\sum_{i=0}^6 a_{zi} S'^i}{\sum_{k=0}^8 a_{pk} S'^k} \quad (3.23)$$

where

$$\begin{aligned} a_{z6} &= 1.0000, & a_{z4} &= 1.9999, & z_{z2} &= 0.2500, \\ a_{z0} &= 0.0000, & a_{p8} &= 1.0000, & a_{p7} &= 1.0458, \\ a_{p6} &= 2.8061, & a_{p5} &= 1.9203, & a_{p4} &= 2.3954, \\ a_{p3} &= 0.9600, & a_{p2} &= 0.7015, & a_{p1} &= 0.1307, \\ a_{p0} &= 0.0625, & \epsilon' &= 11.2390. \end{aligned} \quad (3.24)$$

From the transfer function in Ω' domain, the coupling matrix can be determined [10]. Since the 8th-order dual-passband filter has 6 zeros in finite frequencies, it can be of symmetric canonical structure and its coupling matrix is given by

$$\mathbf{M} = \begin{bmatrix} 0 & 0.8302 & 0 & 0 & 0 & 0 & 0 & -0.0851 \\ 0.8301 & 0 & 0.4080 & 0 & 0 & 0 & 0.1053 & 0 \\ 0 & 0.4080 & 0 & 0.4962 & 0 & 0.5076 & 0 & 0 \\ 0 & 0 & 0.4962 & 0 & -0.2294 & 0 & 0 & 0 \\ 0 & 0 & 0 & -0.2294 & 0 & 0.4962 & 0 & 0 \\ 0 & 0 & 0.5076 & 0 & 0.4962 & 0 & 0.4080 & 0 \\ 0 & 0.1053 & 0 & 0 & 0 & 0.4080 & 0 & 0.8302 \\ -0.0851 & 0 & 0 & 0 & 0 & 0 & 0.8302 & 0 \end{bmatrix}$$

$$R = 0.5229.$$

(3.25)

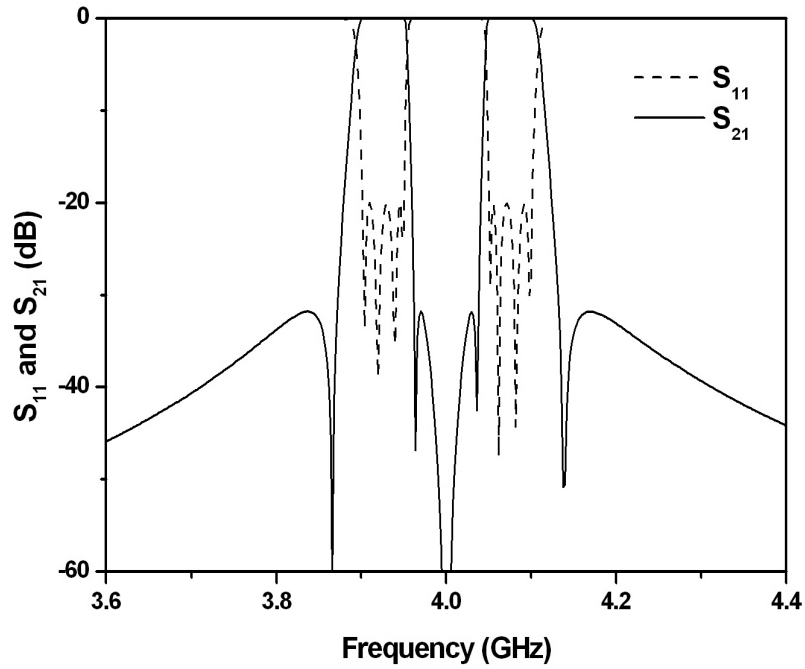


Figure 3.7: The frequency response of the dual-passband filter in real frequency domain.

The matrix similarity transformation can be applied to the coupling matrix to obtain different combinations of positive and negative inter-resonator coupling coefficients or/and different coupling structures (e.g. asymmetric canonical structure) [40][41].

Applying the frequency transformation in (3.16), we can obtain the frequency response of the filter in real frequency domain. Fig. 3.7 shows the frequency response of the filter. Note that the passbands of the filter are 3.90 - 3.95 GHz and 4.05 - 4.10 GHz and attenuation at stopbands is 30 dB, which shows the validity of this proposed synthesis method for dual-passband filter using frequency transformation with prescribed passbands and attenuation at stopbands.

3.3.2 Physical Design and Measurement

The coupling matrix in (3.25) can be realized for many types of filter structures. In this work, we use stripline structure for the filter. Fig. 3.8 shows the conductor layer of the dual-passband filter. This conductor layer is positioned in the middle of two metal-backed

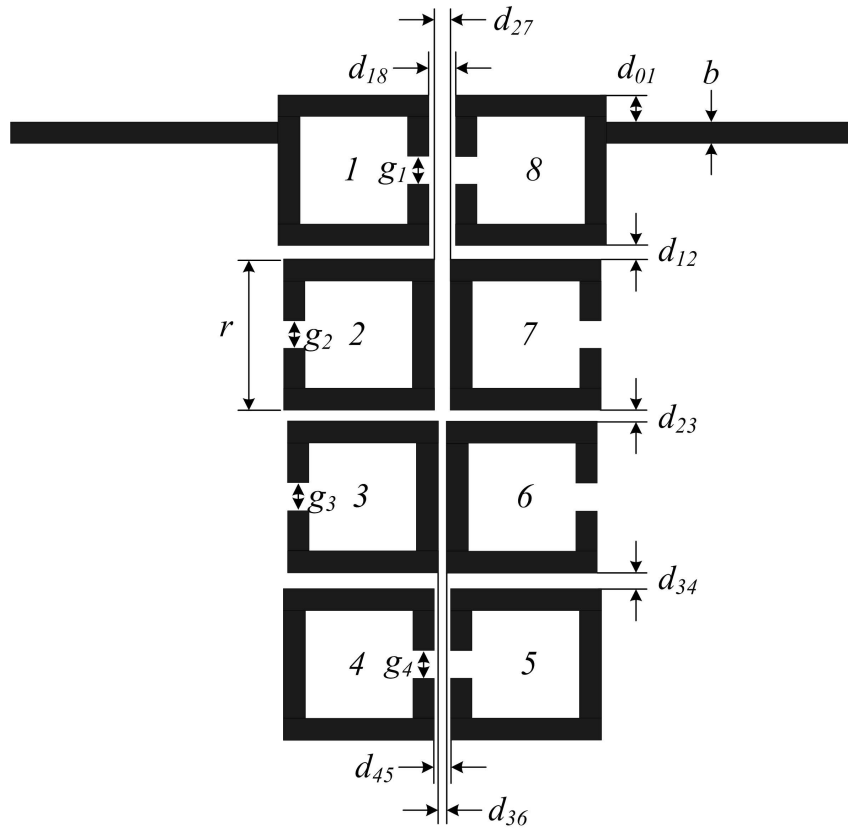


Figure 3.8: The conductor layer of stripline structure for the dual-passband filter.

dielectric layers. The thickness, dielectric constant, and loss tangent of the dielectric layers are 1.574 mm, 2.2, and 0.0009, respectively.

The filter has square open-loop resonators and each of them has a perimeter about one half-wavelength at the center frequency. Any coupling in the filter is that of the proximity coupling, which is through fringe fields. The nature and the extent of the fringe fields determine the nature and the strength of the coupling. At the resonant frequency, each of open-loop resonators has the maximum electric fringe field at the side with an open-gap, and the maximum magnetic fringe field at the opposite side. Because the fringe field exhibits an exponentially decaying character outside the region, the electric fringe field is stronger near the side having the maximum electric field distribution, while the magnetic fringe field is stronger near the side having the maximum magnetic field distribution. It follows that the electric coupling can be obtained if the open-gap sides of two coupled

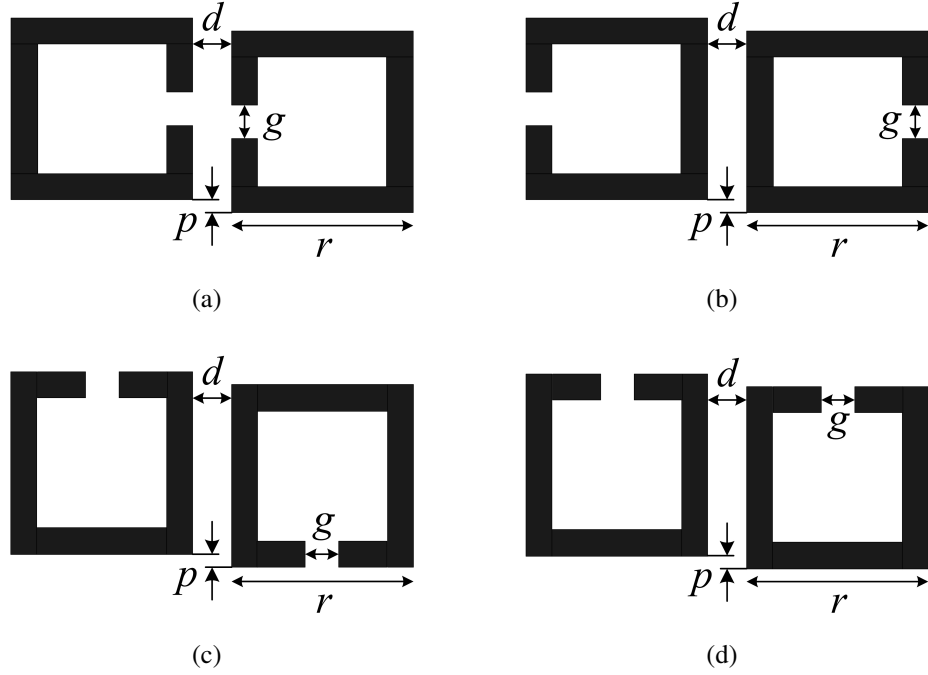


Figure 3.9: Coupling structures of coupled stripline open-loop resonators which are separated by a spacing s and may or may not be subject to an offset p : (a) Electric coupling structure. (b) Magnetic coupling structure. (c) Mixed coupling structure. (d) Mixed coupling structure.

resonators are proximately placed as shown in Fig. 3.9(a), while the magnetic coupling can be obtained if the opposite sides are proximately placed as shown in Fig. 3.9(b). For the coupling structures in Fig. 3.9(c) and Fig. 3.9(d), the electric and magnetic fringe fields at the coupled sides may have comparative distributions so that both the electric and the magnetic coupling occur [42]. In this case, we may need to find out which coupling is dominant so that we can assign positive sign or negative sign for the coupling value of the coupling structures. Since open-loop resonators can provide both the electric and magnetic couplings between two resonators, these can be used for realizing both positive and negative couplings as required by (3.25). In our design, positive and negative signs are assigned to magnetic and electric couplings, respectively. Since $M_{1,8}$ and $M_{4,5}$ are negative, resonator 1 and resonator 8, and resonator 4 and resonator 5 have the electric coupling structure shown in Fig. 3.9(a). Also, resonator 2 and resonator 7, and resonator 3 and resonator 6 have

been determined to have the magnetic coupling structure shown in Fig. 3.9(b), since $M_{2,7}$ and $M_{3,6}$ are positive. This results in that the coupling structures for the other couplings are automatically determined to have mixed coupling structures shown in Fig. 3.9(c) or Fig. 3.9(d). It is of note that the sign of coupling values of these coupling structures does not need to be figured out since these coupling structures can be either positive or negative value as long as $M_{1,2} = M_{7,8}$, $M_{2,3} = M_{6,7}$, and $M_{3,4} = M_{5,6}$ due to the matrix similarity transformation.

Tapping position (d_{01}) is determined by the external coupling coefficient (R) and the spacings between two resonators are determined by inter-resonator coupling coefficients ($M_{i,j}$). The external coupling coefficient can be measured by one-port reflection technique. In this technique, the phase response of reflection coefficient (S_{11}) of one excited resonator is measured and the external coupling coefficient is given by

$$R = \frac{\Delta f_{\pm 90^\circ}}{\Delta f} \quad (3.26)$$

where $\Delta f = f_{b2} - f_{b1}$ and $\Delta f_{\pm 90^\circ}$ are the absolute bandwidth of the filter and the frequency difference of two frequencies at which the phase shift $\pm 90^\circ$ with respect to the absolute phase at the center frequency f_0 , respectively [43]. Resonator-pair measurement is conventional method to experimentally obtain inter-resonator coupling coefficient. In this technique, the two peaks are observed in the amplitude response of transmission coefficient of a circuit consisting of two identical resonators. The inter-resonator coupling coefficient ($M_{i,j}$) between resonator i and resonator j is expressed by

$$M_{i,j} = \frac{f_{p2}^2 - f_{p1}^1}{f_{p2}^2 + f_{p1}^1} \cdot \frac{f_0}{\Delta f} \quad (3.27)$$

where f_{p1} and f_{p2} are the lower and higher frequencies at which the peaks are observed. Based on (3.26) and (3.27), tapping position (d_{01}) and spacings between resonators (s) are determined in such a way that the measured external and inter-resonator coupling coef-

Table 3.1: Physical dimensions of the dual-passband filter.

Parameter	Dimensions (mm)
b	1.26
r	8.10
g_1	1.08
g_2	1.28
g_3	1.28
g_4	1.20
d_{01}	1.70
d_{12}	0.50
d_{23}	0.18
d_{34}	0.78
d_{45}	1.14
d_{36}	0.66
d_{27}	1.38
d_{18}	1.42

ficients are identical to those in (3.25). The full-wave electromagnetic simulator Zeland IE3D is used to calculate the coupling coefficients. The physical dimensions of the filter in Fig. 3.8 are summarized in Table 3.1.

The entire filter structure has also been simulated using Zeland IE3D and Fig. 3.10 compares the simulated and theoretical frequency response of the dual-passband filter. Since the filter synthesis doesn't take into account the losses of the filter, the loss factors are not included in the simulated response in Fig. 3.10 for clear comparison. A good agreement between theoretical and simulated frequency responses is shown. Simulated frequency response has somewhat lower attenuation at higher stopband which is due to asymmetric locations of transmission zeros. It has been reported that the asymmetric frequency response is attributed to the frequency-dependent couplings [44]. The measured response of the fabricated filter (Fig. 3.11) is compared to the simulation one in Fig. 3.12. The simulated response includes loss factors (conductor loss and dielectric loss) in order to take

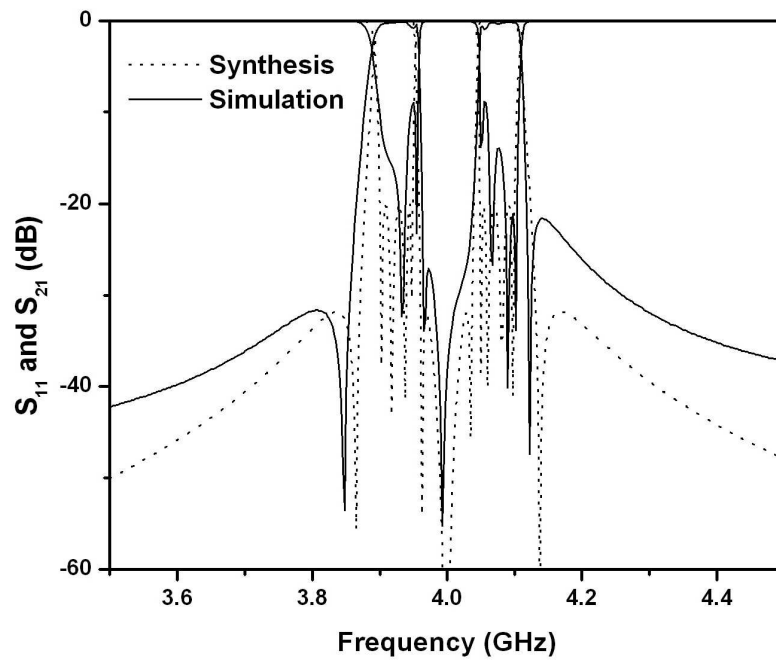


Figure 3.10: Synthesized and simulated frequency response of the dual-passband filter.

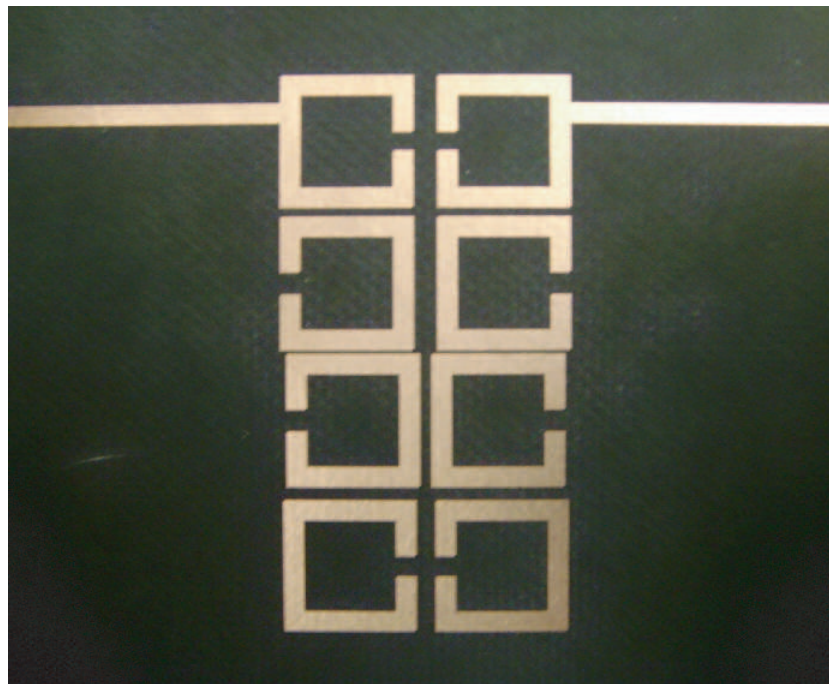
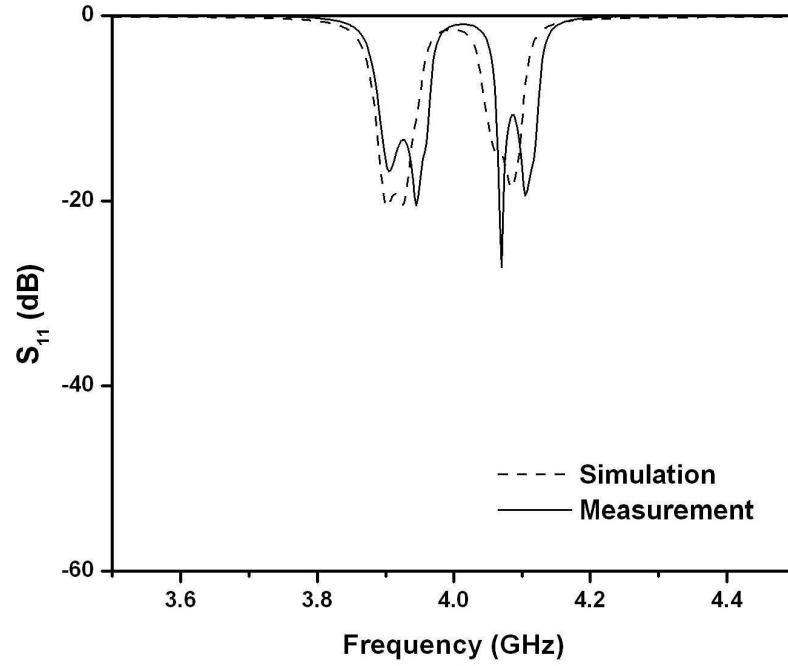
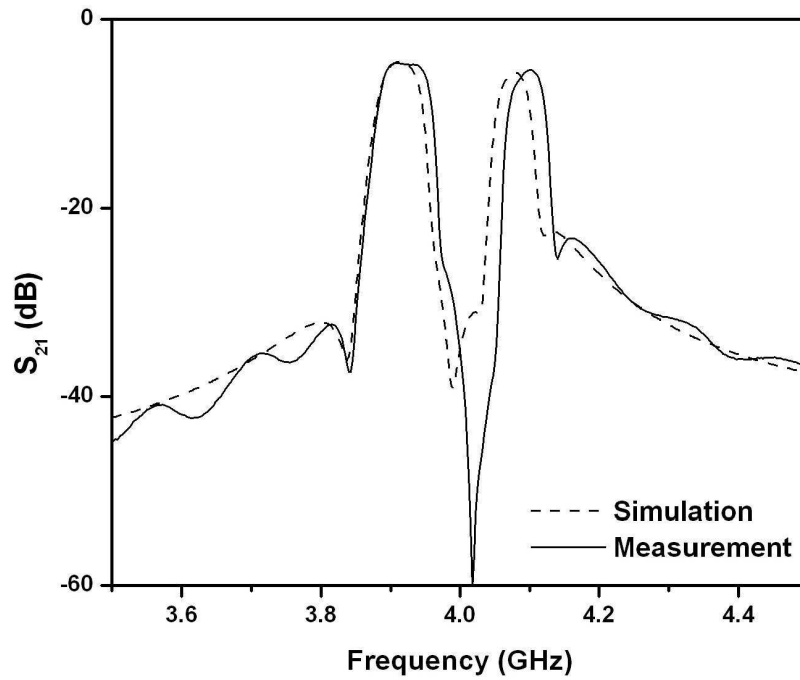


Figure 3.11: The fabricated conductor layer of the stripline structure for the dual-passband filter.



(a)



(b)

Figure 3.12: Frequency response of the dual-passband filter: (a) S_{11} , (b) S_{21} .

into account the losses of the fabricated filter. Measured response shows a reasonably good agreement with the simulated response. There is however, a small frequency shift which can be attributed to the fabrication error.

3.3.3 Sensitivity Considerations

There is random variation in the coupling and resonator tuning states, which is due to component and manufacturing/assembly tolerances [45]. Therefore, the sensitivity analysis is important for filter design, tuning, and fabrication due to aforementioned tolerances. We have carried out the sensitivity analysis in order to see the effect of change of coupling coefficients on the filter response. From these sensitivity analysis, acceptable bounds on the errors in the elements of the coupling matrix can be determined.

In (3.25), many inter-resonator coupling coefficients are zero. In case that the filter is implemented by using coaxial resonators [45] or dual-mode waveguide resonator [10], these zero inter-resonator coupling coefficients are exactly zero. However, in some cases, these coupling coefficients may not be zero in physical design and fabrication. For example, stripline and microstripline resonators use proximity couplings and couplings which are designed to be zero may not be zero due to the fringe fields. Fig. 3.13 and Fig. 3.14 show the frequency response of filter when these coupling coefficients are not zero and vary randomly in a range of ± 0.005 and ± 0.01 , respectively.

Also, all diagonal elements in (3.25), $M_{i,i}$ for $i = 1, 2, \dots, 8$, are zero, which means that all resonators should resonate at the center frequency of the filter. Resonators may not be synchronously tuned at the center frequency and this case has been investigated by applying random variation less than ± 0.005 and ± 0.01 to self-couplings. Nonzero $M_{i,i}$ indicates that i th resonator resonates at

$$f_{ri} = \frac{-M_{i,i}\Delta f + \sqrt{M_{i,i}^2\Delta f^2 + 4f_{b1}f_{b2}}}{2}. \quad (3.28)$$

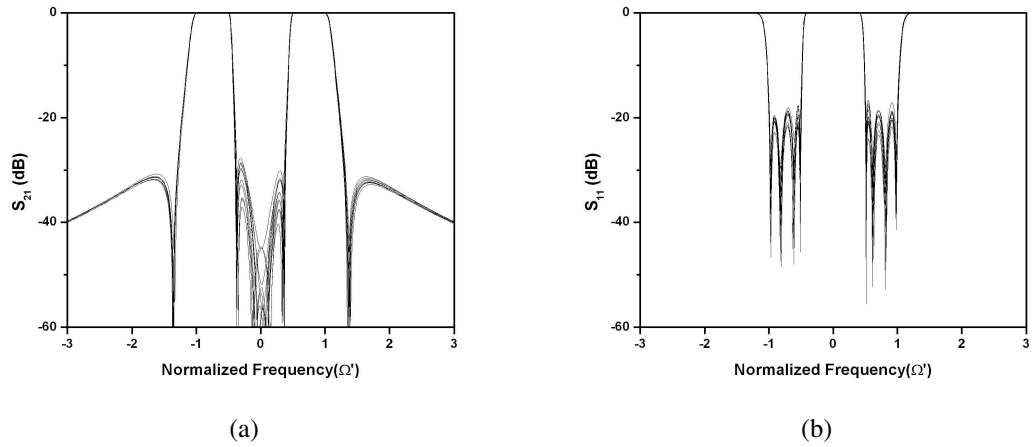


Figure 3.13: Sensitivity to random variation in coupling coefficients. Random variation less than ± 0.005 is applied to all zero inter-resonator couplings in (3.25): (a) S_{21} , (b) S_{11} .

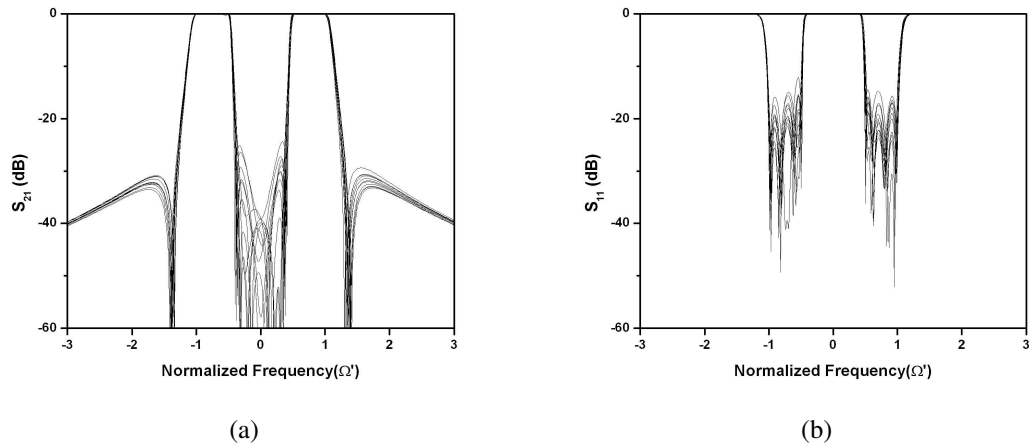


Figure 3.14: Sensitivity to random variation in coupling coefficients. Random variation less than ± 0.01 is applied to all zero inter-resonator couplings in (3.25): (a) S_{21} , (b) S_{11} .

The frequency responses of the sensitivity analysis are shown in Fig. 3.15 and 3.16.

The last analysis has been carried out by applying random variation to nonzero inter-resonator coupling coefficients. Random variation has been set to be less than $\pm 1\%$ and $\pm 5\%$ of original inter-resonator coupling coefficients. Fig. 3.17 and Fig. 3.18 show the results of the quantitative analysis. It is observed that the frequency response variation of

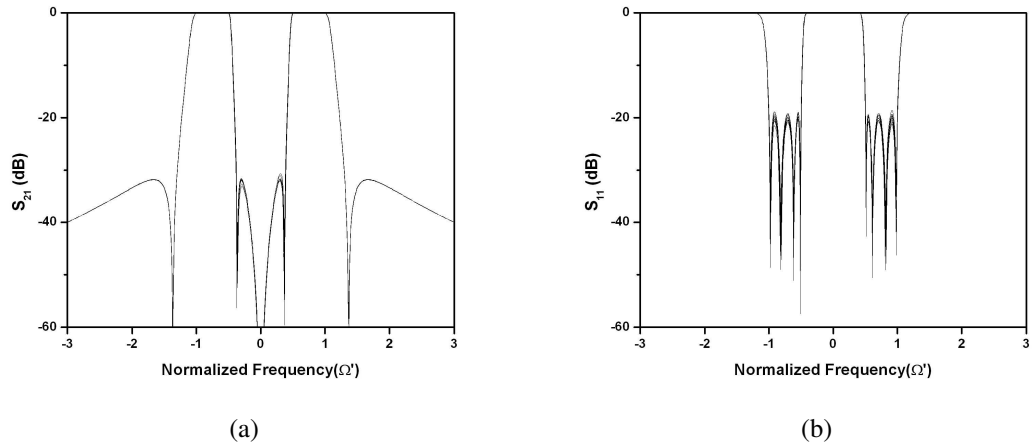


Figure 3.15: Sensitivity to random variation in coupling coefficients. Random variation less than ± 0.005 is applied to all zero self-couplings in (3.25): (a) S_{21} , (b) S_{11} .

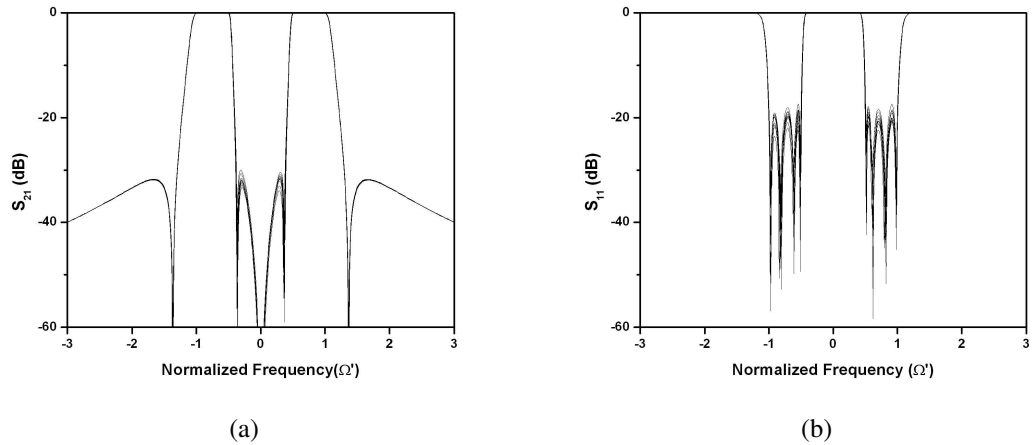


Figure 3.16: Sensitivity to random variation in coupling coefficients. Random variation less than ± 0.01 is applied to all zero self-couplings in (3.25): (a) S_{21} , (b) S_{11} .

transmission coefficient (S_{21}) in the stopband between two passbands is larger than that in the outer stopbands. This is because the stopband between two passbands is crowded with the transmission zeros.

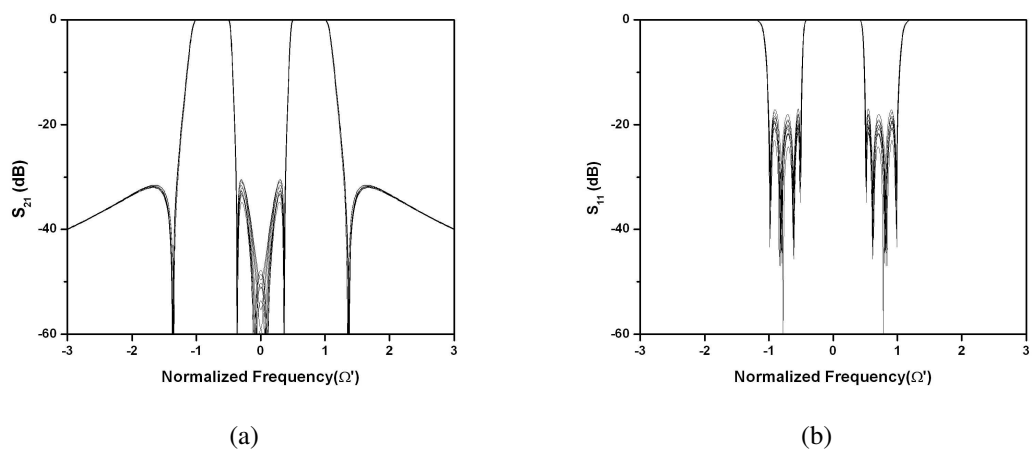


Figure 3.17: Sensitivity to random variation in coupling coefficients. Random variation less than $\pm 1\%$ is applied to all non-zero inter-resonator couplings in (3.25): (a) S_{21} , (b) S_{11} .

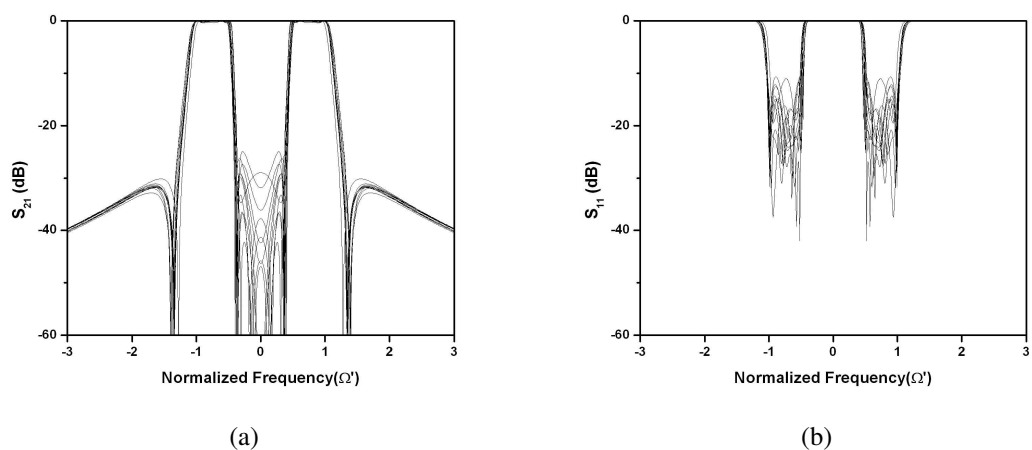


Figure 3.18: Sensitivity to random variation in coupling coefficients. Random variation less than $\pm 5\%$ is applied to all non-zero inter-resonator couplings in (3.25): (a) S_{21} , (b) S_{11} .

3.4 More Examples

In previous section, we dealt with an 8th-order dual-passband filter with repeated transmission zeros at $\Omega' = 0$. In this section, a 4th-order dual-passband filter with repeated transmission zeros at $\Omega' = 0$ and a 8th-order dual-passband filter with no transmission zeros at $\Omega' = 0$ are briefly discussed.

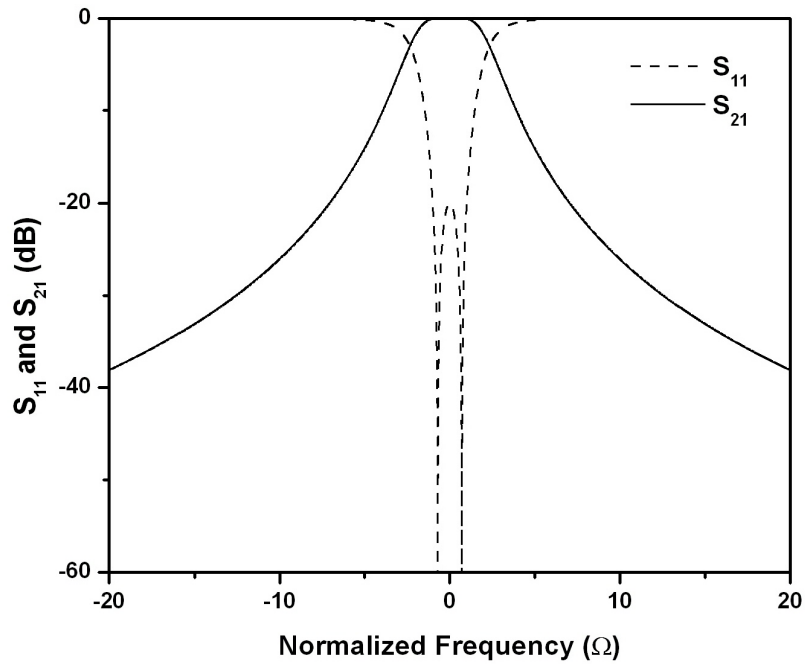


Figure 3.19: Frequency response of a lowpass filter prototype with no transmission zeros at finite frequencies.

Fig. 3.19 shows a 2nd-order lowpass prototype filter with no transmission zeros at finite frequencies in Ω domain. The return loss and the order of the lowpass prototype filter determines the location of the reflection zeros. Using the frequency transformation in (3.7) with $\Omega'_m = 0.9$, we can obtain the location of the reflection zeros and transmission zeros of the 4th-order dual-passband filter in Ω' domain and therefore its frequency response can be obtained as shown in Fig. 3.20. Based on the locations of the reflection zeros and transmission zeros in Ω' domain, the transfer function and coupling matrix can be obtained as described in the previous section. The transfer function is

$$t(S') = \frac{1}{\epsilon'} \frac{S'^2}{\sum_{k=0}^4 a_{pk} S'^k} \quad (3.29)$$

where

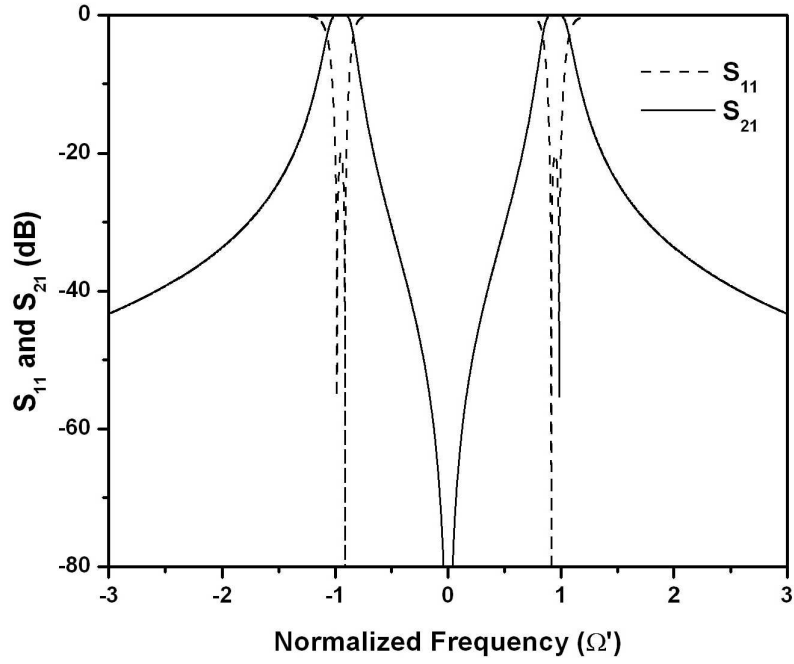


Figure 3.20: Frequency response of a dual-passband filter whose lowpass prototype is shown in Fig. 3.19.

$$\begin{aligned}
 a_{p4} &= 1.0000, & a_{p3} &= 0.29659, & a_{p2} &= 1.8496, \\
 a_{p1} &= 0.2670, & a_{p0} &= 0.8105, & \epsilon' &= 20.507,
 \end{aligned}
 \tag{3.30}$$

and the coupling matrix is

$$M = \begin{bmatrix} 0 & 0.9488 & 0 & -0.1644 \\ 0.9488 & 0 & 0 & 0 \\ 0 & 0 & 0 & 0.9488 \\ -0.1644 & 0 & 0.9488 & 0 \end{bmatrix}
 \tag{3.31}$$

$$R = 0.1483.$$

Using the matrix similarity transformation, we can also have the coupling matrix with

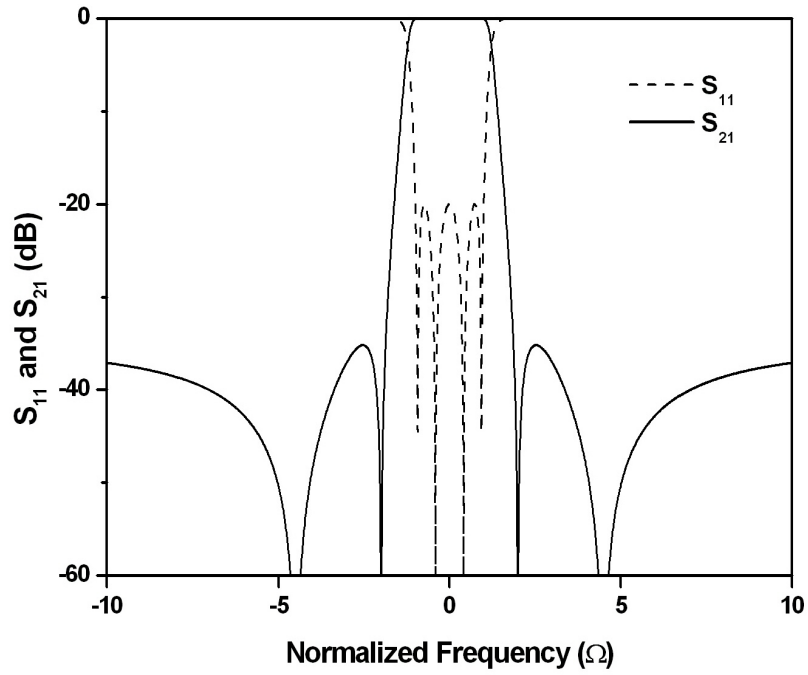


Figure 3.21: Frequency response of a lowpass filter prototype with no transmission zeros at infinite frequencies

positive $M_{1,4}$ and $M_{4,1}$:

$$M = \begin{bmatrix} 0 & 0.9488 & 0 & 0.1644 \\ 0.9488 & 0 & 0 & 0 \\ 0 & 0 & 0 & 0.9488 \\ 0.1644 & 0 & 0.9488 & 0 \end{bmatrix} \quad (3.32)$$

$$R = 0.1483.$$

In case that it is difficult to implement the negative coupling, it is preferred to have the coupling matrix whose elements are all positive such as (3.32). It is interesting to note that there is no direct coupling between resonator 2 and 3 in the coupling matrices in (3.31) and (3.32).

The filter with no transmission zeros at $\Omega' = 0$ can also be synthesized. This kind of

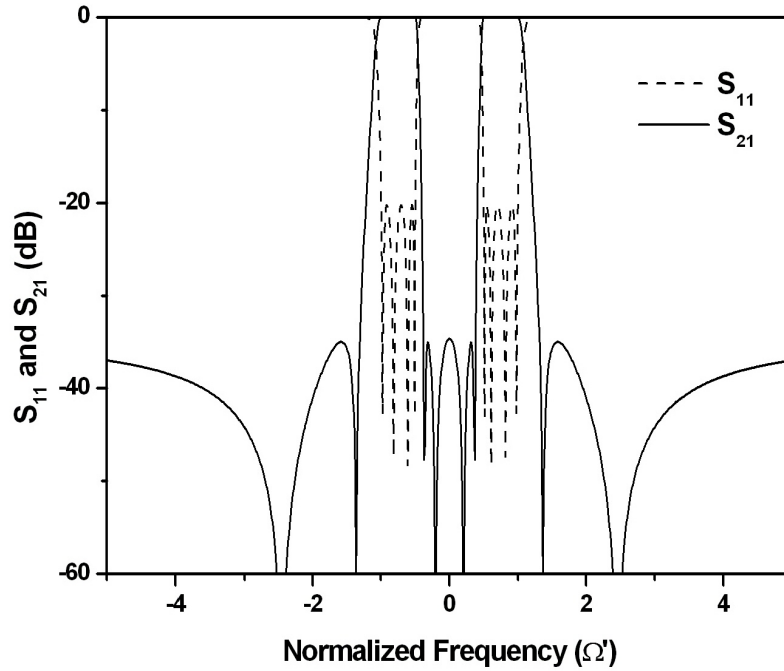


Figure 3.22: Frequency response of a dual-passband filter whose lowpass prototype is shown in Fig. 3.21.

filter can be designed with the lowpass prototype filter having no transmission zeros at infinite frequencies in Ω domain. Fig. 3.21 shows a 4th-order lowpass prototype filter with the transmission zeros at $\pm j2.0$ and $\pm j4.5$. Using the frequency transformation in (3.7), we can obtain the locations of the reflection zeros and transmission zeros of the dual-passband filter in Ω' domain and therefore its frequency response can be obtained as shown in Fig. 3.22. Based on the locations of the reflection zeros and transmission zeros in Ω' domain, the transfer function and coupling matrix can be obtained as described in the previous section. Since the 8th-order filter has 8 transmission zeros in finite frequencies, it might employ the coupling between source and load.

3.5 Asymmetric Dual-Passband Filter Design

We have dealt with a synthesis method for designing symmetric dual-passband filters. The frequency transformation for asymmetric dual-passband filters is given in [37], and it

is possible to obtain two desired passband characteristics. However, it is not clear whether equiripple responses both in the passband and stopband, which enables high frequency selectivity, can be achieved or not.

In this section, we briefly explain the frequency transformation for asymmetric dual-passband filters. The advantage of this frequency transformation is that the attenuation characteristics of low pass prototype is preserved. Therefore it is possible to obtain equiripple responses both in the passband and stopband. Fig. 3.23 shows typical transmission responses of an asymmetric dual-passband filter in Ω and Ω' domains. In Ω' domain, we have asymmetric passbands. Passbands are from -1 to Ω'_{ma} and from Ω'_{mb} to 1 , respectively. Fig. 3.23 shows for the case that $\Omega'_{ma} > 0$ and $\Omega'_{mb} > 0$. Ω'_{ma} and Ω'_{mb} are determined by predetermined passbands in ω or f domains as symmetric dual-passband case.

The frequency transformation for asymmetric dual-passband filters can be obtained by rewriting (3.7) in general form:

$$\begin{aligned}
 S &= \frac{S'}{e_1} + \frac{e_2}{S' - j\Omega'_z} & \text{for } \Omega' > \Omega'_z \\
 S &= - \left(\frac{S'}{e_3} + \frac{e_4}{S' - j\Omega'_z} \right) & \text{for } \Omega' < \Omega'_z
 \end{aligned} \tag{3.33}$$

where e_1 , e_2 , e_3 , and e_4 , are determined by the band edge frequencies in Ω' domain which are also determined by arbitrarily prescribed passbands of the filter. They can be found by solving the simultaneous equations:

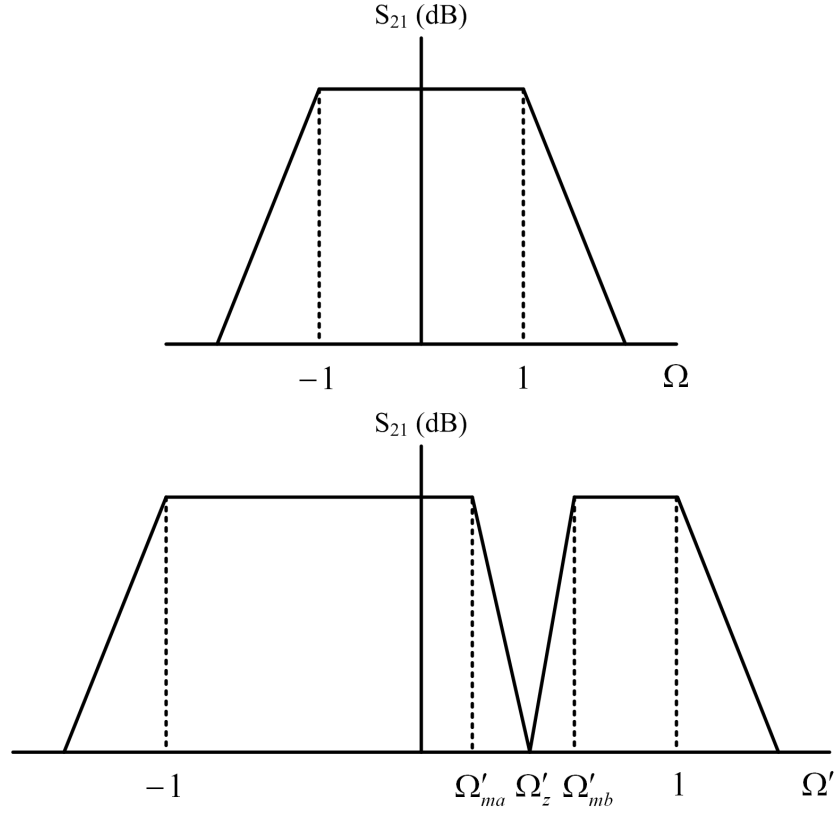
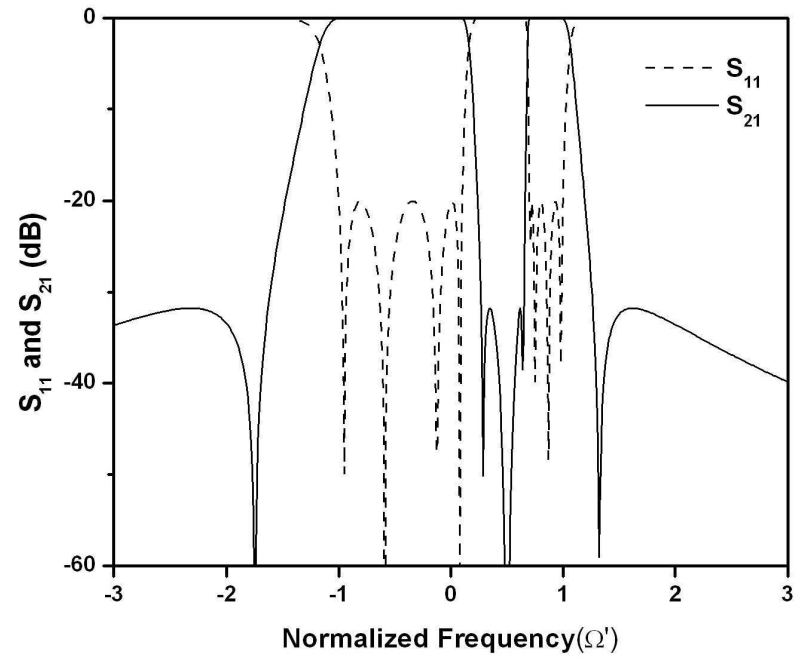


Figure 3.23: A typical transmission response of an asymmetric dual-passband filter in Ω and Ω' domains. Frequency transformation from Ω domain to Ω' domain is performed using (3.33) with $\Omega'_{ma} > 0$, $\Omega'_{mb} > 0$, and $\Omega'_z > 0$.

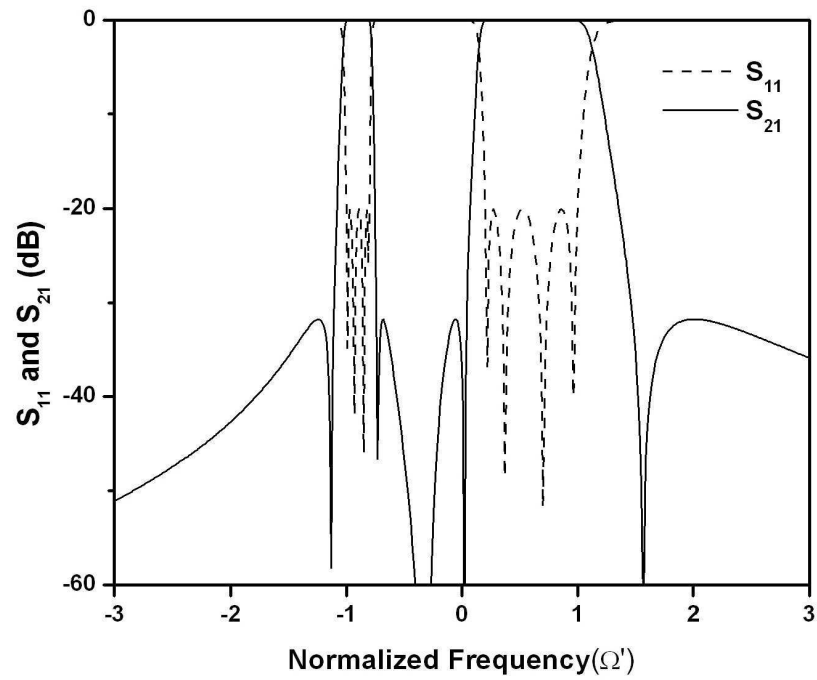
$$\begin{aligned}
 \frac{1}{e_1} - \frac{e_2}{1 - \Omega'_z} &= 1 \\
 \frac{\Omega'_{mb}}{e_1} - \frac{e_2}{\Omega'_{mb} - \Omega'_z} &= -1 \\
 \frac{1}{e_3} + \frac{e_4}{-1 - \Omega'_z} &= 1 \\
 -\frac{\Omega'_{ma}}{e_3} + \frac{e_4}{\Omega'_{ma} - \Omega'_z} &= -1.
 \end{aligned} \tag{3.34}$$

Upper frequency region and lower one is bisected by Ω'_z which can be chosen arbitrarily between Ω'_{ma} and Ω'_{mb} .

Fig. 3.24 shows the frequency response in Ω' domain using the frequency transformation in (3.33) and a lowpass filter prototype in Fig. 3.5. It should be noted that the



(a)



(b)

Figure 3.24: Frequency responses of asymmetric dual-passband filters in Ω' domain : (a) $\Omega'_{ma} = 0.1, \Omega'_{mb} = 0.7, \Omega'_z = 0.5$ (b) $\Omega'_{ma} = -0.8, \Omega'_{mb} = 0.2, \Omega'_z = -0.3$.

frequency transformation in (3.33) is very flexible in designing asymmetric dual-passband filters while preserving the attenuation characteristics of low pass prototype.

Based on the frequency transformation given in (3.33), the locations of the reflection zeros and transmission zeros can be found in Ω' domain, which makes it possible to obtain the transfer function and the coupling matrix.

3.6 Conclusions

This chapter describes a synthesis method for a symmetric dual-passband filter. Frequency transformations are established and applied to the lowpass filter prototype in order to obtain the frequency response of the dual-passband filter. For analytic filter synthesis, the frequency transformations have been given in terms of the prescribed passbands of the dual-passband filter.

To validate the presented synthesis method, the 8th-order dual-passband filter with 6 transmission zeros and two passbands of 3.90 - 3.95 GHz and 4.05 - 4.10 GHz has been designed, fabricated, and measured. The stripline structure has been used for filter design. The measured frequency response of the designed filter has shown a good agreement with the synthesized frequency response. This method has also been applied to the 4th-order dual-passband filter with 2 transmission zeros and 8th-order dual-passband filter with 8 transmission zeros to show the validity of the method.

The frequency transformation for symmetric dual-passband filters has been generalized for asymmetric dual-passband filters. This transformation is found to be flexible enough to allow for designing bandpass filters with two passbands of significantly different bandwidths.

CHAPTER 4

Triple-Passband Microwave Filter

4.1 Introduction

As modern communications systems use a complex arrangement of frequency allocation and spatial coverages, filters are required to have more complicated spectral responses such as elliptic function response for high frequency selectivity, self-equalized response for reduced group delay variation, and multiple-passband response for simultaneous transmission of multiple non-continuous channels.

Recently, microwave bandpass filters with two passbands have been reported. Dual-passband filters can be used to transmit two non-continuous channels through one beam to the same service coverage area. A dual-passband coaxial resonator filter was reported [34] and dual-mode dual-passband circular waveguide resonator filters for satellite applications were reported [11][35]. Furthermore, for reduced group delay variation in passbands, the synthesis method for a self-equalized dual-passband filter is presented in [36]. Analytic synthesis methods for dual-passband filters using frequency transformation techniques have also been of great interests [37][40][46]. However, these analytic synthesis methods are inadequate for designing triple-passband filters.

This work deals with developing a design methodology for triple-passband filters. A frequency transformation is developed for the synthesis of triple-passband filter. The trans-

fer function for the coupling matrix can be obtained from the frequency-transformed locations of reflection zeros and transmission zeros. In cases the frequency selectivity can be compromised, some transmission zeros can be removed to reduce the number of cross-couplings. A minor optimization (or trial-and-error method) is needed to obtain the required frequency response. The proposed method using frequency-transformed locations of reflection zeros and transmission zeros allows for rather accurate determination of initial values. Compared to the direct optimization, this makes it easy to find the desired transfer function with reduced number of transmission zeros. A 6th-order and a 12th-order triple-passband filters are synthesized to validate the proposed method. A 12th-order triple-passband filter is measured and the response shows a good agreement with theory. Finally, the frequency transformation for designing asymmetric triple-passband filters is given and discussed.

4.2 Design Theory

4.2.1 Transfer Fuction

It has been proved that the transmission zeros can be used to split a single passband into multiple passbands. Due to the transmission zeros, the characteristic function of multiple-passband filter can be written as a rational function:

$$K(S') = \frac{\prod_i (S' - S'_{fi})}{\prod_k (S' - S'_{pk})} \quad (4.1)$$

where $S' = j\Omega'$ and Ω' is normalized frequency for multiple-passband filter. S'_f and S'_p are reflection zeros and transmission zeros of the filter, respectively. This characteristic function determines the frequency response of the filter. With the given characteristic function, the transmitted power of the filter can be written as

$$|t(S')|^2 = \frac{1}{1 + \varepsilon'^2 |K(S')|^2} \quad (4.2)$$

where ε' is the ripple constant given by (3.21). Taking only the roots in left-half plane of S' domain, we can obtain the following form of the transfer function.

$$t(S') = \frac{1}{\varepsilon'} \frac{\sum_{i=0}^Z a_{zi} S'^i}{\sum_{k=0}^N a_{pk} S'^k} \quad (4.3)$$

where N and Z are the number of reflection zeros and transmission zeros, respectively. Here, it is assumed that $Z < N$.

The reflection zeros and transmission zeros of the triple-passband filter can be obtained by direct optimization method or analytic method depending on the filtering function. In the following section, we introduce a frequency transformation for finding the locations of reflection zeros and transmission zeros for a desired response analytically.

4.2.2 Frequency Transformation for Tripple-Passband Filters

Fig. 4.1 shows the frequency response of the filter in three different frequency domain. Ω is normalized frequency for single-passband lowpass prototype and Ω' is normalized frequency for triple-passband filter. ω domain is actual frequency domain where the filter operates.

The frequency transformation from Ω to Ω' can be expressed as follows [47]:

$$S = \frac{S'}{c_0} + \frac{c_1}{S' - j\Omega'_z} + \frac{c_1}{S' + j\Omega'_z} \quad (4.4)$$

where $S = j\Omega$ and unknown variables c_0 , c_1 , and Ω'_z are determined by Ω'_a and Ω'_b . Since we are interested in how Ω domain maps to Ω' domain, we rewrite (4.4) so that

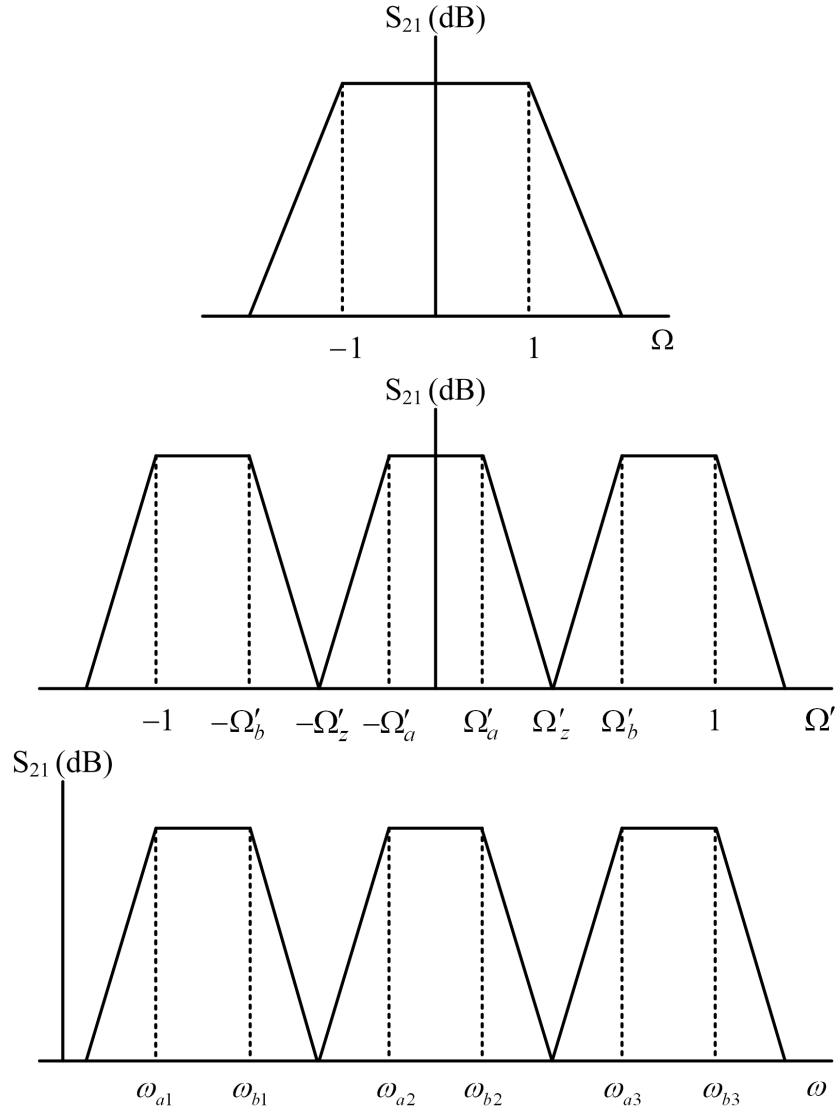


Figure 4.1: The frequency response of the filter in Ω , Ω' , and ω domain. The coupling matrix of the triple-passband filter is obtained from the transfer function in Ω' domain.

$$\Omega = \frac{\Omega'}{c_0} - \frac{c_1}{\Omega' - j\Omega'_z} - \frac{c_1}{\Omega' + j\Omega'_z}. \quad (4.5)$$

1 in Ω domain is transformed to 1 and Ω'_a in Ω' domain. Also, -1 in Ω domain is transformed to Ω'_b in Ω' domain. Therefore, unknown variables in (4.4) can be found by solving the following equations simultaneously.

$$\begin{aligned}
\frac{1}{c_0} - \frac{c_1}{1 - \Omega'_z} - \frac{c_1}{1 + \Omega'_z} &= 1 \\
\frac{\Omega'_b}{c_0} - \frac{c_1}{\Omega'_b - \Omega'_z} - \frac{c_1}{\Omega'_b + \Omega'_z} &= -1 \\
\frac{\Omega'_a}{c_0} - \frac{c_1}{\Omega'_a - \Omega'_z} - \frac{c_1}{\Omega'_a + \Omega'_z} &= 1.
\end{aligned} \tag{4.6}$$

Using (4.4), we can obtain the location of reflection zeros and transmission zeros in Ω' domain analytically. In the case that some of the transmission zeros in Ω' domain are redundant for satisfying the frequency selectivity, these might be removed and other remaining reflection zeros and transmission zeros can be adjusted.

The frequency transformation from Ω' domain to ω domain is well-known transformation and can be expressed as

$$S' = \frac{s}{d_1} + \frac{d_2}{s} \tag{4.7}$$

where $s = j\omega$. This frequency transformation can be rewritten as

$$\Omega' = \frac{\omega}{d_1} - \frac{d_2}{\omega}. \tag{4.8}$$

Considering the fact that 1 and -1 in Ω' domain is transformed to ω_{b3} and ω_{a1} , respectively, we can obtain d_1 and d_2 as follows:

$$\begin{aligned}
d_1 &= \omega_{b3} - \omega_{a1} \\
d_2 &= \frac{\omega_{a1}\omega_{b3}}{\omega_{b3} - \omega_{a1}}.
\end{aligned} \tag{4.9}$$

We can decide Ω'_a and Ω'_b from the fact that -1, $-\Omega'_b$, $-\Omega'_a$, Ω'_a , Ω'_b , and 1 in Ω' domain are transformed to ω_{a1} , ω_{b1} , ω_{a2} , ω_{b2} , ω_{a3} , and ω_{b3} , respectively. Frequency transformation given by (4.8) can also be expressed by using the real frequency variable as

$$\Omega' = \frac{f}{d_1} - \frac{d_2}{f} \quad (4.10)$$

where

$$\begin{aligned} d_1 &= f_{b3} - f_{a1} \\ d_2 &= \frac{f_{a1}f_{b3}}{f_{b3} - f_{a1}}. \end{aligned} \quad (4.11)$$

It is worth while mentioning that frequency transformation technique is for narrowband filters. Therefore, if bandwidths of passbands of the narrowband filter in Ω' domain are identical to each other, it can be approximated that the filter has three passbands with same bandwidth in ω or f domain.

4.3 Filter Synthesis

In this section, a 6th-order and a 12th-order triple-passband filters are synthesized to describe the presented filter synthesis theory.

4.3.1 6th-Order Filter

Fig. 4.2 shows 2nd-order single-passband lowpass prototype in Ω domain. A pair of transmission zeros are located at $S = \pm j25.0$ and return loss is set to be 20 dB. With the given transmission zeros and return loss, the reflection zeros of the filter can be easily found [39]. The reflection zeros are located at $S = \pm j0.707$. Using the frequency transformation given in (4.4), we can find the reflection zeros and transmission zeros of the triple-passband filter in Ω' domain. For $\Omega'_a = 0.055$ and $\Omega'_b = 0.890$, the unknown coefficients in (4.6) are $c_1 = 0.165$, $c_2 = 1.800$, and $\Omega'_z = 0.545$. Fig. 4.3 shows the normalized frequency response of the triple-passband filter. The reflection zeros and transmission zeros in Ω' domain are

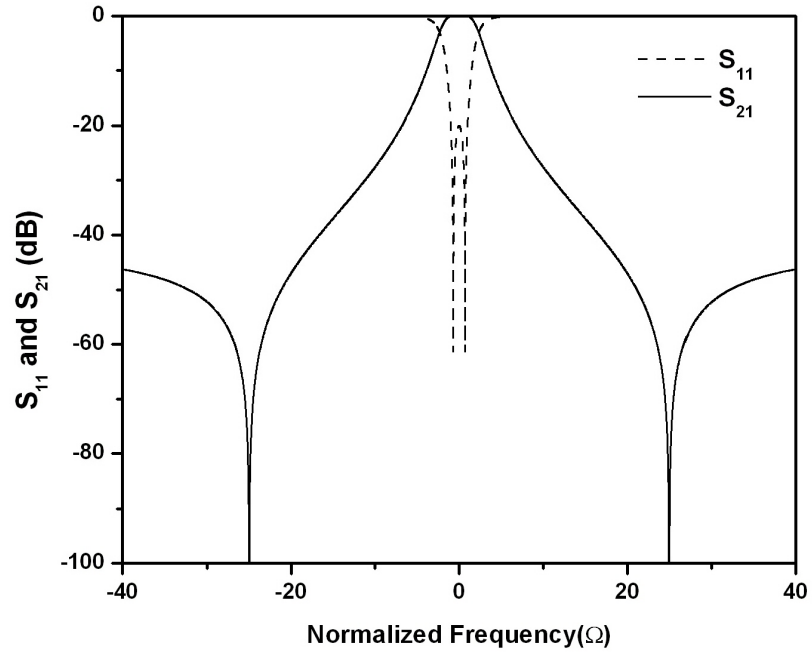


Figure 4.2: The frequency response of a 2nd-order lowpass filter prototype with the transmission zero at $\pm j25.0$ and return loss of 20 dB.

$$\begin{aligned}
 S'_{f1} &= -j0.9814, & S'_{f2} &= -j0.9038, & S'_{f3} &= -j0.0390, \\
 S'_{f4} &= +j0.0390, & S'_{f5} &= +j0.9038, & S'_{f6} &= +j0.9814, \\
 S'_{p1} &= -j4.2650, & S'_{p2} &= -j0.6102, & S'_{p3} &= -j0.4702, \\
 S'_{p4} &= +j0.4702, & S'_{p5} &= +j0.6102, & S'_{p6} &= +j4.2650.
 \end{aligned} \tag{4.12}$$

From (4.1)-(4.2) with obtained S'_{fi} and S'_{pk} in (4.12), the transfer function in the form of (4.3) can be obtained and the non-zero coefficients are as follows:

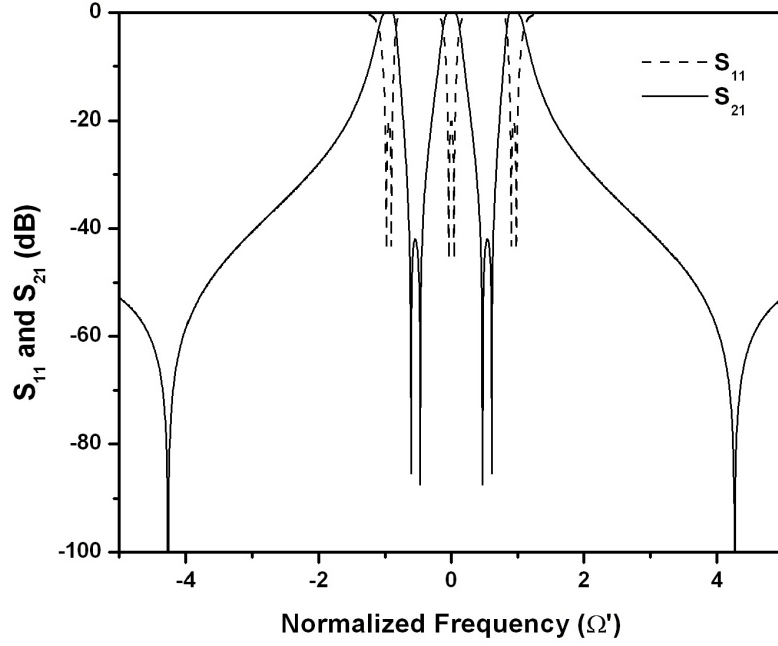


Figure 4.3: The frequency response of a lowpass filter prototype for triple-passband filter.

$$\begin{aligned}
 a_{z0} &= 1.497, & a_{z2} &= 10.877, & a_{z4} &= 18.784, \\
 a_{z6} &= 1.000, & a_{p0} &= 0.012, & a_{p1} &= 0.129, \\
 a_{p2} &= 0.862, & a_{p3} &= 0.583, & a_{p4} &= 1.904, \\
 a_{p5} &= 0.493, & a_{p6} &= 1.000, & \epsilon' &= 125.332.
 \end{aligned} \tag{4.13}$$

Since we have the transfer function in the form of (4.3), the coupling matrix can be obtained easily. Since this 6th-order filter transfer function has 6 transmission zeros, the filter can be implemented in canonical structure with a source-load coupling (see Fig. 4.4). We can also have another transfer function with reduced number of transmission zeros by removing some transmission zeros. The reason of removing some transmission zeros is to reduce the number of cross couplings. For example, we can remove a pair of transmission zeros at $\pm j4.265$ and, using simple trial-and-error (or optimization), the location of reflection zeros and transmission zeros for the desired frequency response can be obtained. To

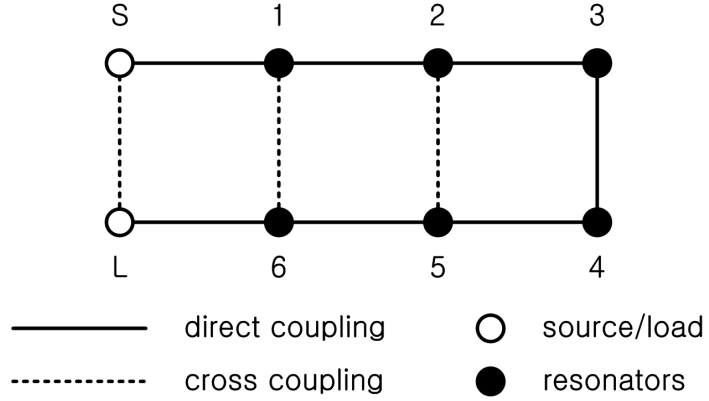


Figure 4.4: The coupling-routing diagram of 6th-order canonical structure filter with a source-load coupling.

preserve the bandwidth of the triple-passband filter, $S_{11}(-1)$ and $S_{11}(1)$ were set to -20 dB and the criteria of $-20.5 \text{ dB} < S_{11}(\Omega'_a \text{ and } \Omega'_b) < -19.5 \text{ dB}$ was used for rearrangement of reflection zeros and transmission zeros. Fig. 4.5 shows the frequency response of the triple-passband filter after removal of a pair of transmission zeros and small adjustment of reflection zeros and transmission zeros. The newly-obtained reflection zeros and transmission zeros in Ω' domain are

$$\begin{aligned}
 S'_{f1} &= -j0.9814, & S'_{f2} &= -j0.9039, & S'_{f3} &= -j0.0386, \\
 S'_{f4} &= +j0.0386, & S'_{f5} &= +j0.9039, & S'_{f6} &= +j0.9814, \\
 S'_{p1} &= -j0.6102, & S'_{p2} &= -j0.4760, & S'_{p3} &= +j0.4760, \\
 S'_{p4} &= +j0.6102.
 \end{aligned} \tag{4.14}$$

From (4.1), (4.2), and (4.14), the coefficients of the transfer function in the form of (4.3) for the frequency response in Fig. 4.5 can be obtained:

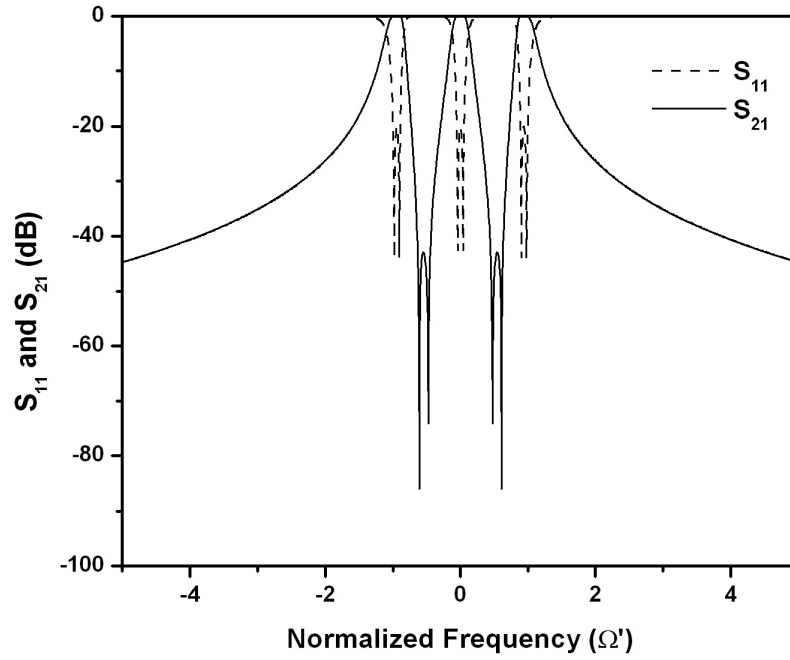


Figure 4.5: The frequency response of a lowpass filter prototype for triple-passband filter. This response is obtained by rearranging the reflection zeros and transmission zeros of the frequency response shown in Fig. 4.3 after removing a pair of outermost transmissions zeros.

$$\begin{aligned}
 a_{z0} &= 0.084, & a_{z2} &= 0.599, & a_{z4} &= 1.000, \\
 a_{p0} &= 0.012, & a_{p1} &= 0.128, & a_{p2} &= 0.861, \\
 a_{p3} &= 0.579, & a_{p4} &= 1.903, & a_{p5} &= 0.492, \\
 a_{p6} &= 1.000, & \epsilon &= 7.247.
 \end{aligned} \tag{4.15}$$

Since the frequency response shown in Fig. 4.5 has 4 transmission zeros, the filter can be implemented in a canonical structure without a source-load coupling. Hence, in this case, we can remove the source-load coupling shown in Fig. 4.4. The corresponding coupling matrix is given in (4.16).

$$\mathbf{M} = \begin{bmatrix} 0 & 0.7660 & 0 & 0 & 0 & -0.2805 \\ 0.7660 & 0 & 0.5431 & 0 & 0.0043 & 0 \\ 0 & 0.5431 & 0 & 0.0043 & 0 & 0 \\ 0 & 0 & 0.0043 & 0 & 0.5431 & 0 \\ 0 & 0.0043 & 0 & 0.5431 & 0 & 0.7660 \\ -0.2805 & 0 & 0 & 0 & 0.7660 & 0 \end{bmatrix} \quad (4.16)$$

$R = 0.2460.$

The reflection zeros and transmission zeros of the filter response in Fig.4.5 can be determined by direct optimization process. The convergence of the optimization depends on the initial values. Therefore, the reflection zeros and transmission zeros in Fig.4.3 which can be easily obtained by the proposed frequency transformation given by (4.4) are good initial values for an optimization process or trial-and-error approach.

4.3.2 12th-Order Filter

Fig. 4.6 shows the frequency response of a 4th-order single-passband lowpass prototype in Ω domain. A pair of transmission zeros are located at $S = \pm j2.0$ and the minimum return loss in the passband is set to be 20 dB. With the given transmission zeros and return loss, the reflection zeros of the filter can be easily found. The reflection zeros are located at $S = \pm j0.933$ and $S = \pm j0.406$. For $\Omega'_a = 0.20$ and $\Omega'_b = 0.60$, the unknown coefficients in (4.4) are $c_1 = 0.600$, $c_2 = 0.267$, and $\Omega'_z = 0.447$. Using the frequency transformation given in (4.4), we can find the reflection zeros and transmission zeros of the triple-passband filter in Ω' domain:

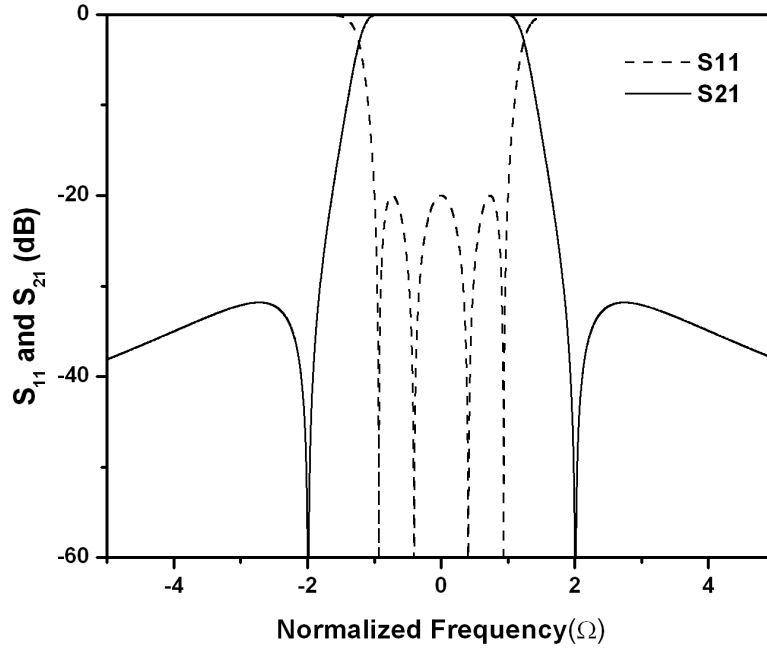


Figure 4.6: The frequency response of a 4th-order lowpass filter prototype with the transmission zero at $\pm j2.0$ and return loss of 20 dB.

$$\begin{aligned}
S'_{f1} &= -j0.9753, & S'_{f2} &= -j0.8108, & S'_{f3} &= -j0.6586, \\
S'_{f4} &= -j0.6052, & S'_{f5} &= -j0.1897, & S'_{f6} &= -j0.0912, \\
S'_{f7} &= +j0.0912, & S'_{f8} &= +j0.1897, & S'_{f9} &= +j0.6052, \\
S'_{f10} &= +j0.6586, & S'_{f11} &= +j0.8108, & S'_{f12} &= +j0.9753, \\
S'_{p1} &= -j1.4450, & S'_{p2} &= -j0.5480, & S'_{p3} &= -j0.4472, \\
S'_{p4} &= -j0.4472, & S'_{p5} &= -j0.3031, & S'_{p6} &= +j0.3031, \\
S'_{p7} &= +j0.4472, & S'_{p8} &= +j0.4472, & S'_{p9} &= +j0.5480, \\
S'_{p10} &= +j1.4450.
\end{aligned} \tag{4.17}$$

The frequency response in Ω' domain is shown in Fig. 4.7. Since the frequency response of 12th-order filter has 10 transmission zeros, the filter can be implemented in the canonical structure of which the coupling-routing diagram is shown in Fig. 4.8. As discussed in

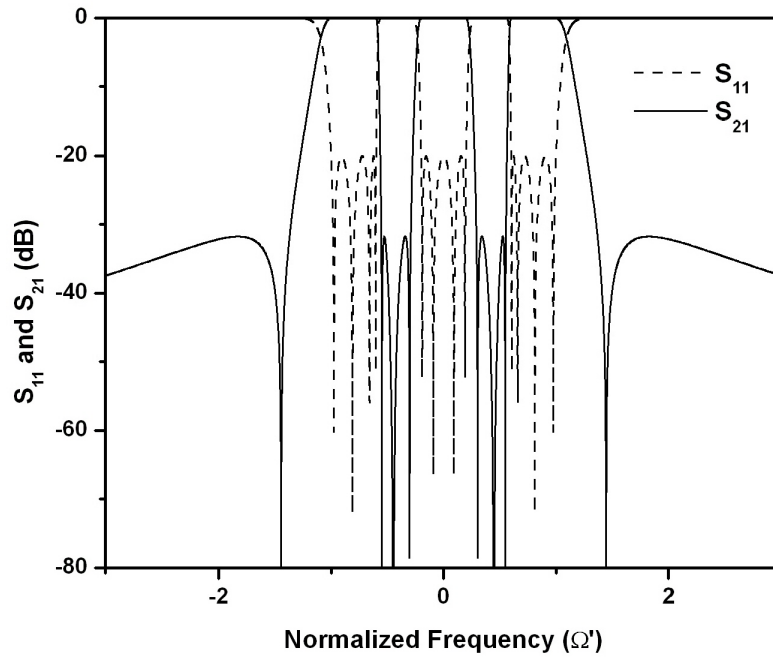


Figure 4.7: The frequency response of a lowpass filter prototype for triple-passband filter.

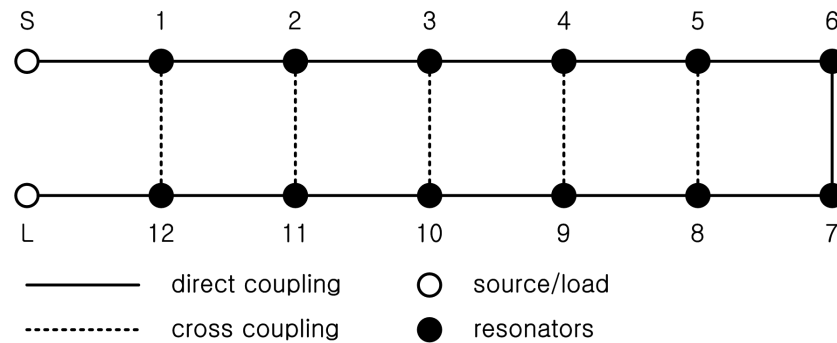


Figure 4.8: The coupling-routing diagram of 12th-order canonical structure filter.

the previous section, the transfer function can be extracted from the locations of reflection zeros and transmission zeros in Ω' domain and finally the coupling matrix can be obtained.

In previous section, we removed a pair of outermost transmission zeros to reduce the number of cross-coupled elements and rearranged the location of the reflection zeros and transmission zeros for required response. In this section, the transmission zeros in stopbands between two passbands are removed. In other word, the overlapped transmission zeros at $\pm\Omega'_z$ are removed and reflection zeros and transmission zeros are rearranged. The

rearranged reflection zeros and transmission zeros are

$$\begin{aligned}
S'_{f1} &= -j0.9900, & S'_{f2} &= -j0.9070, & S'_{f3} &= -j0.7550, \\
S'_{f4} &= -j0.6205, & S'_{f5} &= -j0.1890, & S'_{f6} &= -j0.0860, \\
S'_{f7} &= +j0.0860, & S'_{f8} &= +j0.1890, & S'_{f9} &= +j0.6205, \\
S'_{f10} &= +j0.7550, & S'_{f11} &= +j0.9070, & S'_{f12} &= +j0.9900, \\
S'_{p1} &= -j1.2000, & S'_{p2} &= -j0.3710, & S'_{p3} &= -j0.3050, \\
S'_{p4} &= +j0.3050, & S'_{p5} &= +j0.3710, & S'_{p6} &= +j1.2000.
\end{aligned} \tag{4.18}$$

From (4.1), (4.2), and (4.18), the coefficients of the transfer function in (4.3) can be obtained as follows:

$$\begin{aligned}
a_{z0} &= 0.018, & a_{z2} &= 0.345, & a_{z4} &= 1.671, \\
a_{z6} &= 1.000, & a_{p0} &= 0.0005, & a_{p1} &= 0.0046, \\
a_{p2} &= 0.0320, & a_{p3} &= 0.1398, & a_{p4} &= 0.4947, \\
a_{p5} &= 1.0655, & a_{p6} &= 2.3645, & a_{p7} &= 2.9682, \\
a_{p8} &= 4.4947, & a_{p9} &= 3.3058, & a_{p10} &= 3.5934, \\
a_{p11} &= 1.2589, & a_{p12} &= 1.0000.
\end{aligned} \tag{4.19}$$

Fig. 4.9 shows the frequency response of the filter with reduced number of the transmission zeros. Since the 12th-order filter has 6 transmission zeros, it can have the coupling-routing structure shown in Fig. 4.10. The coupling matrix of the frequency response shown in Fig. 4.9 is given in (4.20).

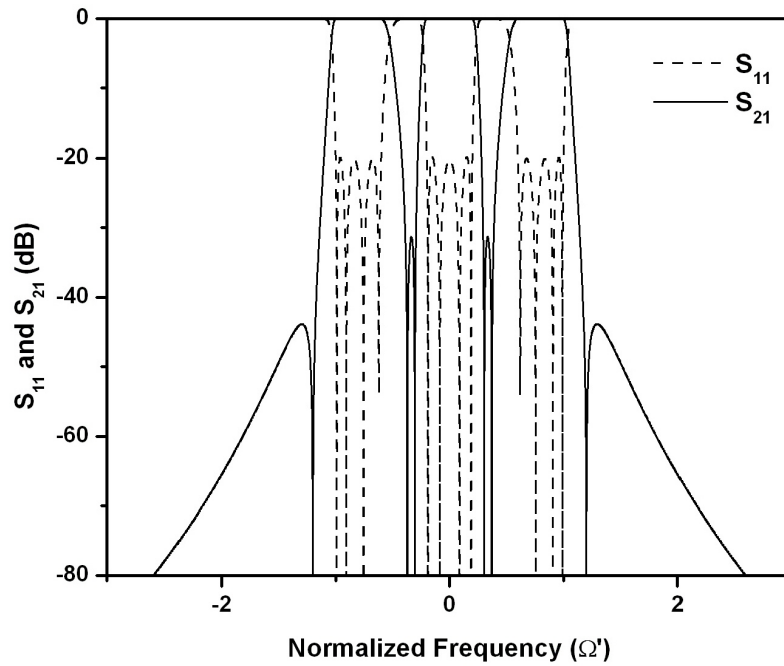


Figure 4.9: The frequency response of a lowpass filter prototype for triple-passband filter. This response is obtained by rearranging the reflection zeros and transmission zeros of the frequency response shown in Fig. 4.7 after removing repeated transmissions zeros at $\pm\Omega'_z$.

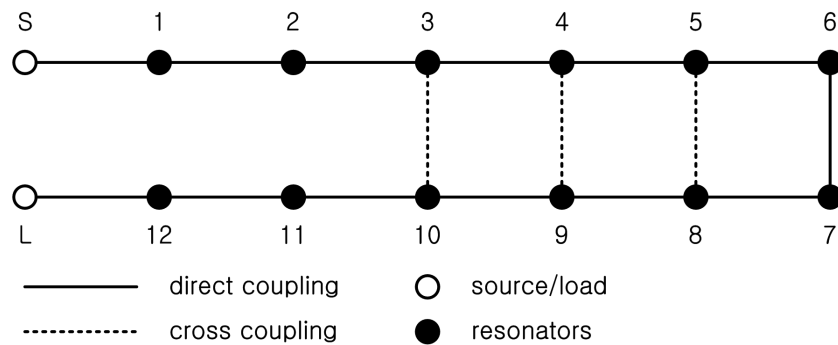


Figure 4.10: The coupling-routing diagram of 12th-order canonical structure filter.

$$\mathbf{M} = \begin{bmatrix}
0 & M_{1,2} & 0 & 0 & 0 & 0 & 0 & 0 & 0 & 0 & 0 & 0 \\
M_{1,2} & 0 & M_{2,3} & 0 & 0 & 0 & 0 & 0 & 0 & 0 & 0 & 0 \\
0 & M_{2,3} & 0 & M_{3,4} & 0 & 0 & 0 & 0 & 0 & M_{3,10} & 0 & 0 \\
0 & 0 & M_{3,4} & 0 & M_{4,5} & 0 & 0 & 0 & M_{4,9} & 0 & 0 & 0 \\
0 & 0 & 0 & M_{4,5} & 0 & M_{5,6} & 0 & M_{5,8} & 0 & 0 & 0 & 0 \\
0 & 0 & 0 & 0 & M_{5,6} & 0 & M_{6,7} & 0 & 0 & 0 & 0 & 0 \\
0 & 0 & 0 & 0 & 0 & M_{6,7} & 0 & M_{7,8} & 0 & 0 & 0 & 0 \\
0 & 0 & 0 & 0 & M_{5,8} & 0 & M_{7,8} & 0 & M_{8,9} & 0 & 0 & 0 \\
0 & 0 & 0 & M_{4,9} & 0 & 0 & 0 & M_{8,9} & 0 & M_{9,10} & 0 & 0 \\
0 & 0 & M_{3,10} & 0 & 0 & 0 & 0 & 0 & M_{9,10} & 0 & M_{10,11} & 0 \\
0 & 0 & 0 & 0 & 0 & 0 & 0 & 0 & 0 & M_{10,11} & 0 & M_{11,12} \\
0 & 0 & 0 & 0 & 0 & 0 & 0 & 0 & 0 & 0 & M_{11,12} & 0
\end{bmatrix}$$

$R = 0.6295.$

(4.20)

In (4.20), $M_{1,2} = M_{11,12} = 0.7558$, $M_{2,3} = M_{10,11} = 0.5568$, $M_{3,4} = M_{9,10} = 0.4677$, $M_{4,5} = M_{8,9} = 0.5718$, $M_{5,6} = M_{7,8} = 0.3003$, $M_{6,7} = 0.1301$, $M_{5,8} = -0.0022$, $M_{4,9} = 0.3638$, and $M_{3,10} = -0.1158$. In addition, the filter can be of cascaded-quadruplet structure (see Fig. 4.11), since the N th-order cascaded-quadruplet structure filter can realize up to $N/2$ transmission zeros. The corresponding coupling matrix is

$$\mathbf{M} = \begin{bmatrix}
0 & M_{1,2} & 0 & M_{1,4} & 0 & 0 & 0 & 0 & 0 & 0 & 0 & 0 \\
M_{1,2} & 0 & M_{2,3} & 0 & 0 & 0 & 0 & 0 & 0 & 0 & 0 & 0 \\
0 & M_{2,3} & 0 & M_{3,4} & 0 & M_{3,6} & 0 & 0 & 0 & 0 & 0 & 0 \\
M_{1,4} & 0 & M_{3,4} & 0 & M_{4,5} & 0 & 0 & 0 & 0 & 0 & 0 & 0 \\
0 & 0 & 0 & M_{4,5} & 0 & M_{5,6} & 0 & M_{5,8} & 0 & 0 & 0 & 0 \\
0 & 0 & M_{3,6} & 0 & M_{5,6} & 0 & M_{6,7} & 0 & 0 & 0 & 0 & 0 \\
0 & 0 & 0 & 0 & 0 & M_{6,7} & 0 & M_{7,8} & 0 & M_{7,10} & 0 & 0 \\
0 & 0 & 0 & 0 & M_{5,8} & 0 & M_{7,8} & 0 & M_{8,9} & 0 & 0 & 0 \\
0 & 0 & 0 & 0 & 0 & 0 & 0 & M_{8,9} & 0 & M_{9,10} & 0 & M_{9,12} \\
0 & 0 & 0 & 0 & 0 & 0 & M_{7,10} & 0 & M_{9,10} & 0 & M_{10,11} & 0 \\
0 & 0 & 0 & 0 & 0 & 0 & 0 & 0 & 0 & M_{10,11} & 0 & M_{11,12} \\
0 & 0 & 0 & 0 & 0 & 0 & 0 & 0 & M_{9,12} & 0 & M_{11,12} & 0
\end{bmatrix}$$

$R = 0.6295.$

(4.21)

In (4.21), $M_{1,2} = M_{11,12} = 0.6069$, $M_{2,3} = M_{10,11} = 0.3438$, $M_{3,4} = M_{9,10} = 0.3239$, $M_{4,5} = M_{8,9} = 0.5030$, $M_{5,6} = M_{7,8} = 0.0070$, $M_{6,7} = 0.7796$, $M_{1,4} = M_{9,12} = 0.4506$, $M_{3,6} =$

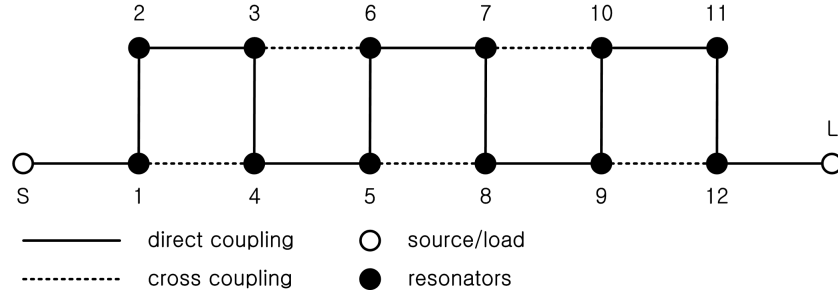


Figure 4.11: The coupling-routing diagram of 12th-order cascaded-quadruplet structure filter.

$$M_{7,10} = -0.4092, \text{ and } M_{5,8} = -0.3993.$$

4.4 Measurements

In this section, the measured result of the 12th-order triple-passband filters is discussed briefly. The coupling matrix obtained in the previous section, (4.20), is used for filter design. The microstrip open-loop resonators are adopted in filter design. The Rogers 5880 substrate with dielectric constant of 2.2 and dielectric thickness of 0.787 mm is used for filter design. Since the design procedure for microstrip open-loop resonator filters are well described in [48], it is not repeated in this thesis.

A 12th-order triple-passband filter is designed to have the center frequency of 2 GHz and the overall bandwidth ($f_{b3} - f_{a1}$) of 200 MHz. Fig. 4.12 shows the microstrip layout of the 12th-order triple-passband filter. The filter has microstripline open-loop resonators and each of them has a perimeter about one half-wavelength at the center frequency. Similar to coupled stripline open-loop resonators (See Chapter 3), coupled microstripline open-loop resonators can have electric coupling, magnetic coupling, and mixed coupling. In this filter design, positive sign is assigned to magnetic coupling and negative sign is assigned to electric coupling. Since $M_{3,10}$ and $M_{5,8}$ are negative, resonator 3 and resonator 10, and resonator 5 and resonator 8 have electric coupling structure. Also, resonator 4 and resonator 9, and resonator 6 and resonator 7 have magnetic coupling since $M_{4,9}$ and $M_{6,7}$ are positive.

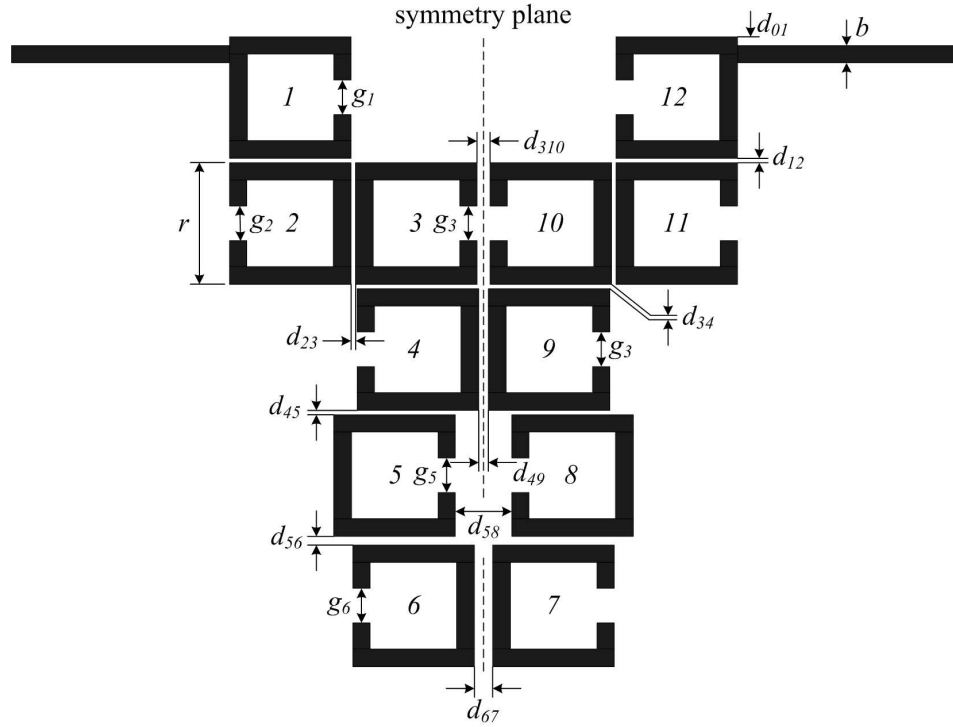
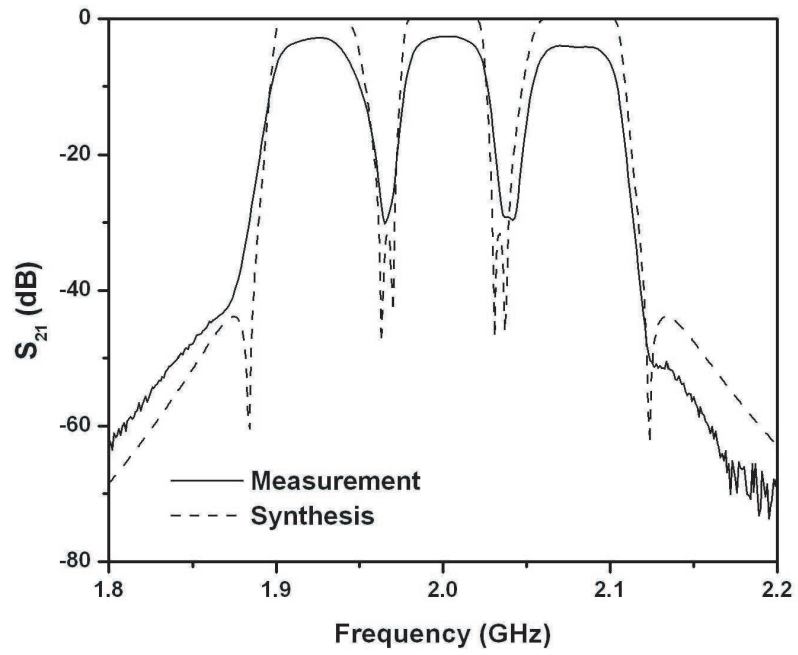


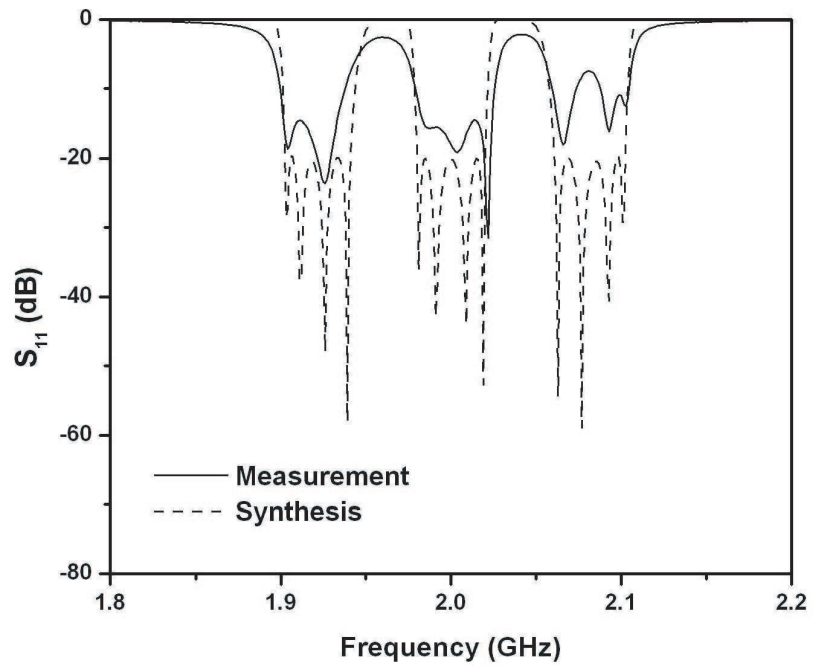
Figure 4.12: The microstrip layout of the 12th-order triple-passband open-loop resonator filter. $b = 2.42$, $r = 17.2$, $g_1 = 2.02$, $g_2 = g_3 = g_4 = g_5 = g_6 = 2.36$, $d_{01} = 0.30$, $d_{12} = 0.40$, $d_{23} = 0.70$, $d_{34} = 0.95$, $d_{45} = 0.52$, $d_{56} = 1.10$, $d_{67} = 3.00$, $d_{58} = 10.10$, $d_{49} = 1.36$, and $d_{310} = 2.10$. All dimensions are in mm.

Other direct couplings (couplings between consecutively-numbered resonators) can be either positive or negative as long as the signs of direct coupling values are symmetric with respect to the symmetric plane (see Fig. 4.12). For example, both $M_{1,2}$ and $M_{11,12}$ can be negative. Also, both $M_{2,3}$ and $M_{10,11}$ can be negative.

Fig. 4.13 show the measured results of the 12th-order triple-passband filter, respectively. Tuning process has been applied to the filter in order to compensate the errors. The potential sources of errors are frequency-dependent coupling coefficients, discrepancies between the actual and desired coupling coefficients, and unwanted couplings [49]. The tuning was mainly applied to the open gap of each resonator by trimming or using some tuning elements as described in [50]. It is shown that three passbands are established and the measured response agrees well with the synthesis results. Although this filter for demonstration has somewhat high insertion loss and rounded passband edges caused by



(a)



(b)

Figure 4.13: The measured and synthesized frequency response of the 12th-order triple-passband open-loop resonator filter.

finite Q-factor of resonators, its performance is good enough to show how the presented synthesis method works.

4.5 Asymmetric Triple-passband filter

Previous sections have dealt with triple-passband filters with symmetric frequency responses. In this section, the frequency transformation for asymmetric triple-passband filters is briefly discussed. Fig. 4.14 shows the transmission responses of an asymmetric triple-passband filter in Ω and Ω' domain. This filter has three passbands which are from -1 to Ω'_{b1} , from Ω'_{a1} to Ω'_{a2} , and from Ω'_{b2} to 1 , respectively. Fig. 4.14 shows the case of $\Omega'_{b1} < 0$, $\Omega'_{a1} < 0$, $\Omega'_{a1} > 0$, and $\Omega'_{b2} > 0$. For asymmetric triple-passband filters, the frequency transformation can be written as follows:

$$S = \frac{S' - j\Omega'_0}{c_0} + \frac{c_1}{S' - j\Omega'_{z1}} + \frac{c_2}{S' - j\Omega'_{z2}} \quad (4.17)$$

where unknown variables c_0 , c_1 , c_2 , Ω'_{z1} , Ω'_{z2} , and Ω'_0 can be determined by solving the following equations simultaneously.

$$\begin{aligned} \frac{1 - \Omega'_0}{c_0} - \frac{c_1}{1 - \Omega'_{z1}} - \frac{c_2}{1 - \Omega'_{z2}} &= 1 \\ \frac{\Omega'_{a2} - \Omega'_0}{c_0} - \frac{c_1}{\Omega'_{a2} - \Omega'_{z1}} - \frac{c_2}{\Omega'_{a2} - \Omega'_{z2}} &= 1 \\ \frac{\Omega'_{b1} - \Omega'_0}{c_0} - \frac{c_1}{\Omega'_{b1} - \Omega'_{z1}} - \frac{c_2}{\Omega'_{b1} - \Omega'_{z2}} &= 1 \\ \frac{\Omega'_{b2} - \Omega'_0}{c_0} - \frac{c_1}{\Omega'_{b2} - \Omega'_{z1}} - \frac{c_2}{\Omega'_{b2} - \Omega'_{z2}} &= -1 \\ \frac{\Omega'_{a1} - \Omega'_0}{c_0} - \frac{c_1}{\Omega'_{a1} - \Omega'_{z1}} - \frac{c_2}{\Omega'_{a1} - \Omega'_{z2}} &= -1 \\ \frac{-1 - \Omega'_0}{c_0} - \frac{c_1}{-1 - \Omega'_{z1}} - \frac{c_2}{-1 - \Omega'_{z2}} &= -1. \end{aligned} \quad (4.18)$$

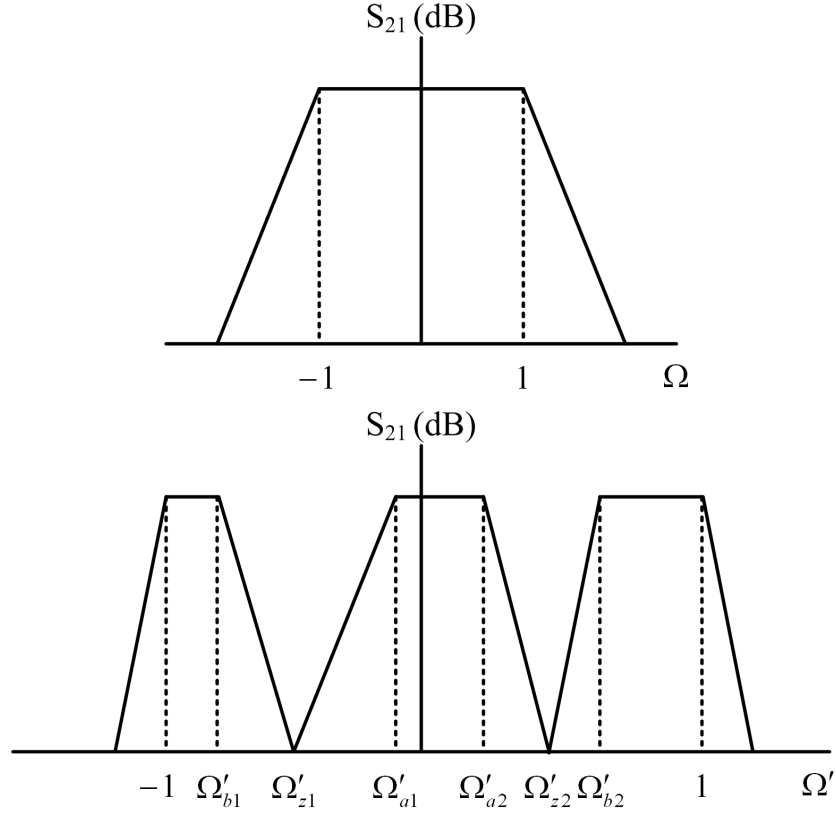


Figure 4.14: The frequency response of the asymmetric triple-passband filter in Ω and Ω' domain.

Fig. 4.15 shows the frequency response of the asymmetric triple-passband filter obtained by using the frequency transformation in (4.17) and a lowpass filter prototype in Fig. 4.6. Three passbands in the Ω' domain are set to be from -1 to $\Omega'_{b1} = -0.80$, from $\Omega'_{a1} = -0.05$ to $\Omega'_{a2} = 0.25$, and from $\Omega'_{b2} = 0.60$ to 1 , respectively. From (4.18), unknown variables are found as $c_0 = 0.4500$, $c_1 = 0.5709$, $c_2 = 0.2597$, $\Omega'_{z1} = -0.6087$, $\Omega'_{z2} = 0.4198$, and $\Omega'_0 = 0.1889$. Note that each passband can be designed to have arbitrary bandwidths.

4.6 Conclusions

This work have presented a synthesis method for triple-passband filters using frequency transformation. This synthesis method is based on the frequency transformation technique.

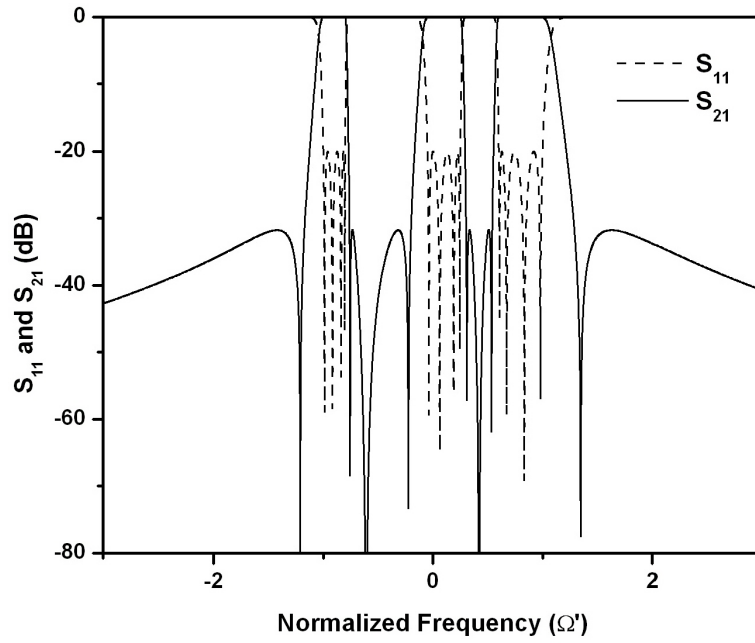


Figure 4.15: The frequency response of an asymmetric triple-passband filter in Ω' domain. $\Omega'_{b1} = -0.80$, $\Omega'_{a1} = -0.05$, $\Omega'_{a2} = 0.25$, and $\Omega'_{b2} = 0.60$.

A 6th-order and a 12th-order triple-passband filters have been synthesized to show the validation of the proposed synthesis approach. The measured result of the 12th-order microstrip open-loop resonator filter has shown a good agreement with the synthesized response. The frequency transformation for asymmetric triple-passband filters has also been presented for general cases. This frequency transformation has been found to be general enough to allow for designing triple-passband filters with arbitrary three passbands.

CHAPTER 5

Tunable Microwave Filter with a Constant Frequency Response

5.1 Introduction

Recently, tunable or reconfigurable microwave filters have found great demands for their applications in adhoc radios and agile radar systems. Diode varactors [51][52][53][54], MEMS (Micro-Electro-Mechanical Systems) capacitors [55][56], and BST (Barium-Strontium-Titanate) varactors [57] have been widely used as tuning elements for such filters.

One of the drawbacks of reported tunable filters is that the frequency response (or bandwidth) is not maintained as the center frequencies are adjusted. In these designs, only the resonant frequencies of resonators are adjusted without adjustment of coupling coefficients. In order to make filters with wide tuning range while maintaining their frequency response, not only the resonant frequencies of resonators but also the coupling coefficients among resonators should be adjusted. Hence, filter architectures that allow for placement of tuning elements for controlling the resonators and all coupling coefficients are needed. However, as the filter structure becomes complex, a systematic tuning strategy is required to achieve a prescribed frequency response.

Tunable filters with nearly same bandwidth over wide tuning range have been reported

recently [58][59]. Although, these filters do not have tuning elements in coupling structures, bandwidths are maintained nearly constant over tuning ranges. In [58], analytic approach to design a combline tunable filter with constant frequency response shape and bandwidth is reported. This design approach could remove the drawbacks of the filter reported in [53]. In [59], a two-pole tunable filter is presented and direct optimization method is used for designing coupling structures for constant bandwidth and insertion loss of the filter. However, a tunable filter with a prescribed filtering function (i.e. Butterworth, Chebyshev) cannot be designed using direct optimization method given in [59].

In this paper, an analytic design method is described for microstrip tunable filters. With this method, the tunable filter can be designed analytically with prescribed frequency response. Two two-pole tunable filters which have tuning range of 1.1 - 1.5 GHz and 2.1 - 2.7 GHz with Chebyshev response are designed for demonstration. Also, 3rd-order and 4th-order tunable filters are designed to show the validation of the proposed analytic design method.

5.2 Design Theory

Fig. 5.1 shows a schematic of a 2nd-order tunable microstrip filter introduced in [59]. This filter employs two step-impedance resonators which are coupled by capacitor circuits. In [59], the capacitance values are determined by an optimization method in order to keep a constant bandwidth and insertion loss within the tuning range.

In this section, we describe an analytic design method for tunable step-impedance microstrip resonator filters [60]. The proposed design method uses analytic approach, hence the optimization process is not required. Also, this method enables designers to realize a filter with prescribed filtering response, which is not easily done with optimization methods. The tunable filter is designed such that the center frequency can be adjusted from 1.1 GHz to 1.5 GHz and the equi-ripple bandwidth and return loss are kept constant to 20 MHz

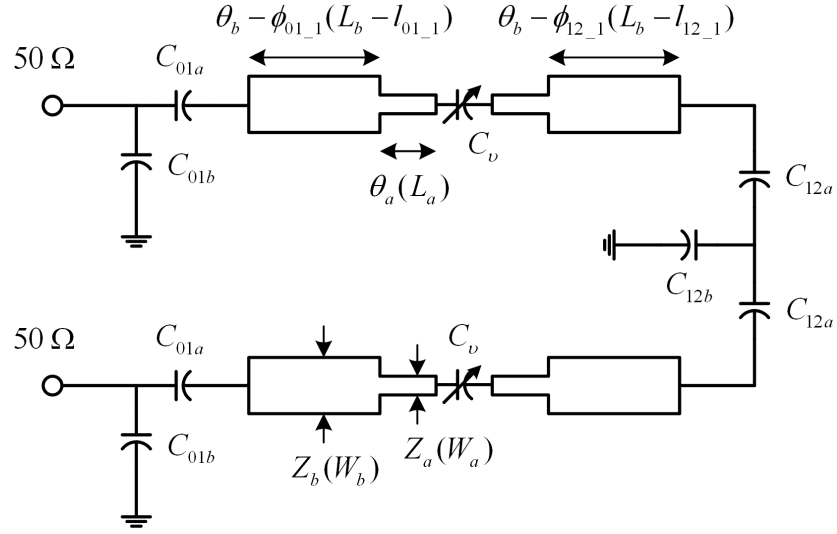


Figure 5.1: A schematic of 2nd-order tunable microstrip filter. Parameters in the parentheses are physical parameters.

and 20 dB, respectively. The filters discussed in this paper are assumed to be implemented on the substrate with the height of 1.28 mm and the dielectric constant of 6.15.

5.2.1 Step-Impedance Resonator

Step-impedance microstrip resonators have been widely applied to microstrip filter design for size reduction and harmonic control. Also, it has been shown that the step-impedance microstrip resonator can have wide tuning range based on varactors' position and the ratio of the length of low-impedance section and that of high-impedance section.

In this work, we use the step-impedance microstrip resonator shown in Fig. 5.2. For resonant frequency and slope parameter calculation, input admittance of the resonator should be derived. Input admittance of the resonator can be derived by using transmission line theory [16]. If fringe capacitance at open ends and parasitic inductance and capacitance at the step discontinuities are ignored, the input admittance, as seen from one end, is given by

$$Y_{in} = jB = jY_b \frac{N}{D} \quad (5.1)$$

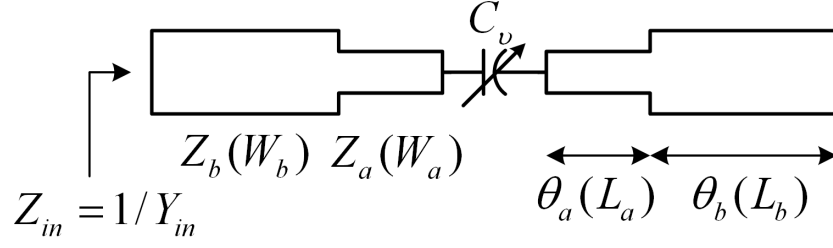


Figure 5.2: A symmetric step-impedance microstrip resonator loaded with a varactor.

where

$$\begin{aligned}
 Y_b &= 1/Z_b \\
 N &= \omega C_v (Z_a^2 Z_b (\tan \theta_b - \tan^2 \theta_a \tan \theta_b + \tan \theta_b \\
 &\quad - \tan^2 \theta_a \tan \theta_b) + 2Z_a \tan \theta_a (Z_b^2 - Z_a^2 \tan^2 \theta_b)) \\
 &\quad + (Z_a \tan \theta_b + Z_b \tan \theta_a)^2 \\
 D &= \omega C_v (Z_a^2 Z_b - 2Z_a^3 \tan \theta_a \tan \theta_b - Z_a^2 Z_b \tan^2 \theta_a \\
 &\quad - Z_a^2 Z_b \tan^2 \theta_b - 2Z_a Z_b^2 \tan \theta_a \theta_b \\
 &\quad + Z_a^2 Z_b \tan^2 \theta_a \tan^2 \theta_b) + Z_a^2 \tan \theta_b + Z_a Z_b \tan \theta_a \\
 &\quad - Z_a Z_b \tan \theta_a \tan^2 \theta_b - Z_b^2 \tan^2 \theta_a \tan \theta_b.
 \end{aligned} \tag{5.2}$$

The resonant frequency can be found by solving $N = 0$. Fig. 5.3 shows resonant frequencies of the step-impedance resonator with $L_a = 10$ mm, $L_b = 24.6$ mm, $W_a = 0.684$ mm ($Z_a = 80$ Ω), and $W_b = 7.274$ mm ($Z_b = 20$ Ω). The resonant frequencies of the step-impedance resonator are calculated to be from $f_1 = 1.079$ GHz to $f_2 = 1.518$ GHz as the capacitance of the varactor varies from 2.25 pF to 0.75 pF. Small discrepancies between the calculated and simulated resonant frequencies are due to the parasitic elements that were ignored in the analytical calculation.

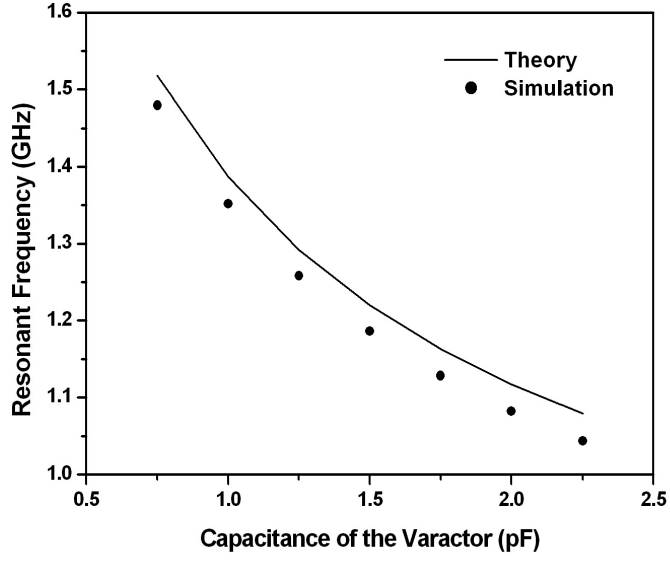


Figure 5.3: The resonant frequencies of the step-impedance resonator.

5.2.2 Coupling Elements

Fig. 5.4 shows a generalized N th-order bandpass filter circuit using admittance inverters. Admittance inverters are determined by the prescribed filter response and fractional bandwidth. For 2nd-order Chebyshev function with 20 dB return loss, the $(N+2) \times (N+2)$ coupling matrix is

$$\begin{aligned}
 \mathbf{M} &= \begin{bmatrix} 0 & M_{01} & 0 & 0 \\ M_{01} & 0 & M_{12} & 0 \\ 0 & M_{12} & 0 & M_{23} \\ 0 & 0 & M_{23} & 0 \end{bmatrix} \\
 &= \begin{bmatrix} 0 & 1.225 & 0 & 0 \\ 1.225 & 0 & 1.660 & 0 \\ 0 & 1.660 & 0 & 1.225 \\ 0 & 0 & 1.225 & 0 \end{bmatrix}.
 \end{aligned} \tag{5.3}$$

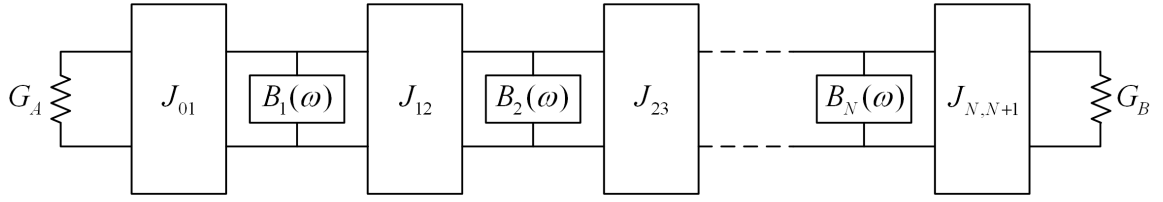


Figure 5.4: A generalized N th-order bandpass filter circuit with admittance inverters.

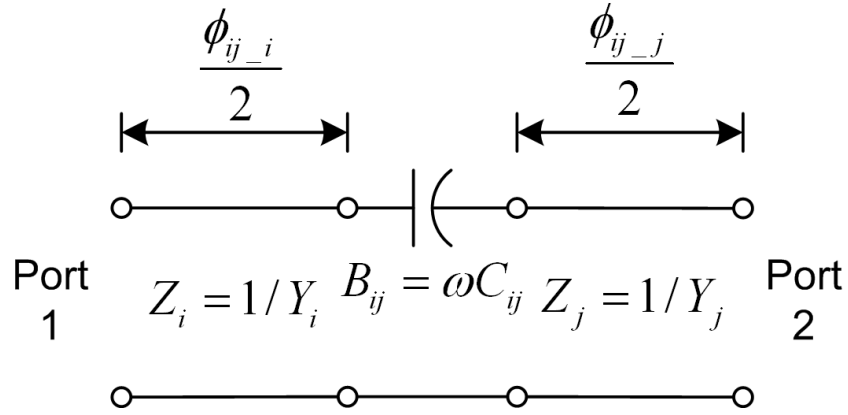


Figure 5.5: An inverter circuit with a series capacitor.

The values of the admittance inverters in terms of elements of the coupling matrix can be obtained from

$$J_{01} = \sqrt{\frac{Y_0 b}{Q_e}} = M_{01} \sqrt{Y_0 b \frac{BW}{f_0}} \quad (5.4)$$

$$J_{12} = M_{12} b \frac{BW}{f_0}$$

where f_0 , BW , and Q_e are the center frequency, the bandwidth, and the external quality factor of the filter, respectively. Also, b is slope parameter of the resonator defined by

$$b = \frac{\omega_0}{2} \left. \frac{dB(\omega)}{d\omega} \right|_{\omega=\omega_0} \quad (5.5)$$

and B is the imaginary part of the resonator input admittance given by (5.1).

There are numerous circuits useful as admittance inverters and a circuit shown in Fig. 5.5 is one of the inverting circuit for capacitor-coupled filters. With given values of admit-

Table 5.1: Design parameters for the 2nd-order tunable filter.

Parameter	f_1	f_2
$C_{01} = C_{23}$	1.861 pF	1.467 pF
$\phi_{01.1} = \phi_{23.2}$	-0.362 radian	-0.378 radian
C_{12}	0.912 pF	0.751 pF
$\phi_{12.1} = \phi_{12.2}$	-0.243 radian	-0.279 radian

tance inverters (J_{ij}), capacitance (C_{ij}) and electrical length of the transmission lines ($\phi_{ij.i}$, $\phi_{ij.j}$) can be calculated using the following equations:

$$\left| \frac{B_{ij}}{\sqrt{Y_i Y_j}} \right| = \frac{\frac{J_{ij}}{\sqrt{Y_i Y_j}}}{\sqrt{\left(1 - \left(\frac{J_{ij}}{Y_i}\right)^2\right) \left(1 - \left(\frac{J_{ij}}{Y_j}\right)^2\right)}}$$

$$\phi_{ij.i} = -\tan^{-1} \left(\frac{2 \frac{Y_j}{B_{ij}}}{\frac{Y_i}{Y_j} - \frac{Y_j}{Y_i} + \frac{Y_i Y_j}{B_{ij}^2}} \right) \quad (5.6)$$

$$\phi_{ij.j} = -\tan^{-1} \left(\frac{2 \frac{Y_i}{B_{ij}}}{\frac{Y_j}{Y_i} - \frac{Y_i}{Y_j} + \frac{Y_i Y_j}{B_{ij}^2}} \right).$$

If $Y_i = Y_j = Y_0$, (5.6) becomes well-known equations [22]:

$$\left| \frac{B_{ij}}{Y_0} \right| = \frac{\frac{J_{ij}}{Y_0}}{1 - \left(\frac{J_{ij}}{Y_0}\right)^2} \quad (5.7)$$

$$\phi_{ij.i} = \phi_{ij.j} = -\tan^{-1} \left(\frac{2B_{ij}}{Y_0} \right).$$

C_{ij} , $\phi_{ij.i}$, $\phi_{ij.j}$ computed at frequency f_1 and f_2 are summarized in Table 5.1. Since

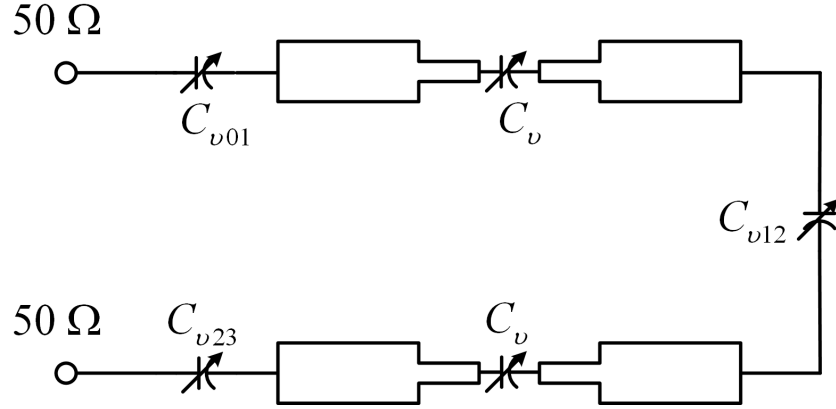


Figure 5.6: A 2nd-order tunable filter with varactors. C_{v01} , C_{v12} , and C_{v23} are for inverter circuit and C_v 's are for adjusting the resonant frequencies of the resonators.

C_{01} , C_{12} , and C_{23} should vary as center frequency of the filter changes, varactors can be used for C_{01} , C_{12} , and C_{23} . Therefore, if we can ignore the difference of ϕ 's at f_1 and f_2 , 2nd-order tunable step-impedance microstrip resonator filter can be designed as shown in Fig. 5.6. However, this filter requires that 5 varactors should be adjusted to have specific values as the center frequency is changed. To rectify this difficulty, an alternate approach is pursued. In this approach, fixed capacitors and transmission line segments are used whose frequency response closely follows those of the desired inverters. It was found that fixed-value capacitors instead of varactors can be used in the inverting circuits [59].

Fig. 5.7 shows the alternative circuit which corresponds to J_{01} inverter. In this filter design, $Z_i = Z_0 = 50 \Omega$ and $Z_j = Z_b$, since port 2 of the circuit in Fig. 5.7 is connected to the low-impedance (Z_b) transmission line section of the resonator. Since the circuit for J_{23} is symmetric to that for J_{01} , only the circuit for J_{01} is discussed in this work. The magnitude of S_{21} of the admittance inverter is given by

$$|S_{21}| = \frac{2 \frac{J_{01}}{\sqrt{Y_0 Y_b}}}{1 + \frac{J_{01}^2}{Y_0 Y_b}}. \quad (5.8)$$

The inverting circuit should have different S_{21} values as the center frequency of the filter is adjusted. In this work, we present simple method to determine the elements of the inverter

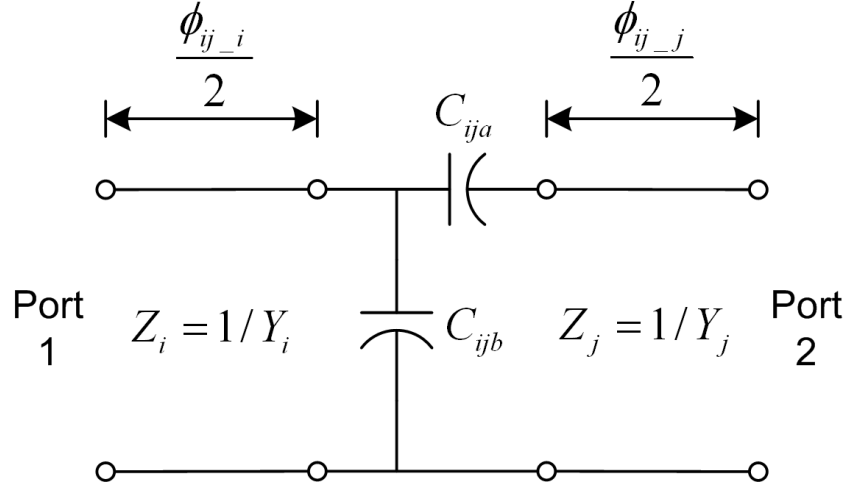


Figure 5.7: An inverter circuit for J_{01} inverter.

circuits. The capacitor values are determined such that the inverting circuit has required $|S_{21}|$ value at $f = f_1$ and $f = f_2$. S_{21} of the circuit in Fig. 5.7 is given by

$$S_{21}(\omega) = \frac{2}{\sqrt{\frac{Z_j}{Z_i} + \frac{1}{j\omega C_{ija}\sqrt{Z_i Z_j}} + j\omega C_{ijb}\sqrt{Z_i Z_j} + \left(1 + \frac{C_{ijb}}{C_{ija}}\right) \sqrt{\frac{Z_i}{Z_j}}}} \quad (5.9)$$

Therefore, simultaneous equations for determining C_{01a} and C_{01b} can be established as follows:

$$\left| \frac{2}{\sqrt{\frac{Z_b}{Z_0} + \frac{1}{j\omega_1 C_{ija}\sqrt{Z_0 Z_b}} + j\omega_1 C_{ijb}\sqrt{Z_0 Z_b} + \left(1 + \frac{C_{ijb}}{C_{ija}}\right) \sqrt{\frac{Z_0}{Z_b}}}} \right| = \frac{2 \frac{J_{01}}{\sqrt{Y_0 Y_b}}}{1 + \frac{J_{01}^2}{Y_0 Y_b}} \Bigg|_{\omega=\omega_1}$$

$$\left| \frac{2}{\sqrt{\frac{Z_b}{Z_0} + \frac{1}{j\omega_2 C_{ija}\sqrt{Z_0 Z_b}} + j\omega_2 C_{ijb}\sqrt{Z_0 Z_b} + \left(1 + \frac{C_{ijb}}{C_{ija}}\right) \sqrt{\frac{Z_0}{Z_b}}}} \right| = \frac{2 \frac{J_{01}}{\sqrt{Y_0 Y_b}}}{1 + \frac{J_{01}^2}{Y_0 Y_b}} \Bigg|_{\omega=\omega_2} \quad (5.10)$$

From (5.10), the values for the capacitors C_{01a} and C_{01b} are found to be $C_{01a}=2.883$ pF, $C_{01b}=1.601$ pF. $\phi_{01,0}$ and $\phi_{01,1}$ can be determined from phase of S_{11} and S_{22} of the capacitor circuit shown in Fig. 5.7. The transmission line sections are added to or absorbed into connecting transmission line on either side. Since the transmission line section of length $\phi_{01,0}$ is added to or absorbed into input feeding transmission line, length $\phi_{01,0}$ is meaningless. Therefore, only $\phi_{01,1}$ is needed and given by

$$\phi_{01,1}(\omega) = \tan^{-1}(S_{22}(\omega)) \quad (5.11)$$

where

$$S_{22}(\omega) = \frac{-\sqrt{\frac{Z_j}{Z_i}} + \frac{1}{j\omega_1 C_{ija} \sqrt{Z_i Z_j}} - j\omega C_{ijb} \sqrt{Z_i Z_j} + \left(1 + \frac{C_{ijb}}{C_{ija}}\right) \sqrt{\frac{Z_i}{Z_j}}}{\sqrt{\frac{Z_j}{Z_i}} + \frac{1}{j\omega_1 C_{ija} \sqrt{Z_i Z_j}} + j\omega C_{ijb} \sqrt{Z_i Z_j} + \left(1 + \frac{C_{ijb}}{C_{ija}}\right) \sqrt{\frac{Z_i}{Z_j}}}. \quad (5.12)$$

From (5.12), $\phi_{01,1}$ can be easily obtained at f_1 and f_2 : $\phi_{01,1}(\omega_1)=-0.430$ radian and $\phi_{01,1}(\omega_2)=-0.517$ radian. Since $\phi_{01,1}$ has negative values, the transmission line section needs to be absorbed into resonator 1, hence the resonator becomes shorter. Also $\phi_{01,1}$ has different values at different frequencies, hence the value of $l_{01,1}$ is chosen to be the average of $l_{01,1}(\omega_1)$ and $l_{01,1}(\omega_2)$.

Fig. 5.8 shows the circuit for J_{12} inverter. In this filter design, $Z_i = Z_j = Z_b$. Similarly to J_{01} inverter circuit, we can determine capacitor values by using the fact that S_{21} of the circuit shown in Fig. 5.8 is

$$S_{21}(\omega) = \frac{2}{2 + 2\frac{C_{ijb}}{C_{ija}} - \frac{j2\omega C_{ija} + j\omega C_{ijb}}{\omega^2 C_{ija}^2 Z_b} + j\omega C_{ijb} Z_b}. \quad (5.13)$$

Simultaneous equations for deciding C_{12a} and C_{12b} are

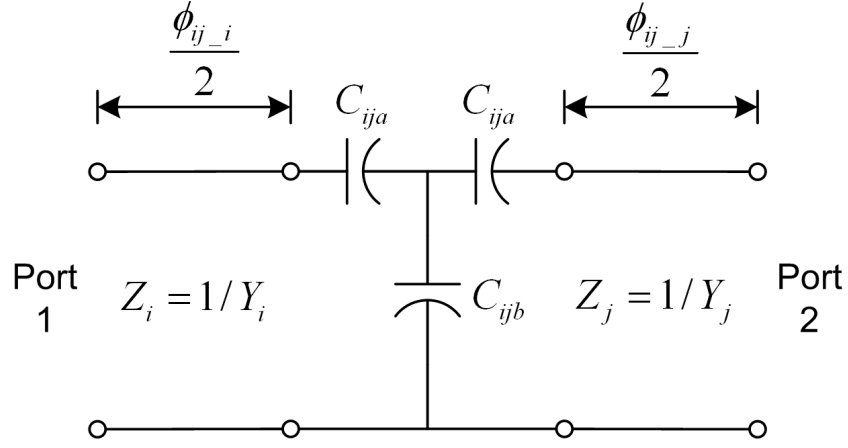


Figure 5.8: An inverter circuit for J_{12} inverter.

$$\left| \frac{2}{2 + 2\frac{C_{ijb}}{C_{ija}} - \frac{j2\omega C_{ija} + j\omega C_{ijb}}{\omega^2 C_{ija}^2 Z_b} + j\omega C_{ijb} Z_b} \right|_{\omega=\omega_1} = \frac{2\frac{J_{12}}{Y_b}}{1 + \frac{J_{12}^2}{Y_b^2}} \quad (5.14)$$

$$\left| \frac{2}{2 + 2\frac{C_{ijb}}{C_{ija}} - \frac{j2\omega C_{ija} + j\omega C_{ijb}}{\omega^2 C_{ija}^2 Z_b} + j\omega C_{ijb} Z_b} \right|_{\omega=\omega_2} = \frac{2\frac{J_{12}}{Y_b}}{1 + \frac{J_{12}^2}{Y_b^2}} .$$

The obtained results by solving (5.14) are $C_{12a}=5.244$ pF, $C_{12b}=13.053$ pF. Similarly, once the values of the capacitors are determined, we can also obtain $\phi_{12,1}$ and $\phi_{12,2}$ using the method applied to $\phi_{01,1}$.

5.2.3 Filter Performance

Fig. 5.1 shows an entire structure of the 2nd-order tunable microstrip filter and Table 5.2 summarizes design results from the proposed analytic approach. These design results are used in circuit simulation for validation of the proposed design method.

Fig. 5.9 shows the simulated frequency responses of the tunable filter designed using the proposed analytic approach. Circuit simulation has been performed using Agilent

Table 5.2: Design result of the tunable filter.

Parameter	Values
L_a	10.000 mm
$L_b-l_{01.1}$	20.244 mm
$L_b-l_{12.1}$	14.155 mm
Z_a	80 Ω
Z_b	20 Ω
C_{01a}	2.883 pF
C_{01b}	1.601 pF
C_{12a}	5.244 pF
C_{12b}	13.053 pF

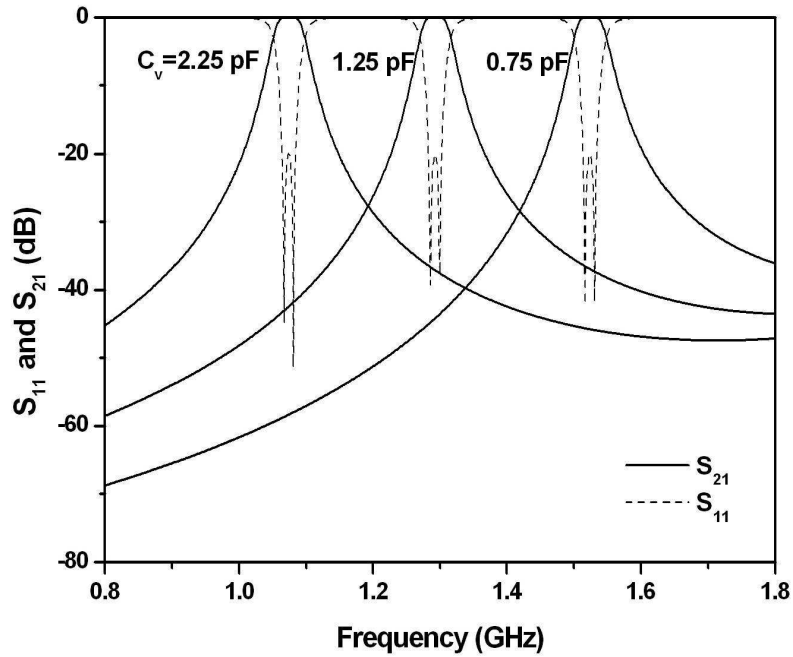


Figure 5.9: Frequency responses of the 2nd-order tunable filter.

Advanced Design System. Since the goal of this work is to provide the design method for tunable filters with prescribed frequency responses, loss factors and other parasitic elements were not taken into account in Fig. 5.9 in order to observe whether the frequency responses varies as the center frequencies of the filters are adjusted by varactors. It is observed that the frequency response of the filter designed using the proposed method rarely

Table 5.3: Design parameters for the 2nd-order tunable filter.

parameter	f_1	f_2
$C_{01} = C_{23}$	0.669 pF	0.602 pF
$\phi_{01.1} = \phi_{23.2}$	-0.295 radian	-0.323 radian
C_{12}	0.269 pF	0.265 pF
$\phi_{12.1} = \phi_{12.2}$	-0.141 radian	-0.178 radian

changes as the center frequency is adjusted by two varactors which are located at the center of each resonator. It is worth mentioning that capacitance of fixed value capacitors can be determined analytically to make the tunable filter have prescribed filtering function.

5.3 Design Example and Measurement

In this section, the design and measurement results of a 2nd-order tunable filter which can be tuned from 2.1 GHz to 2.7 GHz are described for the validation of the presented design method. Also, we discuss practical parameters which need to be considered in actual application. The dielectric constant of the substrate is 6.15 and the dielectric thickness is 1.28 mm (Rogers RO3006). The filter is designed to have Chebyshev function response with 20 dB return loss and the corresponding $(N + 2) \times (N + 2)$ coupling matrix is given in (5.3).

Using the coupling matrix in (5.3) and (5.4)-(5.7), we can compute the required C 's and ϕ 's and they are summarized in Table 5.3. Resonant frequencies and slope parameters are extracted from simulation for accurate design. C_{12} have almost the same value at f_1 and f_2 but C_{01} and C_{23} should vary as center frequency of the filter is adjusted. Therefore, instead of using the capacitor circuit shown in Fig. 5.8, we can use single fixed-value capacitor for C_{12} and set C_{12} value to the average value of those required at f_1 and f_2 for J_{12} inverter. Since two resonators are juxtaposed in layout design, there is gap capacitance between resonators. Hence, C_{12} value should be chosen to be smaller than calculated value. For J_{01}

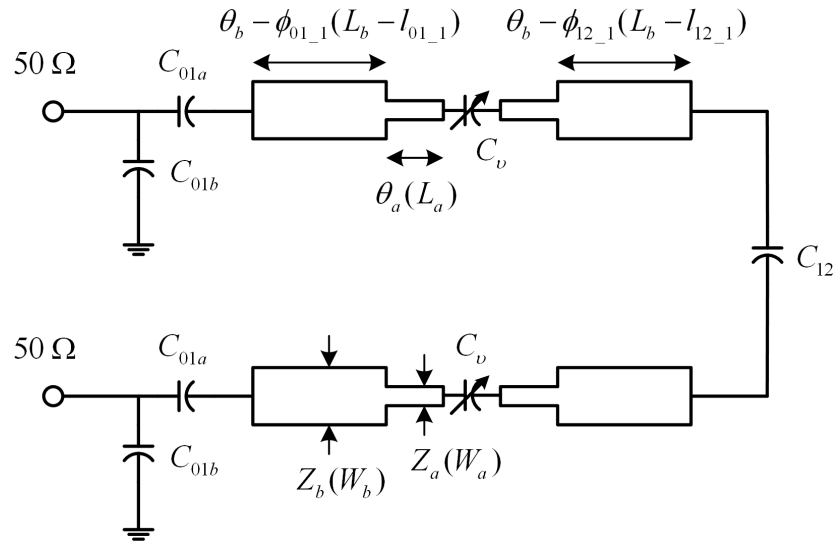


Figure 5.10: The schematic of the 2nd-order tunable microstrip filter.

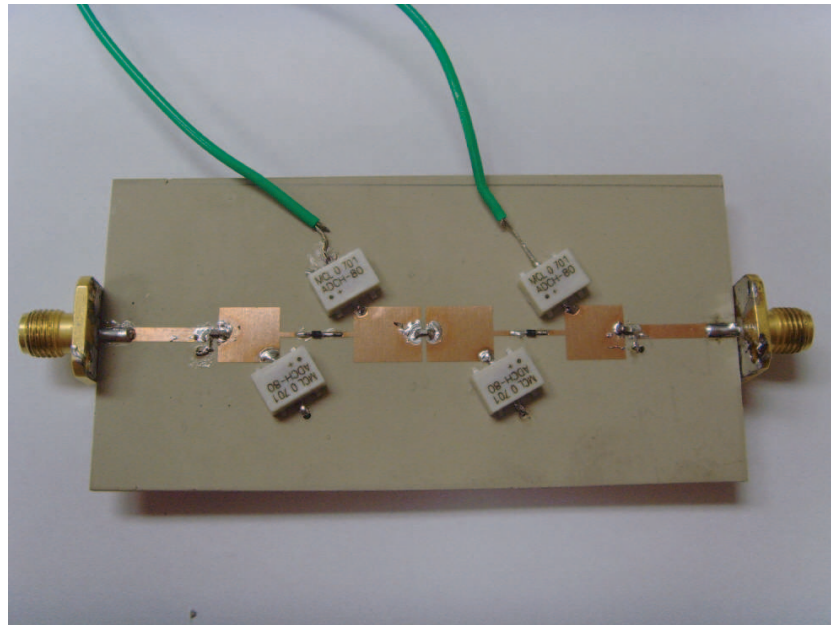
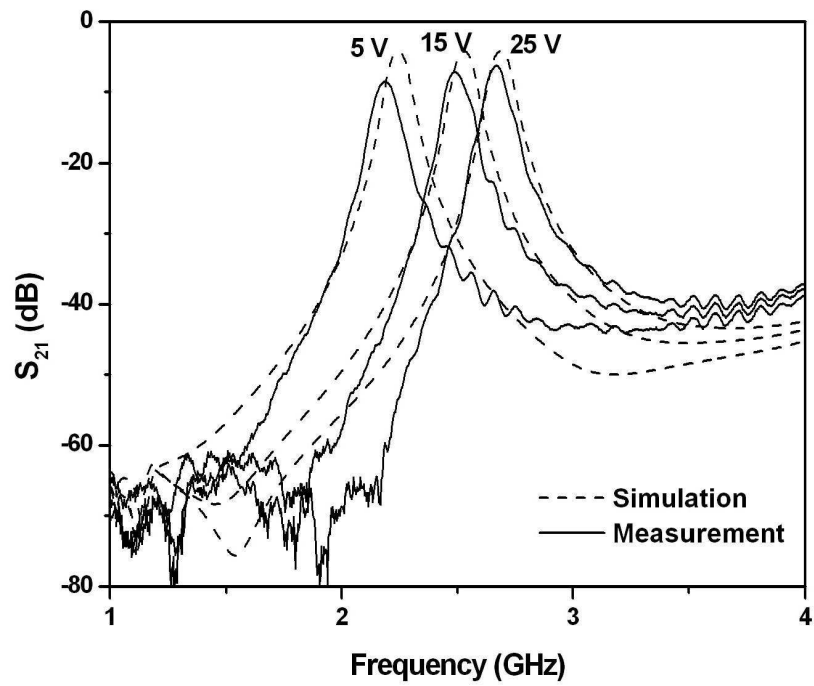


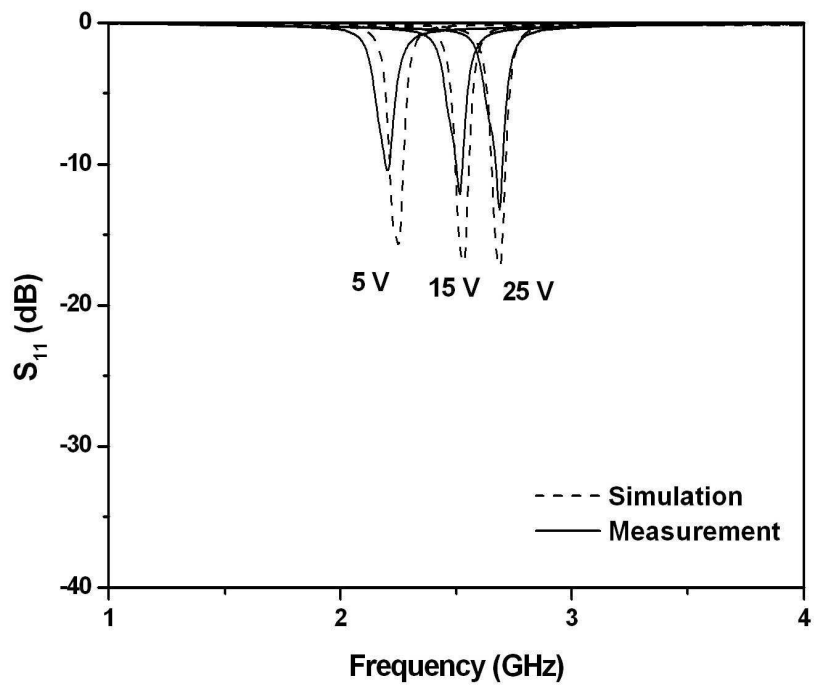
Figure 5.11: The fabricated 2nd-order tunable microstrip filter.

and J_{23} inverter, the capacitor circuit shown in Fig. 5.7 is employed. From (5.10)-(5.12), design parameters are found to be $C_{01a} = 0.831$ pF, $C_{01b} = 0.556$ pF, $\phi_{01_1}(\omega_1) = -0.317$ radian, and $\phi_{01_1}(\omega_2) = -0.366$ radian. l 's are determined to be the average of $l(\omega_1)$ and $l(\omega_2)$.

Fig. 5.10 and Fig. 5.11 show the structure of the 2nd-order tunable microstrip filter and



(a)



(b)

Figure 5.12: Measured and simulated frequency responses of the 2nd-order tunable microstrip resonator filter.

the fabricated filter, respectively. Skyworks varactor SMV1405 is used in this design. The measured frequency responses are compared with the simulated ones in Fig. 5.12. Tuning voltage (V_t) has been increased from 0.5 V to 2.5 V. Electromagnetic field simulation result has been obtained by using Zeland IE3D. Due to the insertion loss of the filter, 3-dB bandwidths, instead of equi-ripple bandwidth, have been observed. 90 MHz 3-dB bandwidth has been observed within whole tuning range in simulation result. Also, it has been measured to be 93.75 MHz at $V_t=0.5$ V and 1.5 V, and 86.25 MHz at $V_t=2.5$ V. We have small bandwidth variation in measurement while the bandwidth is constant in simulation. This is due to the fact that commercially available capacitors which have nearest capacitance values to the desired ones are used in filter fabrication. Also, small discrepancies between simulation and measurement can be attributed to the fabrication error and the tolerances of the capacitors. It should be noted that the shape of frequency responses are maintained within wide tuning range (about 30%).

5.4 Design of Higher-Order Filters

In this section, application of the proposed design method to the higher-order tunable filter is described. The design procedure described in the Section 5.2 is applied to 3rd-order and 4th-order tunable filter design. Also, 20 MHz equi-ripple bandwidth is used in filter design.

For 3rd-order and 4th-order Chebyshev response with 20 dB return loss, the $(N + 2) \times (N + 2)$ coupling matrices are

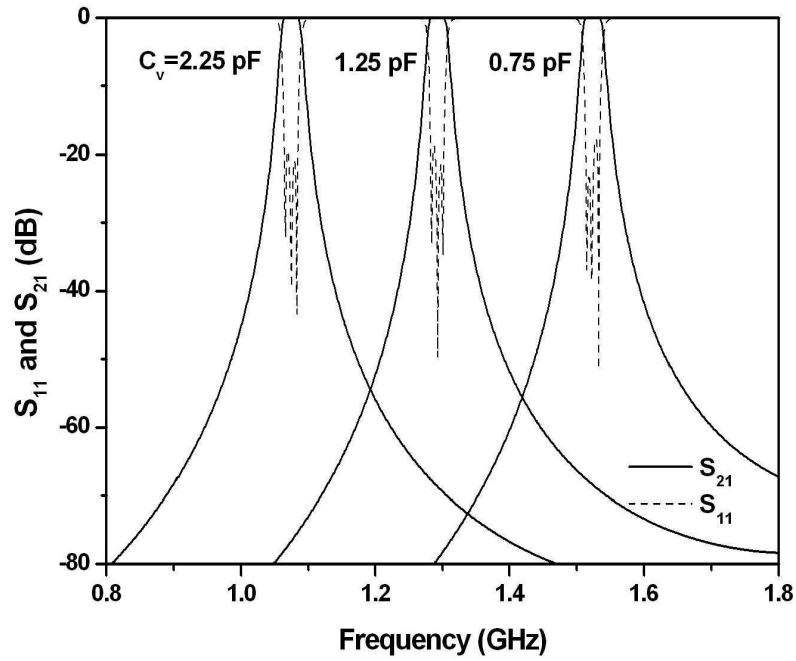


Figure 5.13: Frequency response of a 3rd-order tunable filter. The design parameters are $L_b-l_{01-1}=20.368$ mm, $L_b-l_{12-1}=14.125$ mm, $Z_a=80$ Ω , $Z_b=20$ Ω , $C_{01a}=2.527$ pF, $C_{01b}=1.929$ pF, $C_{12a}=4.751$ pF, $C_{12b}=21.701$ pF. Since the circuit is symmetric, only half of the design parameters are provided.

$$\mathbf{M} = \begin{bmatrix} 0 & 1.082 & 0 & 0 & 0 \\ 1.082 & 0 & 1.030 & 0 & 0 \\ 0 & 1.030 & 0 & 1.030 & 0 \\ 0 & 0 & 1.030 & 0 & 1.082 \\ 0 & 0 & 0 & 1.082 & 0 \end{bmatrix} \quad (5.15)$$

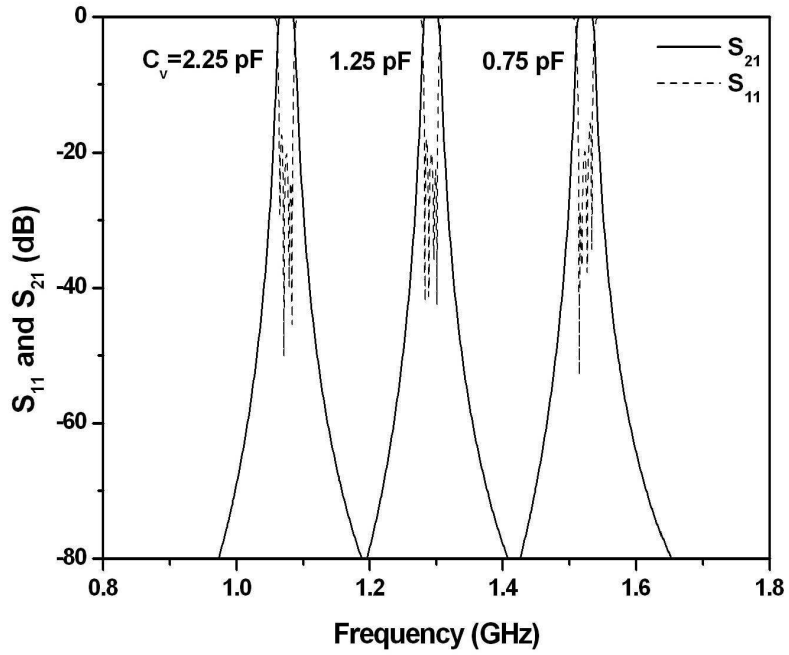


Figure 5.14: Frequency response of a 4th-order tunable filter. The design parameters are $L_b-l_{01,1}=20.424$ mm, $L_b-l_{12,1}=14.130$ mm, $L_b-l_{23,2}=14.130$ mm, $Z_a=80$ Ω , $Z_b=20$ Ω , $C_{01a}=2.416$ pF, $C_{01b}=2.028$ pF, $C_{12a}=4.658$ pF, $C_{12b}=24.616$ pF, $C_{23a}=4.497$ pF, $C_{23b}=32.207$ pF. Since the circuit is symmetric, only half of the design parameters are provided.

$$\mathbf{M} = \begin{bmatrix} 0 & 1.035 & 0 & 0 & 0 & 0 \\ 1.035 & 0 & 0.911 & 0 & 0 & 0 \\ 0 & 0.911 & 0 & 0.700 & 0 & 0 \\ 0 & 0 & 0.700 & 0 & 0.911 & 0 \\ 0 & 0 & 0 & 0.911 & 0 & 1.035 \\ 0 & 0 & 0 & 0 & 1.035 & 0 \end{bmatrix}. \quad (5.16)$$

Based on the coupling matrix and the design procedure described in the previous section, the higher-order tunable filter can also be designed analytically with ease and the simulated frequency responses for the 3rd-order and 4th-order tunable filter are shown in Fig. 5.13 and Fig. 5.14, respectively. In order to show the validity of the proposed design approach,

circuit simulation has been performed using Agilent Advanced Design System. It is shown that the equi-ripple bandwidth is preserved to be 20 MHz with small variation of the return loss over the whole frequency tuning range. Small variation of the return loss is attributed to the approximation made on determining l 's. It can be concluded that this proposed design method make it possible to design higher-order filter analytically and results in same bandwidth with acceptable small variation of the return loss over the entire frequency tuning range.

5.5 Conclusions

In this chapter, an analytic design method for N th-order tunable filters using step-impedance microstrip resonators is presented. For constant frequency response shape and bandwidth over the tuning range, inter-resonator coupling structure and external coupling structures are designed to have specified coupling coefficients at lowest and highest center frequencies.

A 2nd-order tunable microstrip filter which can be tuned from 1.1 to 1.5 GHz has been designed for demonstration of the presented design theory. Also, a 2.1-2.7 GHz tunable filter has been designed and measured to show the validity of the design method. The measured responses agreed well with the simulated ones.

Finally, design results of 3rd-order and 4th-order tunable filters are provided to show that the proposed design method can also be applied to higher-order tunable filter design.

Although this work presents the design theory for bandpass filters coupled by admittance inverters, it can be easily modified for the filters coupled by impedance inverters.

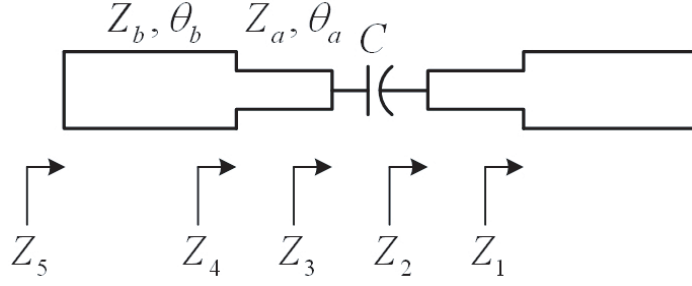


Figure 5.15: A capacitor-loaded step impedance microstrip resonator.

5.6 Appendix I: Step Impedance Resonator

This section provides the equations for deriving the input impedance of the step-impedance microstrip resonator shown in Fig. 5.15. Input impedance at each step discontinuity is derived as follows:

$$Z_1 = \frac{Z_b}{j \tan \theta_b} \quad (5.17)$$

$$\begin{aligned} Z_2 &= Z_a \frac{Z_1 + j Z_a \tan \theta_a}{Z_a + j Z_1 \tan \theta_a} \\ &= Z_a \frac{\frac{Z_b}{j \tan \theta_b} + j Z_a \tan \theta_a}{Z_a + \frac{Z_b \tan \theta_a}{\tan \theta_b}} \\ &= \frac{Z_a Z_b - Z_a \tan \theta_b \tan \theta_a}{j Z_a \tan \theta_b + Z_b \tan \theta_a} \end{aligned} \quad (5.18)$$

$$\begin{aligned} Z_3 &= \frac{Z_a Z_b - Z_a \tan \theta_a \tan \theta_b}{j Z_a \tan \theta_b + Z_b \tan \theta_a} + \frac{1}{j \omega C} \\ &= \frac{Z_a Z_b \omega C - Z_a^2 \tan \theta_a \tan \theta_b \omega C + Z_a \tan \theta_b + Z_b \tan \theta_a}{j \omega C (Z_a \tan \theta_b + Z_b \tan \theta_a)} \end{aligned} \quad (5.19)$$

$$\begin{aligned}
Z_4 &= Z_a \frac{Z_3 + jZ_a \tan\theta_a}{Z_a + jZ_3 \tan\theta_a} \\
&= Z_a \frac{\frac{Z_a Z_b \omega C - Z_a^2 \tan\theta_a \tan\theta_b \omega C + Z_a \tan\theta_b + Z_b \tan\theta_a}{j\omega C (Z_a \tan\theta_b + Z_b \tan\theta_a)} + jZ_a \tan\theta_a}{Z_a + \frac{Z_a Z_b \omega C \tan\theta_a - Z_a^2 \tan^2\theta_a \tan\theta_b \omega C + Z_a \tan\theta_a \tan\theta_b + Z_b \tan^2\theta_a}{\omega C (Z_a \tan\theta_b + Z_b \tan\theta_a)}} \\
&= \frac{Z_a}{j} \frac{\omega C (Z_a Z_b - 2Z_a^2 \tan\theta_a \tan\theta_b - Z_a Z_b \tan^2\theta_a) + Z_a \tan\theta_b + Z_b \tan\theta_a}{\omega C (Z_a^2 \tan\theta_b + 2Z_a Z_b \tan\theta_a - Z_a^2 \tan^2\theta_a \tan\theta_b) + Z_a \tan\theta_a \tan\theta_b + Z_b \tan^2\theta_a}
\end{aligned} \tag{5.20}$$

$$\begin{aligned}
Z_5 &= Z_b \frac{Z_4 + jZ_b \tan\theta_b}{Z_b + jZ_4 \tan\theta_b} \\
&= \frac{Z_b D}{j N}
\end{aligned} \tag{5.21}$$

where

$$\begin{aligned}
D &= \omega C (Z_a^2 Z_b (1 - \tan^2\theta_a) (1 - \tan^2\theta_b) - 2Z_a^3 \tan\theta_a \tan\theta_b - 2Z_a Z_b^2 \tan\theta_a \tan\theta_b) \\
&\quad + Z_a^2 \tan\theta_b + Z_a Z_b \tan\theta_a - Z_a Z_b \tan\theta_a \tan^2\theta_b - Z_b^2 \tan^2\theta_a \tan\theta_b \\
N &= \omega C (Z_a^2 Z_b (\tan\theta_b - \tan^2\theta_a \tan\theta_b + \tan\theta_b - \tan^2\theta_a \tan\theta_b) + 2Z_a \tan\theta_a (Z_b^2 - Z_a^2 \tan^2\theta_b)) \\
&\quad + (Z_a \tan\theta_b + Z_b \tan\theta_a)^2.
\end{aligned} \tag{5.22}$$

5.7 Appendix II: The Inverter Circuit

This section provides the derivation of (5.6). In this section, we use the conversion between S parameters and ABCD parameters with a source admittance Y_i and load admittance Y_j [61]:

$$\begin{aligned}
S_{11} &= \frac{A\sqrt{\frac{Y_i}{Y_j}} + B\sqrt{Y_i Y_j} - \frac{C}{\sqrt{Y_i Y_j}} - D\sqrt{\frac{Y_j}{Y_i}}}{A\sqrt{\frac{Y_i}{Y_j}} + B\sqrt{Y_i Y_j} + \frac{C}{\sqrt{Y_i Y_j}} + D\sqrt{\frac{Y_j}{Y_i}}} \\
S_{12} &= \frac{2(AD - BC)}{A\sqrt{\frac{Y_i}{Y_j}} + B\sqrt{Y_i Y_j} + \frac{C}{\sqrt{Y_i Y_j}} + D\sqrt{\frac{Y_j}{Y_i}}} \\
S_{21} &= \frac{2}{A\sqrt{\frac{Y_i}{Y_j}} + B\sqrt{Y_i Y_j} + \frac{C}{\sqrt{Y_i Y_j}} + D\sqrt{\frac{Y_j}{Y_i}}} \\
S_{22} &= \frac{-A\sqrt{\frac{Y_i}{Y_j}} + B\sqrt{Y_i Y_j} - \frac{C}{\sqrt{Y_i Y_j}} + D\sqrt{\frac{Y_j}{Y_i}}}{A\sqrt{\frac{Y_i}{Y_j}} + B\sqrt{Y_i Y_j} + \frac{C}{\sqrt{Y_i Y_j}} + D\sqrt{\frac{Y_j}{Y_i}}}.
\end{aligned} \tag{5.23}$$

An admittance inverter is defined as a two-port passive circuit of which the input admittance is inversely proportional to the load admittance. Taking the admittance inverter parameter as J , the ABCD matrix of the ideal admittance inverter is expressed as

$$\begin{bmatrix} 0 & \pm \frac{j}{J} \\ \pm jJ & 0 \end{bmatrix}. \tag{5.24}$$

If the inverter is connected to input and output ports whose admittances are Y_i and Y_j , respectively, then S_{21} and S_{11} are

$$\begin{aligned}
S_{21} &= \mp j \frac{2 \frac{J}{\sqrt{Y_i Y_j}}}{1 + \frac{J^2}{Y_i Y_j}} \\
S_{11} &= \frac{1 - \left(\frac{J^2}{Y_i Y_j} \right)}{1 + \left(\frac{J^2}{Y_i Y_j} \right)}.
\end{aligned} \tag{5.25}$$

The other two coefficients S_{12} and S_{22} can also be obtained using (5.24) and $S_{12} = S_{21}$ and $S_{22} = S_{11}$. (5.25) indicates that there is $\pm 90^\circ$ phase difference between transmission and reflection coefficients. Especially, the phase of transmission coefficient is ∓ 90 degree.

We derive (5.6) using the fact that the circuit shown in Fig. 5.5 has the same transmission and reflection properties as the ideal inverter at the frequency of interest. First, we can obtain the B_{ij} using the magnitude of the transmission coefficient. Since the transmission lines attached to the series capacitor in Fig. 5.5 has no effect on the amplitude of the transmission coefficient, for simplicity, the series capacitor only needs to be taken into account in calculating the magnitude of the transmission coefficient. The transmission coefficient of the series element with susceptance B_{ij} shown in Fig. 5.5 is

$$S_{21} = \frac{2}{\sqrt{\frac{Y_i}{Y_j}} + \sqrt{\frac{Y_j}{Y_i}} + \frac{1}{jB_{ij}} \sqrt{Y_i Y_j}}. \tag{5.26}$$

The magnitude of (5.26) is then

$$|S_{21}| = \frac{2}{\sqrt{\frac{Y_i}{Y_j} + \frac{Y_j}{Y_i} + 2 + \frac{Y_i Y_j}{B_{ij}^2}}}. \tag{5.27}$$

Comparing (5.27) with the magnitude of the transmission coefficient of the ideal admittance inverter

$$|S_{21}| = \frac{2 \frac{J}{\sqrt{Y_i Y_j}}}{1 + \frac{J^2}{Y_i Y_j}} \quad (5.28)$$

results in

$$\left| \frac{B_{ij}}{\sqrt{Y_i Y_j}} \right| = \frac{\frac{J_{ij}}{\sqrt{Y_i Y_j}}}{\sqrt{\left(1 - \left(\frac{J_{ij}}{Y_i}\right)^2\right) \left(1 - \left(\frac{J_{ij}}{Y_j}\right)^2\right)}}. \quad (5.29)$$

Next, we determine the length of each transmission line in such a way that the the phases of reflection coefficients at input and output are zero, since those of the ideal inverter are zero from (5.25). The input port reflection coefficient of the series element with susceptance B_{ij} is

$$\begin{aligned} S_{11} &= \frac{\sqrt{\frac{Y_i}{Y_j}} - \sqrt{\frac{Y_j}{Y_i}} + \frac{1}{jB_{ij}} \sqrt{Y_i Y_j}}{\sqrt{\frac{Y_i}{Y_j}} + \sqrt{\frac{Y_j}{Y_i}} + \frac{1}{jB_{ij}} \sqrt{Y_i Y_j}} \\ &= \frac{\frac{Y_i}{Y_j} - \frac{Y_j}{Y_i} + \frac{Y_i Y_j}{B_{ij}^2} - j \frac{2Y_j}{B_{ij}}}{\frac{Y_i}{Y_j} + \frac{Y_j}{Y_i} + 2 + \frac{Y_i Y_j}{B_{ij}^2}}. \end{aligned} \quad (5.30)$$

Hence, the phase of the reflection coefficient is

$$\angle S_{11} = -\tan^{-1} \left(\frac{2 \frac{Y_j}{B_{ij}}}{\frac{Y_i}{Y_j} - \frac{Y_j}{Y_i} + \frac{Y_i Y_j}{B_{ij}^2}} \right). \quad (5.31)$$

The phase of S_{22} can also be obtained in a similar way. Since these phases are not zero, the series element is embedded between uniform transmission lines. Due to the around-

trip along the transmission, double of the electrical length of transmission line should be identical to the phase of corresponding reflection coefficient as given by (5.6). The negative lengths of lines are absorbed in connecting lines.

It has been confirmed that the phase of transmission coefficient of the circuit shown in Fig. 5.5 is 90 degree and the magnitude of reflection coefficient is equal to (5.25) with the parameters given in (5.6). This indicates that the circuit shown in Fig. 5.5 is equivalent to the ideal inverter at certain frequency. The approach described above is also applied to derive (5.9)-(5.14).

CHAPTER 6

Planar Miniaturized Microwave Resonator Filter

6.1 Introduction

In recent years, significant amount of effort has been devoted towards development of high-performance microwave filters. Particular attention has been given to miniaturization, tunability, low insertion loss characteristic, low cost, and multi-passband behavior. Novel topologies employing source-load couplings [62][63] and non-resonating nodes have been reported [64]. Also for tunability, varactors have been used in various filter's resonators [65][66]. The synthesis and realization methods for filters with multiple passband characteristics have also been studied widely [34][35]. To reduce filter dimensions, lumped elements are often used in miniaturized radio frequency (RF) transceivers. However, it is well known that lumped elements at microwave frequencies have very poor quality factors giving rise to significant insertion loss and poor out-of-band rejection. In addition, filter designers must often times deal with undesirable self-resonance behavior of the lumped elements at microwave frequencies. Recently a method for fabricating high performance planar and highly miniaturized microwave filter have been introduced [67]. These filters used slot-line, as opposed to microstrip line or co-planar waveguide, resonators with a unique dual-spiral miniaturized configuration. It was shown that for a miniaturized transmission line type resonator, slot-line resonators provide the highest Q. However, the strong

near-fields around each resonator of these filters can easily interact with what might be placed beneath the dielectric layer. Although transmission zeros can be introduced using a finite ground plane, it is difficult to control their location.

In order to allow vertical integration of other RF components with this filter, this letter presents a modified structure for the miniaturized double-spiral slot-line resonator filter. This structure is formed by placing a conductor plane beneath the slot-line resonators which can shield the backside of a filter formed by these resonators. The back conductor is also used to obtain a controllable source-load coupling that allows placement of transmission zeros in the filter response.

A two-pole miniaturized slot-line resonator filter with two transmission zeros operating at 2.11 GHz is designed and realized to demonstrate the proposed concept. A very good agreement between the simulated results and measured ones is shown.

6.2 Filter Structure and Design

Fig 6.1(a) and 6.1(b) show the structure of two-pole CPW-fed miniaturized slot-line resonator filters one without and one with a back conductor plane. The performance of the conventional slot-line filter (without the back conductor plane) is affected by components or objects placed underneath the resonator and therefore the filter cannot be integrated into multilayer circuits. Although it is possible to introduce transmission zeros in the filter response their locations are mainly affected by the dimensions of the ground plane of the resonator (top layer) and therefore not easily controllable as the size of the top ground plane is a function of transceiver topology and other design rules. The modified filter structure on the other hand shields the resonators from under layers and provides a way to control the location of transmission zeros [68]. To control the transmission zeros, the resonator ground plane on top is split into two parts with a gap shown in Fig. 6.1(b).

To understand the behavior of the proposed filter, let us consider the signal flow graph

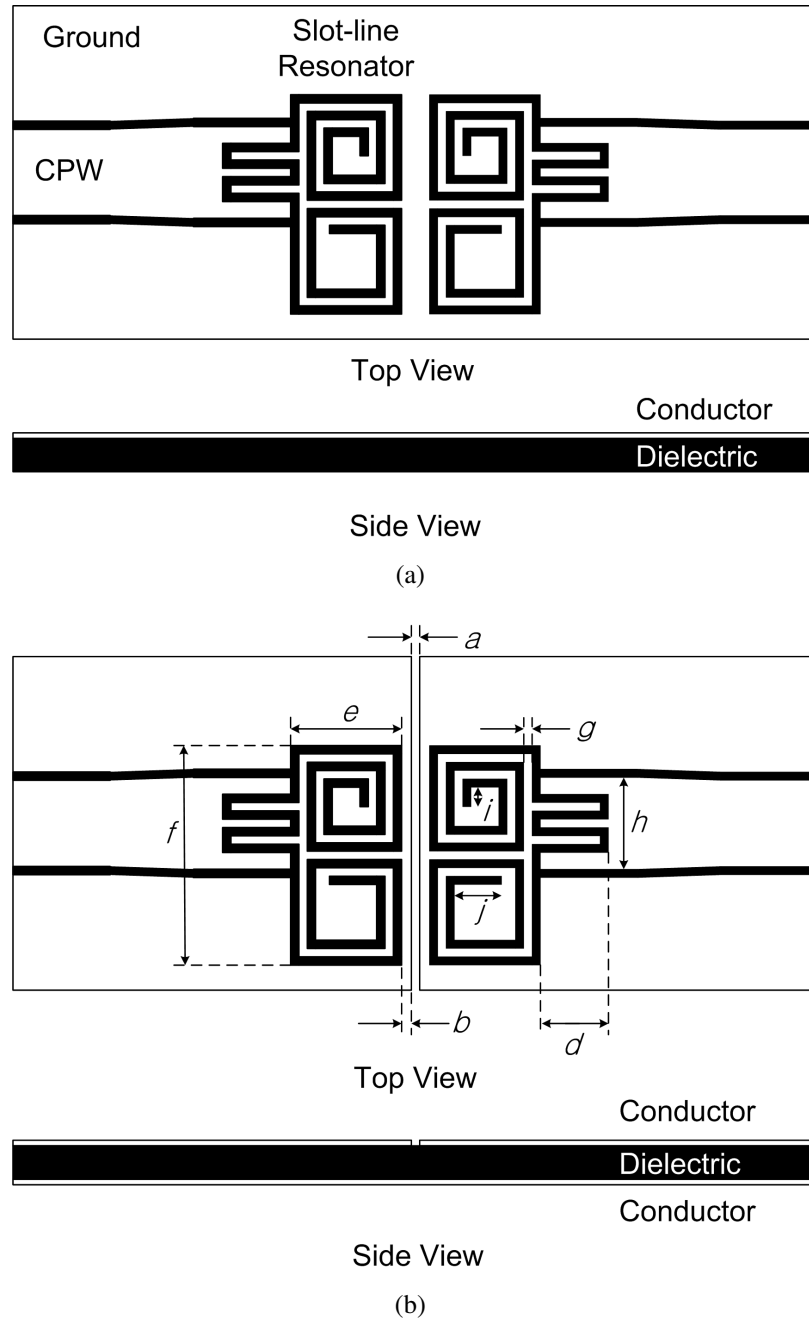


Figure 6.1: Two-pole miniaturized double-spiral slot-line resonator filters: (a) a conventional structure and (b) a novel structure. The dimensions are all in mm and are $a=0.30$, $b=0.35$, $d=2.75$, $e=4.00$, $f=7.90$, $g=0.30$, $h=3.30$, $i=0.70$, and $k=1.70$.

shown in Fig. 6.2. The source-load coupling ($M_{S,L}$) enables the filter to have a pair of transmission zeros.

According to the filter specifications, the transfer function of the filter can be obtained

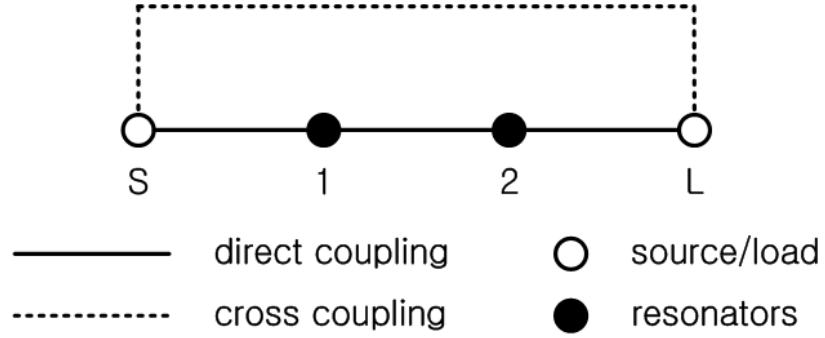


Figure 6.2: Signal flow in the two-pole filter with the source-load coupling.

by the proper choice of reflection zeros and transmission zeros. The transmitted power of an N th-order filter with N finite-frequency transmission zeros can be expressed in terms of the transfer function $t(S)$ and is given in (2.30):

$$|t(S)|^2 = \frac{1}{1 + \frac{\epsilon^2 |F(S)|^2}{\epsilon_R^2 |P(S)|^2}} \quad (6.1)$$

where $S = j\Omega$ and $F(S)$ and $P(S)$ are given by

$$F(S) = \prod_{i=1}^N (S - S_{fi}) \quad (6.2)$$

$$P(S) = \prod_{i=1}^Z (S - S_{pi})$$

where S_{fi} and S_{pi} are reflection zeros and transmission zeros of the filter, respectively. In (6.2), Z is the number of transmission zeros. If the filter has the source-load coupling, N transmission zeros can be realized. The ripple constants ϵ and ϵ_R are given in (2.31) and (2.32):

$$\begin{aligned}\epsilon &= \epsilon_R \sqrt{\frac{1}{10^{R_1/10} - 1} \frac{|P(j\Omega_1)|^2}{|F(j\Omega_1)|^2}} \\ \epsilon_R &= \sqrt{1 + (10^{R_1/10} - 1) \frac{|F(j\Omega_1)|^2}{|P(j\Omega_1)|^2}}\end{aligned}\quad (6.3)$$

where R_1 is the prescribed return loss level in decibels (dB) at $\Omega = \Omega_1$. In general, ϵ_R have a value slightly greater than unity. Also, if the attenuation at $S = \pm j\infty$ is very high, then the ripple factor ϵ_R will be almost unity. In this case, the transmitted power and the ripple factor can be approximated to be

$$|t(S)|^2 = \frac{1}{1 + \epsilon^2 \frac{|F(S)|^2}{|P(S)|^2}} \quad (6.4)$$

$$\epsilon = \sqrt{\frac{1}{10^{R_1/10} - 1} \frac{|P(j\Omega_1)|^2}{|F(j\Omega_1)|^2}}. \quad (6.5)$$

In our filter design, transmission zeros are determined to be at $S_{pi} = \pm j28.0$ with the maximum in-band return loss of 20 dB. From (6.4), the transfer function can be obtained as

$$t(S) = \frac{1}{\epsilon} \cdot \frac{S^2 + a_{z0}}{S^2 + a_{p1}S + a_{p0}} \quad (6.6)$$

where $a_{z0} = 784$, $a_{p1} = 2.991$, $a_{p0} = 5.005$, and $\epsilon = 157.43$. The transmission coefficient S_{21} of the filter is given by

$$S_{21} = 2 \times \mathbf{A}_{N+2,1}^{-1} \quad (6.7)$$

where \mathbf{A}^{-1} is the inverse matrix of \mathbf{A} which is given by

$$\mathbf{A} = \mathbf{R} + S\mathbf{W} + j\mathbf{M}. \quad (6.8)$$

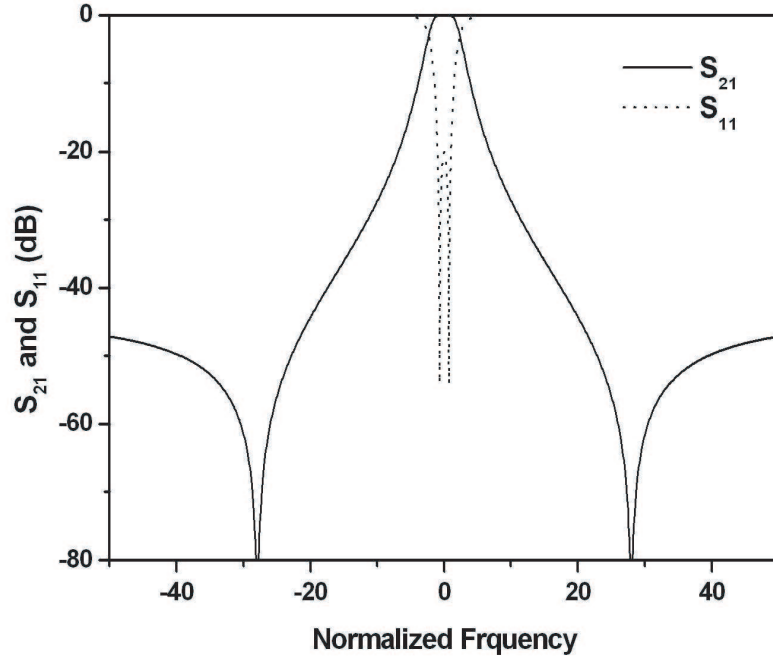


Figure 6.3: Frequency response of the filter with the coupling matrix in (6.9).

Here \mathbf{R} is a $(N+2) \times (N+2)$ matrix whose only nonzero entries are $R_{1,1} = R_{N+2,N+2} = 1$, \mathbf{W} is similar to the $(N+2) \times (N+2)$ identity matrix, except that $W_{1,1} = W_{N+2,N+2} = 0$, and \mathbf{M} is the $(N+2) \times (N+2)$ coupling matrix.

Finally, the $(N+2) \times (N+2)$ coupling matrix of the filter can be obtained by equating (6.6) with (6.7) and is given by

$$\mathbf{M} = \begin{bmatrix} 0 & 1.224 & 0 & 0.003 \\ 1.224 & 0 & -1.661 & 0 \\ 0 & -1.661 & 0 & 1.224 \\ 0.003 & 0 & 1.224 & 0 \end{bmatrix}. \quad (6.9)$$

The frequency response of the filter with the coupling matrix in (6.9) is shown in Fig. 6.3. The filter is designed to have a center frequency of the 2.11 GHz and a bandwidth of 60 MHz.

From the obtained coupling coefficients, the dimensions of the filter can be determined. The coupling coefficient between the source and the load is mainly determined by the distance between the two ground planes, a , and this can be determined by observing the S_{21} response with the following relationship:

$$S_{21} = \frac{2M_{S,L}}{1 + M_{S,L}^2}. \quad (6.10)$$

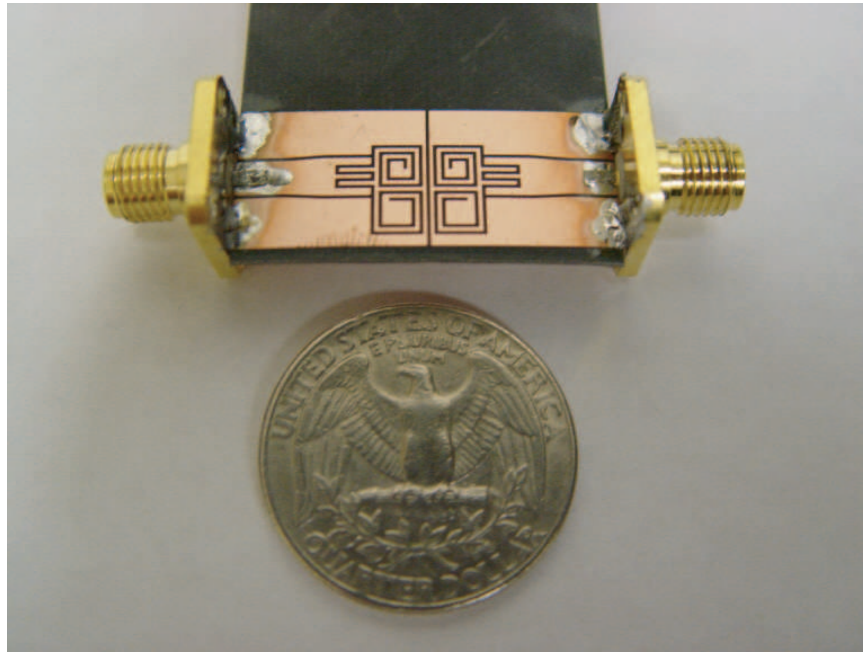
The external coupling coefficients ($M_{S,1}$, $M_{2,L}$) can be varied by changing the finger length d and this can be determined by measuring the phase response of S_{11} with one resonator and using

$$M_{S,1}^2 (= M_{2,L}^2) = \frac{\Delta f_{\pm 90^\circ}}{\Delta f} \quad (6.11)$$

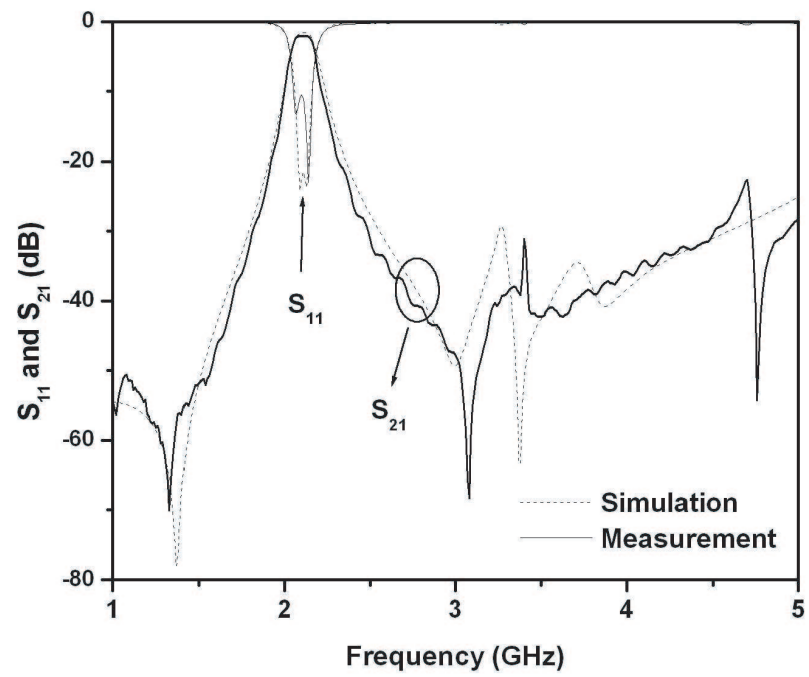
where Δf and $\Delta f_{\pm 90^\circ}$ are the absolute bandwidth of the filter and the frequency difference two frequencies at which the phase shift $\pm 90^\circ$ with respect to the absolute phase at the center frequency f_0 [43].

The coupling between the resonators is mainly determined by the length b . Since this coupling cannot be measured without source-load coupling for this filter structure and all the other couplings are known, the length b has been determined in the presence of source-load coupling and external coupling by matching the measured reflection zero locations to the theoretical ones.

Using this procedure the filter dimensions shown in Fig. 6.1(b) have been found and are given in the caption. All dimensions are in mm and the slot width for both resonators is a fixed value of 0.30 mm.



(a)



(b)

Figure 6.4: (a) Fabricated 2nd-order slot-line resonator filter, (b) The frequency response of the 2nd-order slot-line resonator filter.

6.3 Fabrication and Measurement

A filter is fabricated on a Duroid 5880 substrate with a thickness of 0.787 mm, dielectric constant of 2.2, and loss tangent of 0.0009. Fig. 6.4 shows the fabricated filter and compares the measured and simulated responses of the filter. The measured frequency responses of the filter show a good agreement with the simulated results. Note that a 2nd-order filter can have two transmission zeros and the positions of transmission zeros are nearly identical to each other. If the transmission zeros are designed to locate near to the passband, the filter will have higher frequency selectivity. The simulated and measured insertion losses are 1.7 dB and 2.0 dB. The insertion loss is mainly due to the finite quality factor of the resonator and theoretical value of the insertion loss can be calculated by offsetting S of the matrix SW in (6.8) by a positive real factor δ as follows:

$$SW = \begin{bmatrix} 0 & 0 & 0 & 0 \\ 0 & S + \delta & 0 & 0 \\ 0 & 0 & S + \delta & 0 \\ 0 & 0 & 0 & 0 \end{bmatrix} \quad (6.12)$$

where $\delta = f_0 / (BW \cdot Q_u)$, f_0 is the center frequency, and BW is design bandwidth. Since the unloaded quality factor of the resonator is 110, theoretical insertion loss is calculated to be 1.7 dB. It is of note that the theoretical value is identical to simulated value.

6.4 Conclusion

In this letter, a miniaturized high-Q filter with very high selectivity using a conductor plane backed double-spiral slot-line resonator filter is presented. This filter structure allows vertical integration of multilayer circuits and source-load coupling. A prototype miniaturized 2nd-order slot-line resonator filter at 2.11 GHz is fabricated which occupies an area as small as 8 mm \times 9 mm and presents two transmission zeros. The frequency selectivity

can be adjusted by controlling the location of the transmission zeros. It is also shown that simulation and measured results agree very well.

CHAPTER 7

Conclusions

7.1 Summary

The motivation behind this work was to reduce the size and mass of modern and next-generation wireless systems by developing novel filter architectures as well as design methodologies for the advanced microwave filters. The proposed microwave filters can make a significant impact on the wireless systems by replacing bulky conventional microwave filters. This is accomplished as the size and mass of the entire wireless systems are mainly determined by those filters. Current and future wireless systems, such as mobile and satellite communications systems and radars, rely on wider frequency channels than before, which in turn require more microwave filters for each wireless unit. With the conventional design approach, the number of microwave filters equals that of allocated frequency channels, which results in a substantial increase in size and mass of the wireless systems.

In response to this motivation, this thesis has demonstrated new filter architectures and analytic design methods to be applied to such filters: 1) multiple-passband microwave resonator filters, 2) tunable microwave resonator filters for frequency agility, 3) miniaturized high-performance microwave filters. Existing design theories are not capable of designing these microwave filters in a methodical fashion. Therefore, this work first embarked on

developing new analytic design theories and procedures for such filters. This thesis has demonstrated canonical design procedures for such filters.

7.1.1 Multiple-Passband Microwave Resonator Filters

Conventional wireless communications systems use a bank of microwave filters, one filter for each of the frequency channel. Since multiple frequency channels are established by a number of microwave filters which are connected in parallel using signal dividers and combiners, the size and mass of the wireless system will increase in proportion to the number of frequency channels. To address this issue in the next generation systems, this work provides fundamental theories and analytic design procedures for multiple-passband microwave filters. This work provides frequency transformation techniques for analytic design of multiple-passband microwave filters. Also, these advanced filters enable realization of compact wireless systems. Finally, the electrical performance can be improved since the performance deterioration caused by signal dividers and combiners in conventional wireless systems can be removed.

7.1.2 Tunable Microwave Resonator Filters

Unlike the aforementioned wireless communications systems, frequency-agile wireless systems such as radars and tracking systems use one of a number of allocated frequency channels and change the channel from one to the other as necessary. Since these systems use many frequency channels, a switched bank of microwave filters is required, which also results in increased size of frequency-agile wireless systems. For size reduction, a switched bank of microwave filters can be replaced by a single tunable microwave filter which can be electrically adjusted to operate at different channels. In this case, the tunable filter should exhibit same performance as it operates at the different frequency channels.

This work provides two-dimensional microwave tunable filter architecture and analytic

design procedure for such filter. It is of note that this proposed analytic procedure produces filters that exhibit identical electrical performance at all of the various frequency channels.

7.1.3 Miniaturized Microwave Resonator Filters

In general, miniaturized microwave filters exhibit higher signal losses and lower selectivity compared to their physically larger counterparts. In other words, two important electrical performance characteristics of the microwave filter, small signal losses and high frequency-selectivity, are not affordable for miniaturized microwave filters. This work focused on improving electrical performance of small-size microwave filters. It presented transmission zero technique for electrical design of miniaturized microwave filters with aforementioned good performance characteristic.

7.2 Future Work

This work can be of help to future researchers in the following area.

7.2.1 Non-Planar Miniaturized Microwave Resonator Filter

There has been increasing demand for the development of miniaturized and high performance microwave and millimeter wave filters. With increasing demand for the development of miniaturized and high performance microwave and millimeter wave filters, numerous techniques and methodologies have been presented for reducing the size and volume of the filters. Especially, most techniques are for planar structure filters. Step-impedance resonator, miniature open-loop resonator, and miniature hairpin resonator have been presented for compact filter structure. Also, in the previous chapter, the miniaturized planar microwave filter with slot-line resonators has been discussed. Although the planar structure filters have good compatibility with other planar structure components such as amplifiers, mixers, and oscillators, they suffers from the insertion loss due to the quality factor of the

planar structure resonators. Since, in general, the quality factor is proportional to the volume of the resonator, the non-planar structure resonators have higher quality factor than planar structure resonators. Dielectric-loaded cavity filters, bulk acoustic wave filters [69], and Low Temperature Co-fired Ceramic (LTCC) filters can be categorized into the non-planar miniaturized filter. The concept of dielectric resonators was proposed in 1930s and was brought into practical use for miniaturizing microwave filters in the early 1960s. In general, cylindrical dielectric resonators and coaxial block dielectric resonators have been widely used in various applications. RF filtering in mobile terminals is dominated by surface acoustic wave and bulk acoustic wave based filters due to their high performance, small size, and low cost. As compared to SAW filter technology, BAW filter solutions can provide lower insertion loss, better frequency selectivity due to the higher quality factor [69]. The reason for this is that BAW is trapped inside the body of the device material while SAW is trapped on the surface. The LTCC technology is a very widely used multilayer technology for designing miniaturized RF passive components, owing to its three-dimensional (3-D) integration capabilities, process tolerance, and low dielectric loss [70]. It provides an ability to embed passive components in layers while the active elements are mounted on the surface layer [71].

In this work, an air-filled meander resonator filter is proposed. The resonator is miniaturized by meandering the structure and it has low loss due to the air-filled structure. Since the resonator has meandering structure, it is difficult to implement using conventional fabrication processes such as milling process. Hence, a newly-developed fabrication process called ultrasonic consolidation process can be used to implement such structure.

Fig 7.1 shows a two-pole filter with miniaturized meander resonators. The resonator is coupled by a microstrip line through a slot on the ground plane of substrate and inter-resonator coupling is achieved by a slot on the vertical wall. The proposed resonator structure can be attached to the bottom layer of a microstrip line structure. Since this filter doesn't take the place of top surface of the circuit, we can save the space of top surface and

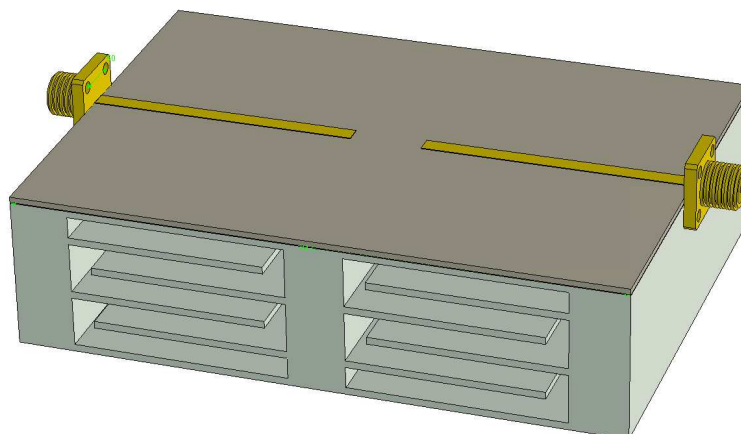


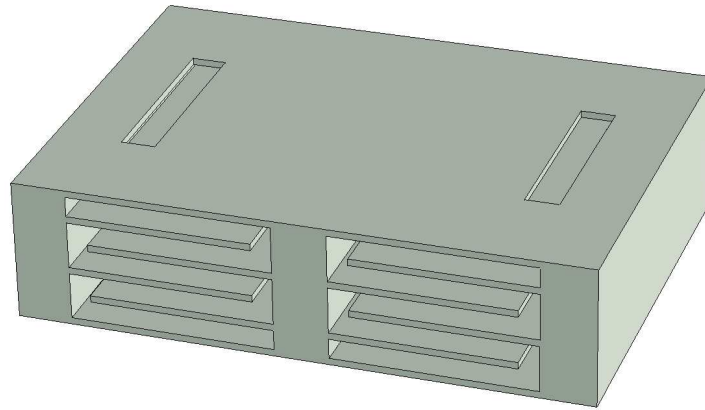
Figure 7.1: The miniaturized two-pole filter with meandered resonators

overall circuit size can be reduced.

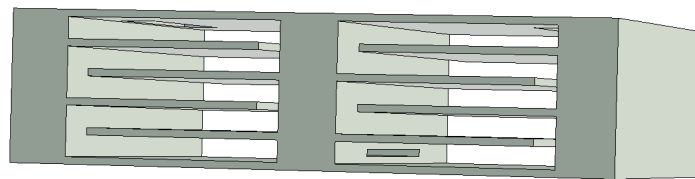
The size and the quality factor of the resonator depends on the number of layers, the height of each layer, and the width of the resonator. Generally, the quality factor is inversely proportional to the volume of the resonator. Hence, the trade-off between the size and the quality factor should be performed.

The resonator of the filter shown in Fig. 7.1 is designed to have the center frequency of 1.0 GHz. The resonator has 5 layers and the height of each layer is designed to be 3 mm. The width (from one open end to the other) and the length (from one vertical wall to the other) of the resonator are 40 mm and 30 mm, respectively. If the meandered layer is stretched out, the total length will be about 150 mm and this is approximately equivalent to the half of the wavelength.

Fig 7.3 shows the simulated frequency response of the two-pole filter with miniaturized meander resonators. The simulation was performed with the assumption that substrate of the microstrip structure is Rogers 5880 and the resonator is made of aluminum. The minimum return loss are shown to be 20 dB and and insertion loss is 0.6 dB. The quality



(a)



(b)

Figure 7.2: Enlarged view for the meandered resonators in Fig. 7.1.

factor of each resonator is calculated to be higher than 600.

In this work, the main issue is to validate the proposed filter structure by implementation and measurement. Also, making the filter shielded from the surroundings and designing higher-order filters are the other main issue.

The resonator structure shown in Fig. 7.2 can be fabricated using ultrasonic consolidation process. Ultrasonic consolidation is a micro-friction process. It differs substantially from other direct metal processes in that the technologies of ultrasonic joining are applied to produce true metallurgical bonds between layers of metal without melting [72]. The

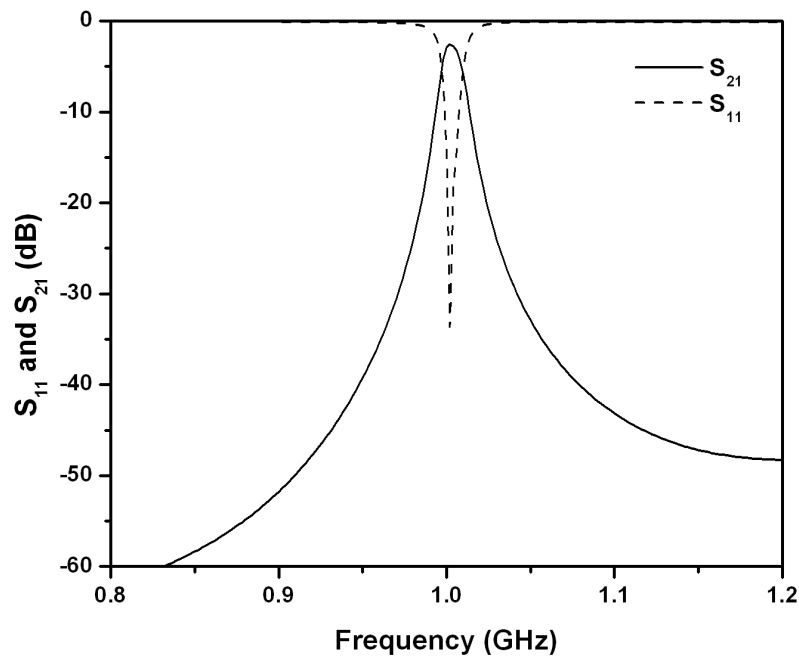


Figure 7.3: The frequency response of the miniaturized filter shown in Fig. 7.1

layer being consolidated is translated against the previously built volume at very high (ultrasonic) frequency, and with low amplitude. As the surfaces vibrate against each other, surface contaminants such as oxides are fractured and displaced. These atomically clean surfaces are then brought into close contact under modest pressures at temperatures that typically do not exceed half the melting point of the metal.

Due to its unique properties, the ultrasonic consolidation process can be of help to design and fabrication of non-planar miniaturized microwave filters as well as other microwave components.

7.2.2 High-Pass Filter for the Receiver of Frequency-Modulated Continuous-Wave Radar

Frequency-Modulated Continuous-Wave (FMCW) radar uses frequency modulation of the waveform to allow a range measurement and the target range is determined by the range-related frequency difference between the echo-frequency ramp and the frequency of

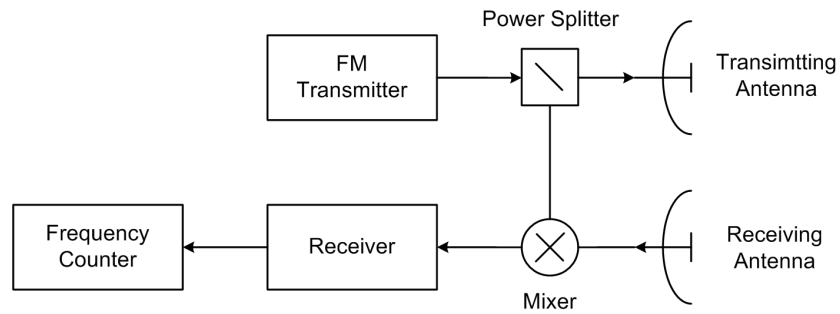


Figure 7.4: A block diagram of an FMCW radar system.

the ramp being transmitted.

FMCW radar has found many applications such as vehicle collision avoidance systems, helicopter landing systems, and ice layer detecting systems. For example, a FMCW radar for measuring snow thickness use frequency range of 2-8 GHz with the frequency sweep time of 10 msec [73]. Due to the large frequency range, the radar use YIG oscillator for signal generation. Also, FMCW has been used for a X-band collision avoidance radar which has 1.5 GHz bandwidth and 256 usec sweep time [74]. In this system, FM signal is generated by VCO which is controlled by a RAM table and a digital-to-analog converter (DAC).

A W-band FMCW radar for helicopter landing systems has also been demonstrated [75]. In this radar system, a direct digital synthesizer was used to generate the baseband frequency modulated (FM) signal with fast sweep time (40 usec). Fast sweep time is essential for almost real-time range detection and high resolution in range detection. This baseband FM signal then has been up-converted to S-band and W-band consecutively.

A block diagram of FMCW radar for measuring range is shown in Fig. 7.4 [76]. The transmitter frequency is changed as a function of time in a know manner. In practical FMCW radar, the frequency cannot be continually changed in one direction only. Therefore, the transmitter emits waves of a frequency that varies with time, oscillating above and below the mean frequency, as in the triangular-frequency-modulation waveform shown in Fig. 2. The modulation need not necessarily be triangular; it can be sawtooth, sinusoidal,

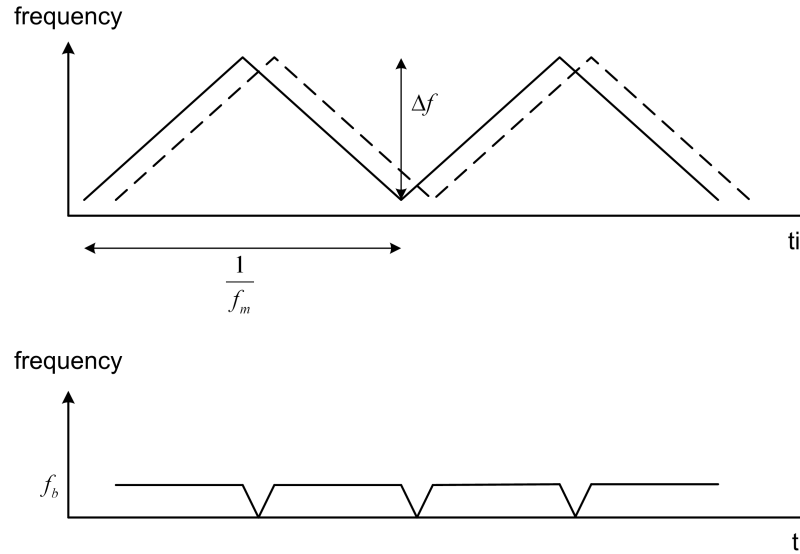


Figure 7.5: A transmitting, receiving, and beat frequency of an FMCW radar.

or some other shape. The waves arrive at the receiver both by a direct connection and by reflection from the target. Since the trip to the target and return takes time, the received frequency curve is displaced along the time axis relative to the transmitted frequency. Also there might be a displacement along the frequency axis due to doppler effect. This can be disregarded for stationary target.

The resulting beat frequency as a function of time is also shown in Fig. 7.6 for triangular modulation. The beat note is of constant frequency except at the turn-around region. If the frequency is modulated at a rate f_m over a range Δf , the beat frequency is

$$f_b = \frac{4Rf_m\Delta f}{c} \quad (7.1)$$

where c is the speed of light and R is the range. Thus the measurement of the beat frequency determines the range R .

The block diagram for the receiver is shown in Fig. 7.6 [75]. An amplifier is inserted at the first stage, followed by a splitter. Two outputs are provided by a splitter at the receiver. One is the direct baseband signal while the other is routed through a highpass filter whose amplitude response below cutoff frequency is proportional to f^4 . The inclusion

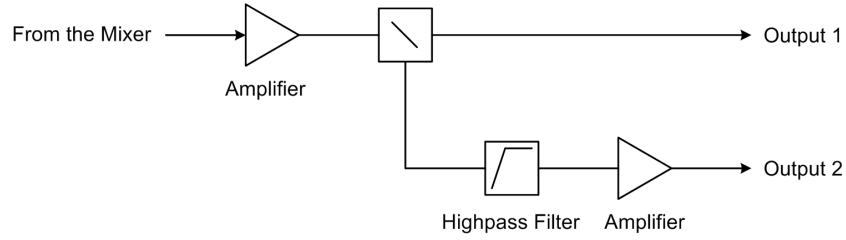


Figure 7.6: The block diagram of the receiver.

of the highpass filter is that the range, in FMCW radars, is converted to frequency and a monostatic radar has a R^{-4} amplitude variation with the range of a target. This highpass filter compensates for that, and decrease the dynamic range required from the analog-to-digital converter (ADC). However, for the close targets, the highpass filter has very high attenuation (above 60 dB), and the signal is lost in the noise floor. Thus, both outputs are provided in the receiver board.

For amplitude response which is proportional to f^4 , the highpass filter should be of 4th order and have butterworth response. The frequency response of this highpass filter in the normalized frequency domain is shown in Fig. 7.7. Both return loss and insertion loss are 3.0103 dB at cutoff frequency which is set to be 1. Below cutoff frequency, amplitude of transmission coefficient is almost proportional to f^4 . However, the high attenuation at low frequencies make the receiver have two pathes as shown in Fig 7.6. Hence, the receiver can have only one path if the filter with decent, but not very high, attenuation at low frequencies is provided.

Since highpass filters can be designed by using the lowpass-to-highpass frequency transformation, we begin highpass filter design with lowpass prototype filter design. Fig. 7.8 shows the frequency response of the 4th-order butterworth-response lowpass prototype filter without transmission zeros at finite frequencies and 4th-order butterworth-response lowpass prototype filter with transmission zeros at $S = \pm j4.0$. Since these filters have infinite attenuation at $S = \pm j\infty$ and $S = \pm j4.0$, the corresponding highpass filters will have signal loss if used in the receiver board of the above-described FMCW radar. By using complex transmission zeros at stopband, we can avoid infinite attenuation at certain fre-

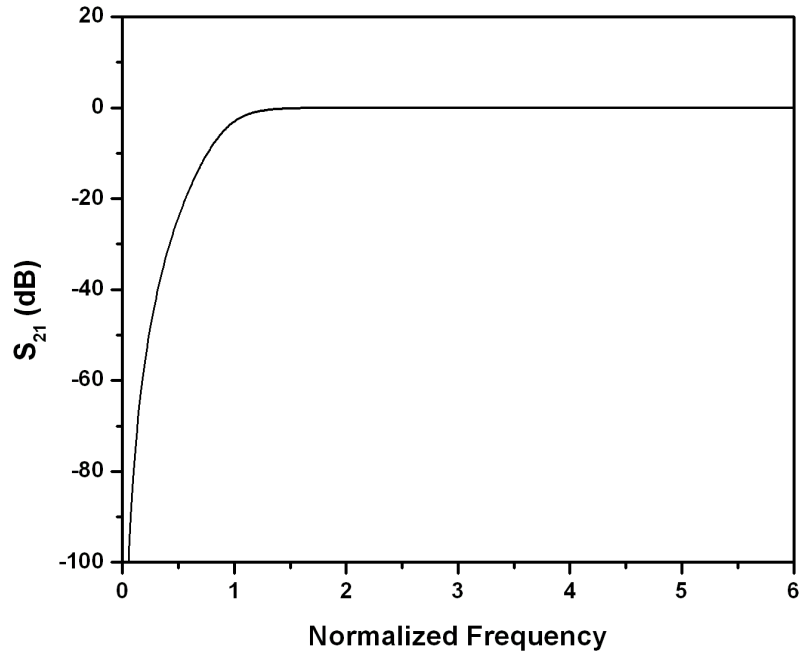
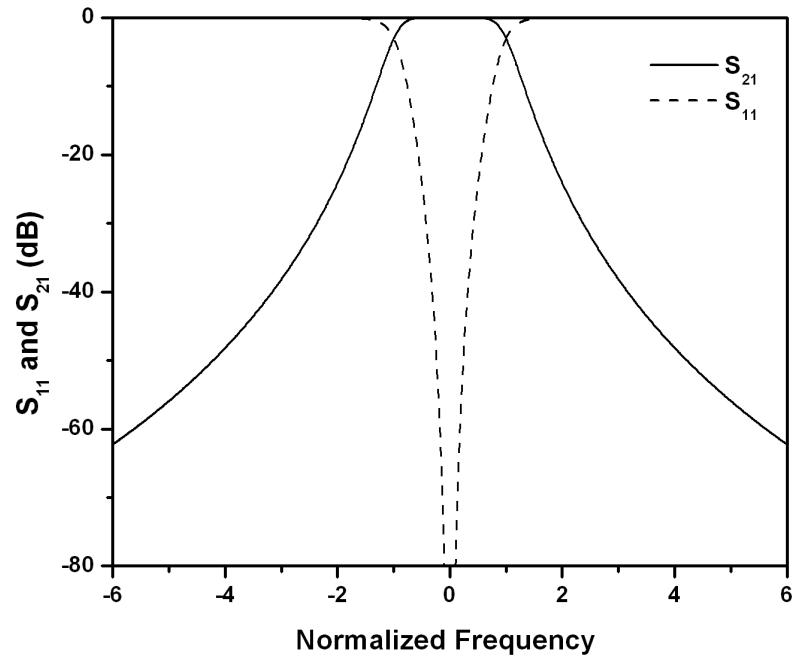


Figure 7.7: The amplitude response of the normalized butterworth-response highpass filter. The cutoff frequency is at $\Omega = 1$.

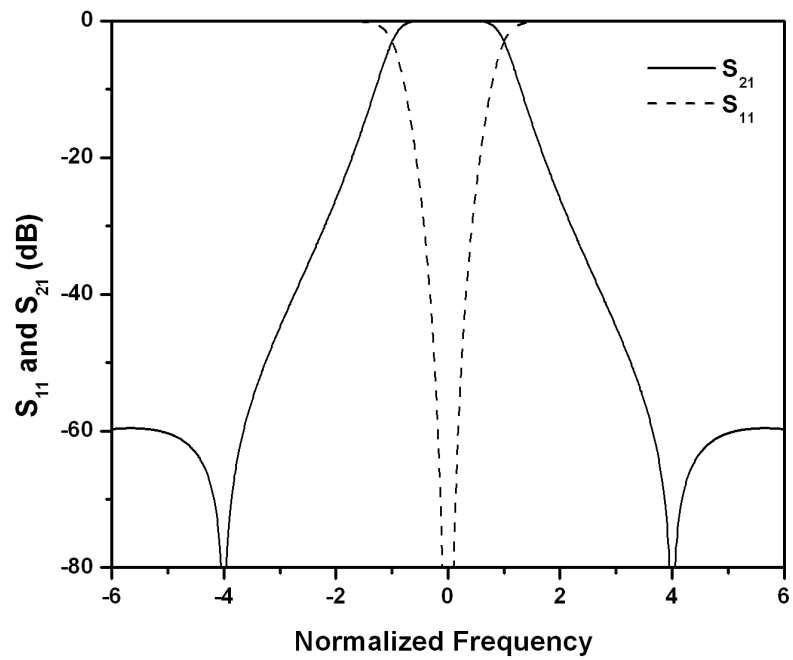
quencies theoretically. However, there is no lowpass prototype presented for this frequency response. Hence, in this work, an approximation method is used for developing the lowpass prototype filter with no infinite attenuation.

Fig. 7.9(a) shows a 4th-order lowpass prototype filter with a pair of transmission zeros at finite frequencies. The frequency response shown in Fig. 7.8(b) can be achieved by using the prototype shown in Fig. 7.9(a). Since all reflection zeros are at $S_f = j0$ and a pair of finite-frequency transmission zeros are at $S_p = \pm j4.0$, the transmitted power is expressed as

$$\begin{aligned}
 |t(S)|^2 &= \frac{1}{1 + \epsilon^2 |K(S)|^2} \\
 &= \frac{1}{1 + \epsilon^2 \frac{|F(S)|^2}{|P(S)|^2}}
 \end{aligned} \tag{7.2}$$



(a)



(b)

Figure 7.8: Amplitude responses of 4th-order lowpass prototype filters: (a) with no transmission zeros; (b) with transmission zeros at $S = \pm j4.0$.

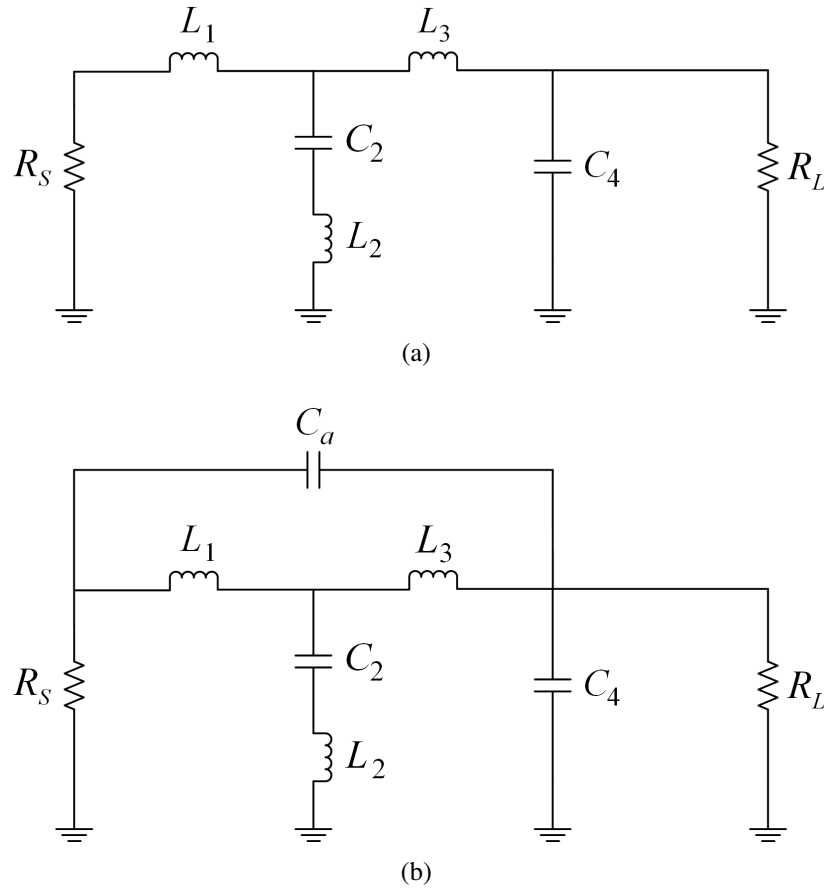


Figure 7.9: Amplitude responses of 4th-order lowpass prototype filters: (a) with no transmission zeros; (b) with transmission zeros at $S = \pm j4.0$.

where $S = j\Omega$ and $F(S)$ and $P(S)$ are given by

$$\begin{aligned}
 F(S) &= \prod_{i=1}^N (S - S_{fi}) \\
 P(S) &= \prod_{i=1}^Z (S - S_{pi})
 \end{aligned}
 \tag{7.3}$$

where S_{fi} and S_{pi} are reflection zeros and transmission zeros of the filter, respectively. From (2.25), the ripple factor ϵ is found to be 15 for $R_1 = 3.0103$ at $\Omega_1 = 1$. The return loss $R_1 = 3.0103$ dB results in $A_1 = 3.0103$ dB. From the transmitted power, the transfer function can be found and is given by

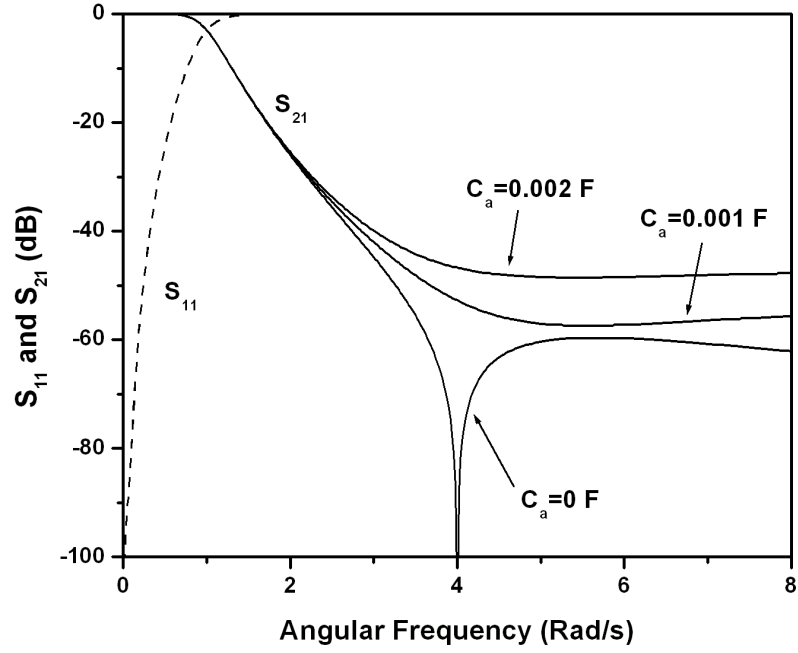


Figure 7.10: The frequency response.

$$t(S) = \frac{1}{\epsilon} \cdot \frac{S^2 + a_{z0}}{S^4 + a_{p3}S^3 + a_{p2}S^2 + a_{p1}S + a_{p0}} \quad (7.4)$$

where $a_{z0} = 16$, $a_{p3} = 2.638$, $a_{p2} = 3.480$, $a_{p1} = 2.698$, and $a_{p0} = 1.067$.

Since the transmission coefficient of the lowpass prototype shown in Fig. 7.9(a) can be derived easily in terms of prototype elements, we can find prototype elements by equating the transmission coefficient of the prototype and the transfer function in (7.4). The prototype elements are found to be $R_S = 1 \Omega$, $L_1 = 0.6771 \text{ H}$, $C_2 = 1.7206 \text{ F}$, $L_2 = 0.0363 \text{ H}$, $L_3 = 1.852 \text{ H}$, $C_4 = 0.8097 \text{ F}$, and $R_L = 1 \Omega$. In order to remove the infinite attenuation at $S = \pm j4.0$, a capacitor denoted C_a is added as shown in Fig. 7.9(b). Fig 7.10 shows a frequency response of the filter prototype shown in Fig. 7.9(b) with various values of C_a .

Based on the design of lowpass filter prototype with no infinite attenuation, we can remove high attenuation of the highpass filter at low frequencies, which allows that the receiver can be designed to have only one path instead of two paths shown in Fig. 7.6. This highpass filter is expected to compensate the amplitude variation of the received signal

from the target keeping the signal for the close target alive, which leads to the effective increase of the dynamic range of the analog-to-digital converter.

BIBLIOGRAPHY

BIBLIOGRAPHY

- [1] A. I. Zverev, *Handbook of Filter Synthesis*. New York: John Wiley & Sons, 1967.
- [2] J. Helszajn, *Synthesis of Lumped Element, Distributed and Planar Filters*. London: McGraw-Hill, 1990.
- [3] S. B. Cohn, "Direct-coupled-resonator filters," *Proc. of the IRE*, vol. 45, no. 2, pp. 187–196, Feb. 1957.
- [4] S. Darlington, "Synthesis of reactance four poles which produce prescribed insertion loss characteristics," *J. Math. Phys.*, vol. 18, pp. 257–353, Sept. 1939.
- [5] V. E. Boria and B. Gimeno, "Waveguide filters for satellies," *IEEE Microwave*, vol. 8, no. 5, pp. 60–70, Oct. 2007.
- [6] R. M. Kurzok, "General three-resonator filters in waveguide," *IEEE Trans. Microwave Theory Tech.*, vol. 14, no. 1, pp. 46–47, Jan. 1966.
- [7] ———, "General four-resonator filters at microwave frequencies," *IEEE Trans. Microwave Theory Tech.*, vol. 14, no. 6, pp. 295–296, June 1966.
- [8] R. Levy and S. B. Cohn, "A history of microwave filters research, design and development," *IEEE Trans. Microwave Theory Tech.*, vol. 32, no. 9, pp. 1055–1067, Sept. 1984.
- [9] R. D. Richtmyer, "Dielectric resonator," *J. Applied Physics*, vol. 10, pp. 391–398, June 1939.
- [10] A. E. Williams, "A four-cavity elliptic waveguide filter," *IEEE Trans. Microwave Theory Tech.*, vol. 18, no. 12, pp. 1109–1114, Dec. 1970.
- [11] S. Holme, "Multiple passband filters for satellite applications," in *20th AIAA Int. Commun. Satellite Syst. Conf. and Exhibit.*, 2002, paper AIAA-2002-1993.
- [12] W. J. Keane, "Narrow-band YIG filters aid wide-open receivers," *Microwaves*, vol. 17, no. 9, pp. 50–56, Sept. 1978.
- [13] ———, "YIG filters aid wide open receivers," *Microwave Journal*, vol. 17, no. 8, pp. 295–308, Sept. 1980.

- [14] J. S. Hong and M. J. Lancaster, "Compact microwave elliptic function filter using novel microstrip meander open-loop resonators," *Electronics Letters*, vol. 32, no. 6, pp. 563–564, Mar. 1996.
- [15] G. F. Craven and C. K. Mok, "The design of evanescent mode waveguide bandpass filter for a prescribed insertion loss characteristic," *IEEE Trans. Microwave Theory Tech.*, vol. 19, no. 3, pp. 295–308, Mar. 1971.
- [16] D. M. Pozar, *Microwave Engineering*. Wiley, 2005.
- [17] F. F. Kuo, *Network Analysis and Synthesis*. John Wiley & Sons, Inc., 1966.
- [18] R. J. Cameron, "General coupling matrix synthesis methods for Chebyshev filtering functions," *IEEE Trans. Microwave Theory Tech.*, vol. 47, no. 4, pp. 433–442, Apr. 1999.
- [19] A. E. Atia and A. E. Williams, "Narrow-bandpass waveguide filters," *IEEE Trans. Microwave Theory Tech.*, vol. 20, no. 4, pp. 258–265, Apr. 1972.
- [20] R. J. Cameron, C. M. Kudsia, and R. R. Mansour, *Microwave Filters for Communication Systems: Fundamentals, Design, and Applications*. Wiley, 2007.
- [21] F. Seyfert and S. Billa, "General synthesis techniques for coupled resonator networks," *IEEE Microwave*, vol. 8, no. 5, pp. 98–104, Oct. 2007.
- [22] G. L. Matthaei, L. Young, and E. M. T. Jones, *Microwave Filters, Impedance-Matching Networks, and Coupling Structures*. Norwood, MA: Artech House, Inc., 1980.
- [23] M. Uhm, J. Lee, I. Yom, and J. Kim, "General coupling matrix synthesis method for microwave resonator filters of arbitrary topology," *ETRI Journal*, vol. 28, no. 2, pp. 223–226, Apr. 2006.
- [24] J. B. Thomas, "Cross-coupling in coaxial cavity filters-A tutorial overview," *IEEE Trans. Microwave Theory Tech.*, vol. 51, no. 4, pp. 1368–1376, Apr. 2003.
- [25] J. A. Ruiz-Cruz, C. Wang, and K. A. Zaki, "Advances in microwave filter design techniques," *Microwave Journal*, vol. 51, no. 11, pp. 26–44, Nov. 2008.
- [26] A. Woode and J. Petit, "Investigation into multipactor breakdown in satellite microwave payload," *ESA Journal*, vol. 14, no. 4, pp. 467–478, 1990.
- [27] ———, "Design data for the control of multipactor discharge in spacecraft microwave and RF systems," *Microwave Journal*, vol. 35, no. 1, pp. 142–155, Jan. 1992.
- [28] C. Wang and K. A. Zaki, "Dielectric resonators and filters," *IEEE Microwave Magazine*, vol. 8, no. 5, pp. 115–127, Oct. 2007.
- [29] S. J. Fiedziuszko, "Dual-mode dielectric resonator loaded cavity filters," *IEEE Trans. Microwave Theory Tech.*, vol. 30, no. 9, pp. 1311–1316, Sept. 1982.

- [30] J. F. Liang and W. D. Blair, "High-Q TE_{01} mode DR filters for PCS wireless base stations," *IEEE Trans. Microwave Theory Tech.*, vol. 46, no. 9, pp. 1311–1316, Sept. 1982.
- [31] M. Makimoto and S. Yamashita, *Microwave Resonators and Filter for Wireless Communication: Theory, Design, and Application*. Berlin, Germany: Springer, 2001.
- [32] C. M. Kudsia, "A generalized approach to the design and optimization of symmetrical microwave filters for communications systems," Ph.D. dissertation, Dept. Eng., Concordia Univ., Quebec, QC, Canada, 1978.
- [33] G. Pfitzenmaier, "An exact solution for a six-cavity dual-mode elliptic bandpass filter," in *IEEE MTT-S Int. Microwave Symp. Dig.*, San Diego, CA, 1977, pp. 400–403.
- [34] D. R. Jachowski, "Folded multiple bandpass filter with various couplings," U.S. Patent 5 410 284, Apr. 25, 1995.
- [35] J. Lee, M. S. Uhm, and I.-B. Yom, "A dual-passband filter of canonical structure for satellite applications," *IEEE Microwave Wireless Compon. Lett.*, vol. 14, no. 6, pp. 271–273, June 2004.
- [36] J. Lee, M. S. Uhm, and J. H. Park, "Synthesis of self-equalized dual-passband filter," *IEEE Microwave Wireless Compon. Lett.*, vol. 15, no. 4, pp. 256–258, Apr. 2005.
- [37] G. Macchiarella and S. Tamiazzo, "Design techniques for dual-passband filters," *IEEE Trans. Microwave Theory Tech.*, vol. 53, no. 11, pp. 3265–3271, Nov. 2005.
- [38] R. Cameron, M. Yu, and Y. Wang, "Direct-coupled microwave filters with single and dual stopbands," *IEEE Trans. Microwave Theory Tech.*, vol. 53, no. 11, pp. 3288–3297, Nov. 2005.
- [39] S. Amari, "Synthesis of cross-coupled resonator filters using an analytical gradient-based optimization technique," *IEEE Trans. Microwave Theory Tech.*, vol. 48, no. 9, pp. 1559–1564, Nov. 2000.
- [40] R. J. Cameron and J. D. Rhodes, "Asymmetric realizations for dual-mode bandpass filters," *IEEE Trans. Microwave Theory Tech.*, vol. 29, no. 1, pp. 51–58, Jan. 1981.
- [41] C.-S. Ahn, J. Lee, and Y.-S. Kim, "Design flexibility of an open-loop resonator filter using similarity transformation of coupling matrix," *IEEE Microwave Wireless Compon. Lett.*, vol. 15, no. 4, pp. 262–264, Apr. 2005.
- [42] J.-S. Hong and M. J. Lancaster, "Couplings of microstrip square open-loop resonators for cross-coupled planar microwave filters," *IEEE Trans. Microwave Theory Tech.*, vol. 44, no. 12, pp. 2099–2109, Dec. 1996.
- [43] R. S. Kwok and J.-F. Liang, "Characterization of high-Q resonators for microwave-filter applications," *IEEE Trans. Microwave Theory Tech.*, vol. 47, no. 1, pp. 111–114, Jan. 1999.

- [44] J. S. Hong and M. J. Lancaster, "Theory and experiment of novel microstrip slow-wave open-loop resonator filters," *IEEE Trans. Microwave Theory Tech.*, vol. 45, no. 12, pp. 2358–2365, Dec. 1997.
- [45] R. J. Cameron, A. R. Harish, and C. J. Radcliffe, "Synthesis of advanced microwave filters without diagonal cross-couplings," *IEEE Trans. Microwave Theory Tech.*, vol. 50, no. 12, pp. 2862–2872, Dec. 2002.
- [46] J. Lee and K. Sarabandi, "A synthesis method for dual-passband microwave filters," *IEEE Trans. Microwave Theory Tech.*, vol. 55, no. 6, pp. 1163–1170, June 2007.
- [47] ———, "Design of triple-passband microwave filters using frequency transformations," *IEEE Trans. Microwave Theory Tech.*, vol. 56, no. 1, pp. 187–193, Jan. 2008.
- [48] J. S. Hong and M. J. Lancaster, *Microstrip Filters for RF/Microwave Applications*. New York: Wiley, 2001.
- [49] J.-S. Hong, M. J. Lancaster, and J.-C. Mage, "Cross-coupled HTS microstrip open-loop resonator filter on LAO substrate," in *IEEE MTT-S Int. Microwave Symp. Dig.*, 1999, pp. 1559–1562.
- [50] J.-S. Hong and M. J. Lancaster, "Design of highly selective microstrip bandpass filters with a single pair of attenuation poles at finite frequencies," *IEEE Trans. Microwave Theory Tech.*, vol. 48, no. 7, pp. 1098–1107, July 2000.
- [51] M. Makimoto and M. Sagawa, "Varactor tuned bandpass filters using microstrip-line ring resonators," in *IEEE MTT-S Int. Microwave Symp. Dig.*, 1986, pp. 411–414.
- [52] S. R. Chandler, I. C. Hunter, and J. G. Gardiner, "Active varactor tunable bandpass filter," *IEEE Microwave Guided Wave Lett.*, vol. 3, no. 3, pp. 70–71, Mar. 1993.
- [53] A. R. Brown and G. M. Rebeiz, "A varactor-tuned RF filter," *IEEE Trans. Microwave Theory Tech.*, vol. 48, no. 7, pp. 1157–1160, July 2000.
- [54] C.-Y. Chang and T. Itoh, "A varactor-tuned, active microwave bandpass filter," in *IEEE MTT-S Int. Microwave Symp. Dig.*, 1990, pp. 499–502.
- [55] R. M. Borwick, III, P. A. Stupar, J. F. DeNatale, R. Anderson, and R. Erlandson, "Variable MEMS capacitors implemented into RF filter systems," *IEEE Trans. Microwave Theory Tech.*, vol. 51, no. 1, pp. 315–319, Jan. 2003.
- [56] H.-T. Kim, J.-H. Park, Y.-K. Kim, and Y. Kwon, "Low-loss and compact V-band MEMS-based analog tunable bandpass filters," *IEEE Microwave Wireless Compon. Lett.*, vol. 11, no. 11, pp. 432–434, Nov. 2002.
- [57] J. Nath, D. Ghosh, J.-P. Maria, A. I. Kingon, W. Fathelbab, P. D. Franzon, and M. B. Steer, "An electronically tunable microstrip bandpass filter using thin-film Barium-Strontium-Titanate (BST) varactors," *IEEE Trans. Microwave Theory Tech.*, vol. 53, no. 9, pp. 2707–2711, Sept. 2005.

- [58] B.-W. Kim and S.-W. Yun, "Varactor-tuned combline bandpass filter using step-impedance microstrip lines," *IEEE Trans. Microwave Theory Tech.*, vol. 52, no. 4, pp. 1279–1283, Apr. 2004.
- [59] B. Kapilevich, "A varactor-tunable filter with constant bandwidth and loss compensation," *Microwave Journal*, vol. 50, no. 6, pp. 106–114, June 2007.
- [60] J. Lee and K. Sarabandi, "An analytic design method for microstrip tunable filters," *IEEE Trans. Microwave Theory Tech.*, vol. 56, no. 7, pp. 1699–1706, July 2008.
- [61] D. A. Frickey, "Conversion between S , Z , Y , h , $ABCD$, and T parameters which are valid for complex source and load impedances," *IEEE Trans. Microwave Theory Tech.*, vol. 42, no. 2, pp. 205–211, Feb. 1994.
- [62] J. R. Montejo-Garai, "Synthesis of N -even order symmetric filters with (n) transmission zeros by means of source-load cross coupling," *Electronics Letters*, vol. 36, no. 3, pp. 232–233, Feb. 2000.
- [63] S. Amari, U. Rosenburg, and J. Bornemann, "Adaptive synthesis and design of resonator filters with source/load-multiresonator coupling," *IEEE Trans. Microwave Theory Tech.*, vol. 50, no. 9, pp. 1969–1978, Aug. 2002.
- [64] S. Amari and U. Rosenburg, "New building blocks for modular design of elliptic and self-equalized filters," *IEEE Trans. Microwave Theory Tech.*, vol. 52, no. 2, pp. 721–736, Feb. 2004.
- [65] A. Tombak, J.-P. Maria, F. T. Ayguavives, Z. Jin, G. T. Stauf, A. I. Kingon, and A. Mortazawi, "Voltage-controlled RF filters employing thin-film barium-strontium-titanate tunable capacitors," *IEEE Trans. Microwave Theory Tech.*, vol. 51, no. 2, pp. 462–467, Feb. 2003.
- [66] L.-H. Hsieh and K. Chang, "Tunable microstrip bandpass filters with two transmission zeros," *IEEE Trans. Microwave Theory Tech.*, vol. 51, no. 2, pp. 520–525, Feb. 2003.
- [67] R. Azadegan and K. Sarabandi, "Miniature high-Q double-spiral slot-line resonator filters," *IEEE Trans. Microwave Theory Tech.*, vol. 52, no. 5, pp. 1548–1557, May 2004.
- [68] J. Lee and K. Sarabandi, "A miniaturized conductor-backed slot-line resonator filter with two transmission zeros," *IEEE Microwave Wireless Compon. Lett.*, vol. 16, no. 12, pp. 660–662, Dec. 2006.
- [69] F. Z. Bi and B. P. Barber, "Bulk acoustic wave RF technology," *IEEE Microwave Magazine*, vol. 9, no. 5, pp. 65–80, Oct. 2008.
- [70] C. F. Chang and S. J. Chung, "Bandpass filter of serial configuration with two finite transmission zeros using LTCC technology," *IEEE Trans. Microwave Theory Tech.*, vol. 53, no. 7, pp. 2383–2388, July 2005.

- [71] W. Y. Leung, K. K. M. Cheng, and K. L. Wu, "Multilayer LTCC bandpass filter design with enhanced stopband characteristics," *IEEE Microwave Wireless Compon. Lett.*, vol. 12, no. 7, pp. 240–242, July 2002.
- [72] D. R. White, "Ultrasonic consolidation of aluminum tooling," *Advanced Material & Processes*, vol. 161, no. 1, pp. 64–65, Jan. 2003.
- [73] S. Krishnan, "Modeling and simulation analysis of an fmcw radar for measuring snow thickness," Master's thesis, Dept. of Electrical Eng. and Computer Science, Univ. of Kansas, Lawrence, KS, 2004.
- [74] L. P. Ligthart, U. Akpinar, P. J. F. Swart, A. John, and R. H. Jansen, "35 GHz FM-CW radar modules," in *Int. Sym. on Physics and Engineering of Microwaves, Millimeter and Submillimeter Waves*, 2001, pp. 841–845.
- [75] M. Rangwala, J. Lee, and K. Sarabandi, "Design of FMCW millimeter-wave radar for helicopter assisted landing," in *IEEE Int. Geoscience and Remote Sensing Symp.*, 2007, pp. 4183–4186.
- [76] L. N. Ridenour, *Radar System Engineering*. Lexington, MA: Boston Technical Publishers, 1964.